# SYNTHESIS OF INTERNALLY FUNCTIONALIZED SILICA NANOPARTICLES FOR THERANOSTIC APPLICATIONS

by

Nathan Isaac Walton

A dissertation submitted to the faculty of
The University of Utah
in partial fulfillment of the requirements for a degree of

Doctor of Philosophy

Department of Chemistry

The University of Utah

August 2013

# The University of Utah Graduate School

## STATEMENT OF DISSERTATION APPROVAL

The dissertation of **Nathan Isaac Walton**

has been approved by the following supervisory committee members:

| | | |
|---|---|---|
| **Ilya Zharov** | , Chair | **06/04/2013** Date Approved |
| **Scott L. Anderson** | , Member | **06/04/2013** Date Approved |
| **Charles B. Grissom** | , Member | **06/04/2013** Date Approved |
| **Kenneth J. Woycechowsky** | , Member | **06/04/2013** Date Approved |
| **Ling Zang** | , Member | **07/22/2013** Date Approved |

and by **Henry S. White**, Chair of the Department of **Chemistry**

and by Donna M. White, Interim Dean of The Graduate School.

# ABSTRACT

This thesis addresses the synthesis and characterization of novel inorganic silica nanoparticle hybrids. It focuses in large part on their potential applications in the medical field. Silica acts as a useful carrier for a variety of compounds and this thesis silica will demonstrate its use as a carrier for boron or gadolinium. Boron-10 and gadolinium-157 have been suggested for the radiological treatment of tumor cells through the process called neutron capture therapy (NCT). Gadolinium is also commonly used as a Magnetic Resonance Imaging (MRI) contrast agent. Particles that carry it have potential theranostic applications of both imaging and treating tumors.

Chapter 1 presents a background on synthetic strategies and usages of silica nanoparticles, and NCT theory.

Chapter 2 describes a procedure to create mesoporous metal chelating silica nanoparticles, mDTTA. This is achieved via a co-condensation of tetraethoxysilane (TEOS) and 3-trimethoxysilyl-propyl diethylenetriamine (SiDETA) followed by a post-synthesis modification step with bromoacetic acid (BrAA). These particles have a large surface area and well-defined pores of ~2 nm. The mDTTA nanoparticles were used to chelate the copper(II), cobalt(II) and gadolinium(III). The chelating of gadolinium is the most interesting since it can be used as a MRI contrast agent and a neutron capture therapeutic. The synthetic procedure developed also allows for the attachment of a

fluorophore that gives the gadolinium chelating mDTTA nanoparticles a dual imaging modality.

Chapter 3 presents the synthetic method used to produce two classes of large surface area organically modified silica (ORMOSIL) nanoparticles. Condensating the organosilane vinyltrimethoxysilane in a micellar solution results in nanoparticles that are either surface rough (raspberry-like) or mesoporous nanoparticles, which prior to this thesis has not been demonstrated in ORMOSIL chemistry. Furthermore, the vinyl functionalities are modified, using hydroboration, to make the nanoparticles into water-dispersible boron carriers that also have potential boron neutron capture therapy (BNCT) applications.

Lastly, Chapter 4 provides a general description of NCT, specifically that involving boron-10 and gadolinium-157. It further describes the synthetic methodology used in producing fatty acid coated boron nanoparticles (BNPs). The BNPs are encapsulated with silica to add a hydrophilic shell so that they can potentially be used in biological systems as BNCT agents. The silica shell is also modified with a fluorophore, dansyl chloride, so that the particle hybrid could be imaged during cell studies.

TABLE OF CONTENTS

# LIST OF ABBREVIATIONS

| | |
|---|---|
| Å | Angstrom |
| $-COO^-$, -COOH | Carboxylate, Carboxylic Acid Group |
| °C | Degrees Celsius |
| K | Degrees Kelvin |
| ρ | Density |
| eV, keV, MeV | Electron Volt, Kilo Electron Volt, Mega Electron Volt |
| mg, g, kg, | Milligram, Gram, Kilogram |
| -OH | Hydroxyl Group |
| mL, L | Milliliter, Liter |
| cm, μm, nm | Centimeter, Micrometer, Nanometer |
| mV | Millivolt |
| mol | Mole |
| M | Molar |
| ppm | Parts Per Million |
| % | Percent |
| r | Radius |
| Si-OH | Silanol |
| $cm^{-1}$ | Wavenumber |
| $\%W_{loss}$ | Weight Loss |

| | |
|---|---|
| Au | Gold |
| APTES | Aminopropyltriethoxy Silane |
| $^{10}B$, B-10 | Boron-10 Isotope |
| $B@SiO_2$ | Silica Coated Boron Nanoparticle |
| $B_2O_3$ | Born Oxide |
| BET | Brunauer–Emmett–Teller |
| $BH_3THF$ | Borane Tetrahydrofuran |
| BNCT | Boron Neutron Capture Therapy |
| BNP | Elemental Boron Nanoparticle |
| BPA | p-Boronophenylalanine |
| $Br_2$ | Bromine |
| BrAA | Bromoacetic Acid |
| BSH | Mercapto-undecahydro-closo-dodecaborate |
| $CaCl_2$ | Calcium Chloride |
| CdSe | Cadmium Selenide |
| $Co^{2+}$ | Cobalt(II) |
| $CoCl_2$ | Cobalt Chloride |
| CT | X-ray Computed Tomography |
| CTAB | Cetyl Trimethylammonium Bromide |
| $Cu^{2+}$ | Copper(II) |
| $CuCl_2 \cdot 2H_2O$ | Cupric Chloride Dihydrate |
| DETA | Diethylenetriamine |
| DETA-MSNP | DETA Containing Mesoporous Silica Nanoparticle |

| | |
|---|---|
| DLS | Dynamic Light Scattering |
| DNA | Deoxyribonucleic Acid |
| DOX | Doxorubicin |
| DTTA | Diethylenetriaminetetraacetic Acid |
| DTTA-MSNP | DTTA Containing Mesoporous Silica Nanoparticle |
| EDTA | Ethylenetriaminetetraacetic Acid |
| EDS | Energy-dispersive X-ray Spectroscopy |
| EG | Ethylene Glycol |
| Eq | Equation |
| $Fe_2O_3$ | Iron Oxide |
| FITC | Fluorescein Isothiocyanate |
| $^{157}Gd$ | Gadolinium Isotope 157 |
| $Gd^{3+}$ | Gadolinium(III) |
| $GdCl_3 \cdot 6H_2O$ | Gadolinium Chloride Hexahydrate |
| HCl | Hydrochloric Acid |
| $H_2O$ | Water |
| IR | Infrared Spectroscopy |
| $KMnO_4$ | Potassium Permaganate |
| KOH | Potassium Hydroxide |
| LET | Linear Energy Transfer |
| MRI | Magnetic Resonance Imaging |
| MSN | Mesoporous Silica Nanoparticle |
| mvSNP | Mesoporous Vinyl Silica Nanoparticle |

| | |
|---|---|
| MW | Molecular Weight |
| $N_2$ | Nitrogen |
| $NaH_2PO_4$ | Monobasic Sodium Phosphate |
| NaOH | Sodium Hydroxide |
| $Na_2EDTA{\cdot}2H_2O$ | Disodium Ethylenetriaminetetraacetic Acid Dihydrate |
| $Na_2HPO_4$ | Dibasic Sodium Phosphate |
| NCI | National Cancer Institute |
| $NH_4OH$ | Ammonium Hydroxide |
| ORMOSIL | Organically Modified Silica |
| QD | Quantum Dots |
| rvSNP | Surface-Rough Vinyl Silica Nanoparticle |
| SiDETA | 3-trimethoxysilylpropyl Diethylenetriamine |
| SiDTTA | 3-Trimethoxysilylpropyl diethylenetriaminetetraacetic Acid |
| SiDTTA-Gd | 3-Trimethoxysilylpropyl Diethylenetriaminetetraacetic Acid Chelating Gadolinium |
| $SiO_2$ | Silica |
| $Si(OEt)_3$ | Triethoxy Silane |
| STEM | Scanning Transmission Electron Microscopy |
| svSNP | Solid Vinyl Silica Nanoparticle |
| T-mDTTA-Gd | Gadolinium chelating mesoporous silica nanoparticles synthesized by Taylor group. |
| TAT | Targeted Alpha Therapy |
| TEM | Transmission Electron Microscopy |
| TEOS | Tetraethoxy Silane |
| TGA | Thermogravimetric Analysis |

| | |
|---|---|
| THF | Tetrahydrofuran |
| TMB | Mesitylene, 1,3,5-Trimethylbenzene |
| TNT | Trinitrotoluene |
| UND Acid | Undecenoic Acid |
| UND-BNP | Undecenoic Acid Coated Boron Nanoparticles |
| UV/Vis | Ultraviolet/Visible |
| vSNP | Vinyl Silica Nanoparticle |
| VTMS | Vinyltrimethoxy Silane |
| $W_{sp}$ | Weight of a Single Particle |

LIST OF FIGURES

LIST OF SCHEMES

LIST OF TABLES

Table Page

# ACKNOWLEDGEMENTS

As a graduate student, the first person I should thank is Dr. Ilya Zharov, who kindly let me into his lab, let me design my own experiments, and was there for guidance when the universe and the world of chemistry felt like they were against me. Without him, I would not be the chemist I am today and I hope I use the foundation that he has given me to better my scientific knowledge. I wish him the best in getting graduate students, like myself, to further develop their chemical knowledge and their Ph.D.s.

I would like to thank Dr. Zhe Gao and Dr. Eric Brozek, who have helped me tremendously in my research. Dr. Gao and I worked on my first project together and I consider it a pleasure to have been able to work with her. Dr. Brozek acted as a second mentor, helped me enter the field of silica nanoparticle chemistry, and I am glad he considers me a friend.

I would also like to thank the Zharov group, Amir Khabibullin, Robert Haynes, Patrick Kolbay, Erica Green, and Dr. Patricia Ignacio-DeLeon, who have become my longtime friends. We have had some good times throughout my five years of doctoral work and I hope we have many more after.

Throughout my graduate work, I have had the help and support of many people whom I would name specifically. This would make this section as long as a chapter in my thesis, so I will single out two: Dr. Paulo Perez, who participated greatly in my boron

nanoparticle research and Michael Standing of BYU, who took the amazing TEM images of my hundreds of samples.

The greatest thanks I can give are to my parents (Michael and Phyllis) and siblings (Judith, Josie, Kathy, and Adam), who have gone above and beyond in encouragement and support. Mom and Dad, thank you for being around and reading all my chemistry papers and specifically this thesis. What would I do without you?

# CHAPTER 1

# BACKGROUND

## 1.1 Introduction

Theranostics is a novel approach to multifunctional agents that combine diagnostic (often imaging) and therapeutic (often combined with targeted delivery) functions in treatment of various diseases, and in particular, in the treatment of cancer. The combination of several modalities allows for the simultaneous imaging and treatment of tumors by a single construct. This design has become of particular interest with silica nanoparticles because of their surface modification chemistry and drug encapsulation properties.[1]

Theranostic constructs often incorporate tumor targeting ligands, groups which selectively and tightly bind receptors over expressed by the tumor cells (e.g. folic acid receptors, integrins). The attachment of a targeting ligand to the silica surface typically involves the use of a primary amine group (e.g. 3-aminopropyltriethoxysilane) reacting with the carboxylic acid group of the targeting species. For example, it has been demonstrated that silica modified with 3-aminopropyltriethoxysilane bound to folic acid has a much greater uptake into pancreatic tumor cells than silica nanoparticles that do not have folic acid on their surface.[2]

There are essentially two methods in imaging inside the body, Magnetic Resonance Imaging (MRI) and Computed Tomography (CT). Synthesizing silica

nanoparticles with biologically relevant imaging modality can prove difficult. The MRI agents gadolinium and superparamagnetic iron oxide have been the focus for introducing an imaging modality to silica nanoparticles.[2,3] In addition, nanoparticles that can incorporate bismuth (CT contrast agent) have recently been suggested.[4]

Mesoporous silica nanoparticles have been demonstrated to be useful as a drug delivery agent since the drug can be trapped in their pores. This process requires a release mechanism so that the drug can exit the pores inside the cancer cell.[1] Although small molecule drug treatment of cancer is widely used, it is not without limitations and disadvantages. There is an alternative cancer treatment called Neutron Capture Therapy that does not require a release of drug molecules.

Multiple approaches have been proposed for the preparation of theranostic constructs, including liposomes,[5-9] dendrimers ,[10,11]polymers,[12-16] and nanoparticles.[17-26] Of the latter, inorganic nanoparticles in general, and silica nanoparticles in particular, are very attractive due to their ease of formation, diverse surface chemistry, and biocompatibility. The focus of this dissertation is on the preparation of internally functionalized silica nanoparticles for theranostic applications.

The study of inorganic nanoparticles is a burgeoning area in the field of nanoscience. Inorganic nanoparticles have become of particular interest for their potential use in a variety of applications, such as sensing,[27] delivery,[28] electronics,[29] energy,[30] imaging,[31] therapeutics,[32,33] and separations.[34,35] Inorganic nanoparticles can be metallic, semiconductor, or dielectric. Metallic (i.e. gold and silver) and semiconductor (i.e. titania and cadmium selenide) nanoparticles demonstrate optical and electronic properties that are size and shape dependent.[36,37] Dielectric nanoparticles (e.g. silica), although lacking

dependent optical and electronic properties, can be synthesized in a broader range of sizes than other inorganic nanoparticles. Because they maintain their inert and hydrophilic properties, they are useful as carriers. Silica nanoparticles are especially valuable for many fields because they can be used as carriers of fluorescent dyes, other nanoparticles, various organic groups, and drug molecules.

In 1960, synthesizing silica nanoparticles involved the combustion of a silicon tetrachloride.[38] The sizes of these silica nanoparticles were less than 100 nm; however, the resultant particles were prone to severe aggregation and size polydispersity. Werner Stöber, Fink, and Bohn saw the necessity to synthesize uniform, nonagglomerating silica nanoparticles for analytical and other applications.[39] The method developed by Stöber et al. is still very popular, and other synthetic strategies are currently available, such as tailoring[40-48] the aforementioned method or the use of reverse phase microemulsion.[49]

The inherent inertness of silica nanoparticles does not, at first, seem to offer many applications when compared to conductive and semiconductive nanoparticles. They have no optical or electronic properties, are thermally and chemically stable, and relatively hydrophilic. By modifying the traditional synthetic procedures, however, silica can become a phosphor carrier, which can improve the luminescence because its inert matrix prevents energy loss.[50] It can also act as a nanoparticle carrier,[51] imparting hydrophilic properties while protecting the cargo from the environment or *vice versa*.

Modification of the silica surface with organosilanes, utilizing surface silanols, can endow it with additional properties while minimizing disadvantages, thus creating an improved silica nanoparticle. Reactive sites for polymerization and other organic reactions can be achieved through the addition of organosilanes to the surface.[52] Because

organosilanes impart changes in hydophilicity, or charge, to the surface of these particles,[53] guest species can be trapped on to the surface by noncovalent interactions, such as electrostatic interactions between surface and guest species. All of the endowed organic properties also make silica nanoparticles potentially useful in separations (i.e. chromatography[54] and inorganic membranes[55]).

ORMOSILs (Organically Modified Silica) are silica nanoparticles made solely from organosilanes.[56] Although more recently developed and less studied, ORMOSILs provide the same advantages as do silica nanoparticle without the necessity of post-modifications. These particles also possess higher densities of organic functionalities throughout the entire particle, which makes them highly effective as guest carriers for drug delivery,[57] and in catalysts.[58] Additionally, their greater organic group density results in more groups that can be modified by traditional synthetic techniques, such as converting an alkene to a borate through hydroboration.

Processes that increase the surface area to volume ratio of silica nanoparticles can be used to increase the accessibility and/or density of silanols, or organic groups, for modification. This can be achieved by either making the surface-rough[59] or by preparing mesoporous nanoparticles.[60,61] This becomes important when considering silica nanoparticles for drug delivery,[62] adsorption,[63] or creating superhydrophic surfaces.[64] To make surface-rough particles, silica nanoparticles are either co-condensed with large amounts of organosilanes,[59] etched,[64] or smaller particles are bonded to their surface.[65] For the mesoporous particle preparation, a surfactant is used to generate a micellar solution. The micelles in the solution act as a template around which the silica precursor condenses, thus creating particles with mesopores.

Silica nanoparticles act as superb carriers for a multitude of different species, whether they are luminescent species within the body of the particles or another nanoparticle. Their applications depend on their cargo. Silica nanoparticles can be synthetically modified in a variety of ways to improve them as carriers. The purpose of this chapter is to provide a background and a history of silica nanoparticle development from solid spherical structures to high surface area structures, and to discuss their applications. The following chapters will discuss the synthesis of hybrid silica nanoparticles for theranostics, experiments with them, results, and conclusions of the studies.

## 1.2 Formation of Silica Nanoparticles

Although there are many methods to synthesize silica nanoparticles,[40-48] the typical procedures require hydrolysis and condensation steps in the presence of a catalyst (Scheme 1.1). Particle formation is initiated when an alkoxy silane is hydrolyzed, creating reactive silanols group in place of the ether. The silanols then undergo polymerization with other precursor units leading to dimers and oligomers, which supersaturate the solution and precipitate out to become distinct nuclei that grow into the larger silica networks. The final product of the condensation reaction can be either a silica gel or silica nanoparticles (Figure 1.1). [53,66]

The catalyst is the controlling factor of the final product. There are two types of catalysts that can be used for hydrolysis/condensation, either acid (e.g. HCl) or base (i.e. NaOH or $NH_4OH$). When an acid catalyst is used, creating a low pH environment, the

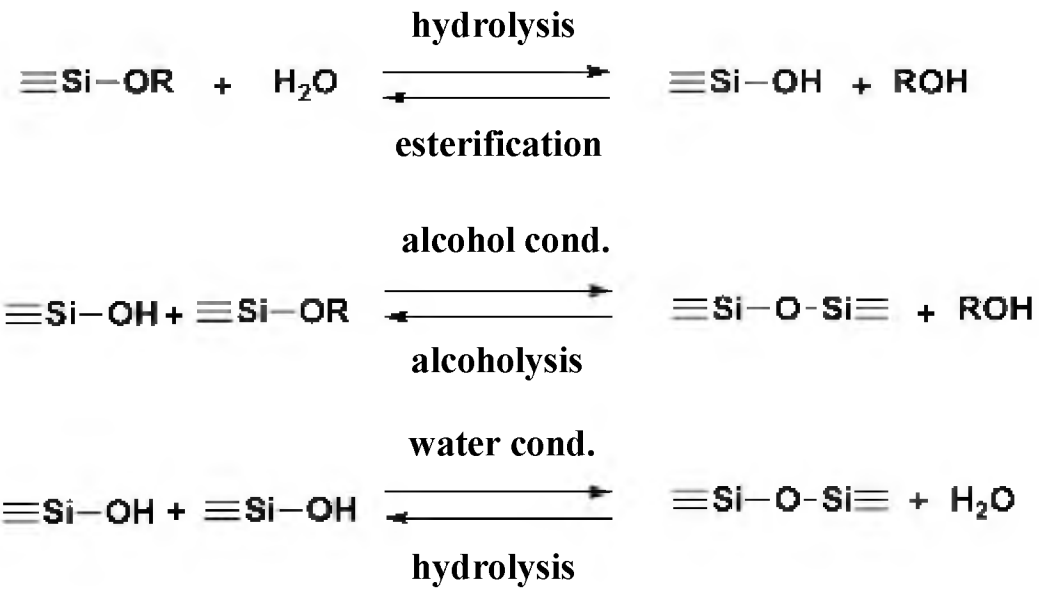


Scheme 1.1: Reaction intermediates in sol-gel synthesis.

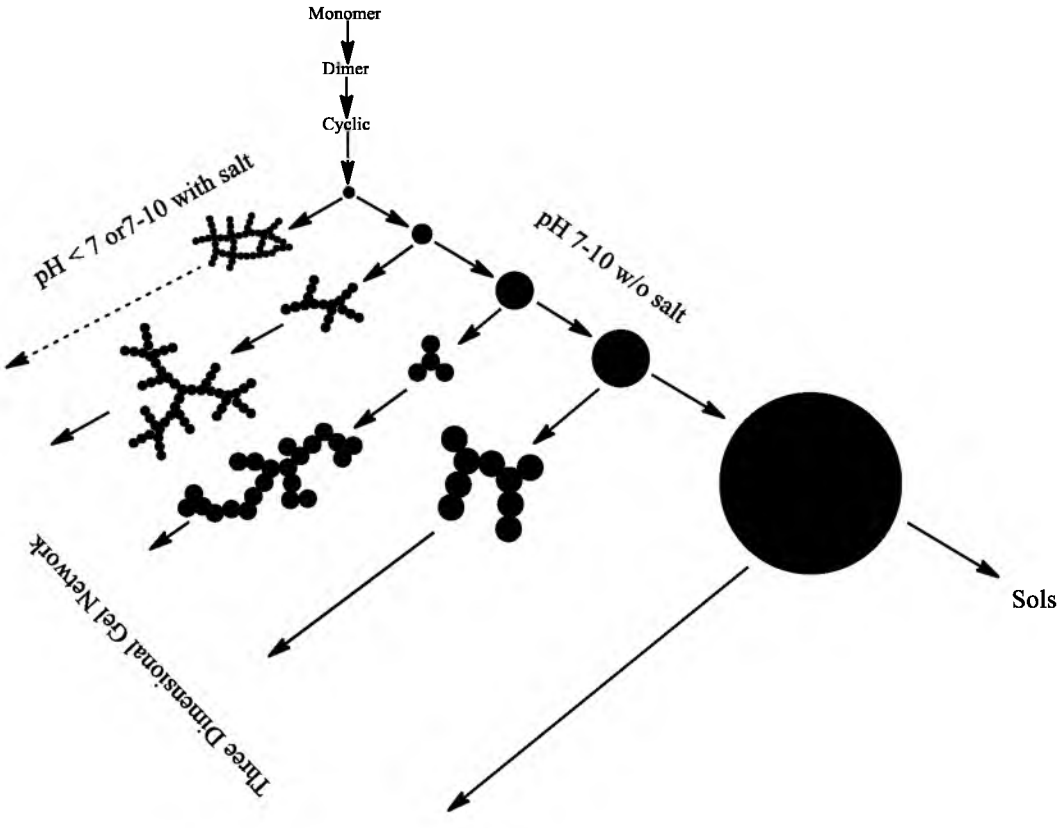


Figure 1.1: Sol-gel products resulting from different reaction conditions.[53]

silanols remain protonated. The lack of any significant repulsion between growing nuclei creates extended polymer chains that cross-link. This results in a three-dimensional gel.[66] A base catalyst produces a high pH environment that deprotonates the silanols, creating negative charge on the surface of the growing nuclei. The resultant electrostatic repulsion between the nuclei prevents the cross-linking of the silica intermediates between the growing particles, preventing aggregation.[53]

## 1.3 Stöber Method Silica Particles Synthesis

The Stöber method was first introduced in 1968 as a procedure to synthesize uniform silica nanoparticles.[39] Since its inception, it is probably the most popular and widely developed method of silica nanoparticle preparation.

Stöber et al. synthesized silica nanoparticles with the hydrolysis and condensation of tetraethoxy silane (TEOS) in water, ammonium hydroxide ($NH_4OH$), and alcohol (i.e. methanol and ethanol) solution. When TEOS is added to the rapidly stirred solution, the mixture quickly becomes opaque, indicating that TEOS is being hydrolyzed and condensing into nuclei, which grow into distinct, monodisperse nanoparticles (Scheme 1.2). The silica particles are collected via centrifugation and washed to remove the unreacted precursor and the catalyst.

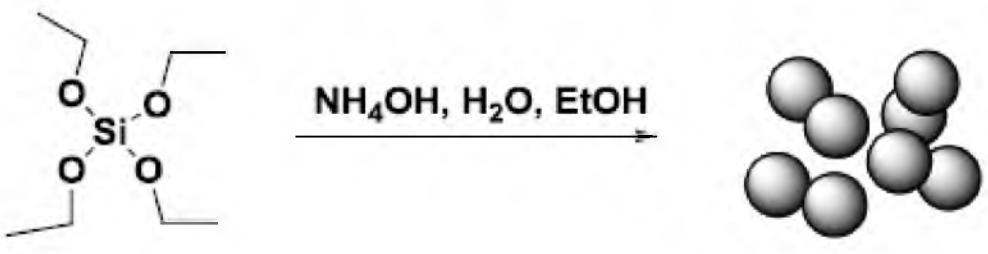


Scheme 1.2: Stöber method.

By controlling the environment in which the silica nanoparticle intermediates are made, particles with sizes ranging from 50 nm[67] to 2 μm[68] in diameter can be synthesized. The size of the silica nanoparticles is tuned by adjusting the solution temperature,[69-71] $NH_4OH$[72] and/or alcohol concentration, or by using a different alcohol as a co-solvent.[73] Increasing the temperature of the solution results in the synthesis of particles with smaller diameters (base on the Lifschitz-Slyozov-Wagner equation). Multiple factors such as surface energy, diffusion and growth rates, and equilibrium solubility are affected by changes in solution temperature.[74] Increasing the concentration of $NH_4OH$ accelerates the rate of hydrolysis leading to more oligomer intermediates, which quickly leads to supersaturation, thus increasing the rate of the condensation and producing larger silica particles. Additionally, decreasing the polarity of the solution by increasing the alcohol concentration or changing the alcohol used as a co-solvent causes the silica intermediates to become insoluble in solution. This insolubility decreases the concentration needed for supersaturation and forces early nucleation. Oligomers that did not nucleate then deposit on the nuclei, instead of reaching supersaturation, creating larger particles.

## 1.4 The Use of Organosilanes for Surface Modification of Silica Nanoparticles

Organosilanes are one of the few chemicals that react with the inert silica nanoparticles utilizing their surface silanols. Organosilanes are silanes that can undergo hydrolysis and condensation to provide organic functionalities to the silica nanoparticle surface. There are many advantages to modifying silica nanoparticles with organosilanes. For example, polymerization reactions[35] or other chemical attachments (i.e. binding antibodies or fluorophores) can be performed.[75] Also, polarity changes to the particles

using alkyl silanes (e.g. vinyltrimethoxy silane) allow them to be dispersed in more hydrophobic environments.[76]

There are two methodologies to attach organosilanes to silica, "grafting to" and co-condensation (Scheme 1.3).[77] The "grafting to" approach involves the post-modification of silica nanoparticles with another hydrolysis/condensation reaction in the presence of the organosilane. This approach provides a defined spherical structure with a known surface area that has organic functionalities solely on its surface. Multiple layers of organic functionalities can be added because the organosilanes introduce new silanols during hydrolysis/condensation that can undergo further condensation. For monolayers, the density of the organic group on the surface is dependent on the available silanols (~2-3 Si-OH per $nm^2$), but due to condensation between organosilanes, a greater surface coverage is often observed.[78]

The co-condensation method involves the condensation of TEOS with the organosilanes, which incorporates organic groups into the silica matrix. This creates a higher density of available organic functionalities but may have an unwanted effect on nanoparticle size and shape.[59,79]

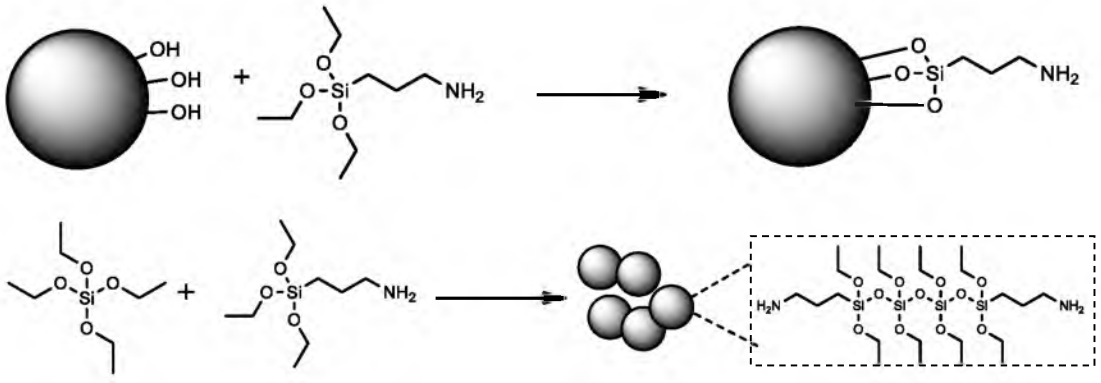


Scheme 1.3: Example of "grafting to" and co-condensation products.

## 1.5 Silica Nanoparticles as Carriers of Fluorophores, Nanoparticles, and Ions

Fluorophores are used in bioimaging or labeling, but organic fluorophores (e.g. FITC) are highly susceptible to photobleaching and low quantum yield,[77] and inorganic nanoparticle fluorophores (e.g. quantum dots) are highly toxic.[75,80] Silica nanoparticles can help to ameliorate these problems.[75,77] The hydrophilic and inert nature of silica nanoparticles makes them useful carriers for both fluorophores and inorganic nanoparticles to be used in biological systems, because they can be transported to cells via the circulatory system without being degraded by biological catalysts. Silica, by encapsulating organic fluorophores, protects the dyes from photobleaching, thus improving fluorescence lifetime and increasing its quantum yield. For inorganic nanoparticles, silica creates a protective shell so that the bare inorganic particles are sequestered from the biological environment. This prevents the inorganic nanoparticles from creating oxidative species or leaching toxic heavy metals.[80]

The two typical methods to encapsulate a species within silica are the Stöber method and reverse phase microemulsion.[75] Encapsulating organic fluorophores using the Stöber method is most effective when attaching the fluorophore to an organosilane and performing a co-condensation reaction. This allows the dye to be covalently incorporated on the surface and throughout the silica matrix. The dyes on the surface can be protected, like the core fluorophores, by adding another layer of silica around the nanoparticle post-synthesis (Scheme 1.4).

Reverse phase microemulsion encapsulates the organic fluorophore by placing the TEOS and dye into the same micelle. As the TEOS condenses, the dye is passively trapped in the silica matrix. This process can result in dye leakage from the particle,

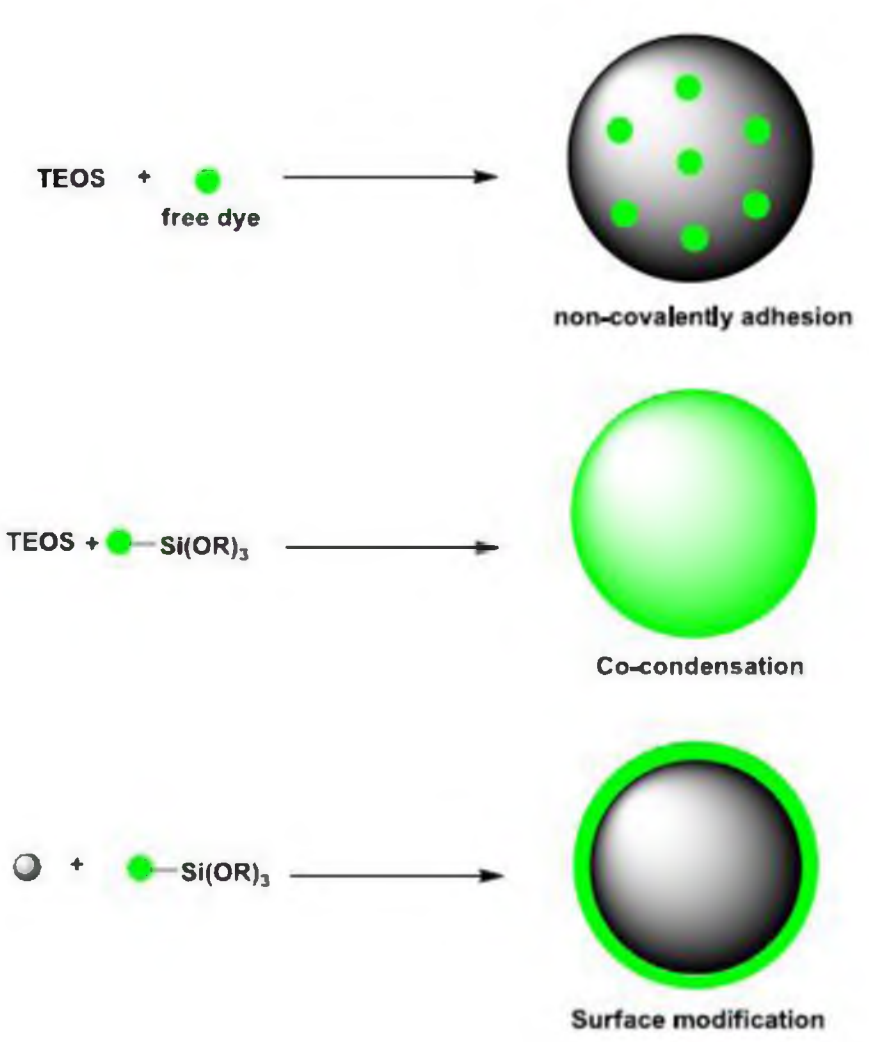


Scheme 1.4: Generating fluorescent silica nanoparticles.

because the dye is not covalently attached (Scheme 1.4). This can be corrected by using a cationic fluorophore, such as ruthenium(II) chloride hexahydrate, which electrostatically binds to the negatively charged silica. This passive encapsulation can be also performed using the Stöber method.

The highly fluorescent, organic dye-containing silica nanoparticles have been shown to be useful for biological applications. When their surfaces are modified with targeting or recognition groups, they can provide optical differentiation of cell lines or DNA sequences.[81,82] These particles can also be used as detectors, if the fluorescence of

the dye is affected by the environment. This was demonstrated when detecting trinitrotoluene (TNT) with fluorescein isothiocyanate (FITC).[77]

When encapsulating inorganic nanoparticles within silica, whether for fluorophores (e.g. CdSe) or for other applications (i.e. $Fe_2O_3$, Au), the same methods, Stöber and microemulsion, can be implemented to create core-shell nanostructures (Scheme 1.5).[77] The core-shell structure is a direct result of the silica not being able to incorporate the inorganic nanoparticle in its matrix during the condensation. Encapsulation involving the Stöber method is used when organosilanes cannot be bonded to the inorganic nanoparticle. This failure results in a dependency on noncovalent interaction between TEOS and inorganic particles and may result in some particles not being encapsulated.

The encapsulation of quantum dots (QDs) by silica demonstrates a significant reduction, or removal, of toxic effects. Such encapsulated QDs have been used for cell imaging and, after modifying the silica shell, have been able to target/label different tumor cells.[75,77,83] Furthermore, changing the cargo that silica encapsulates has given core-shell silica nanoparticles applications in MRI contrast when carrying

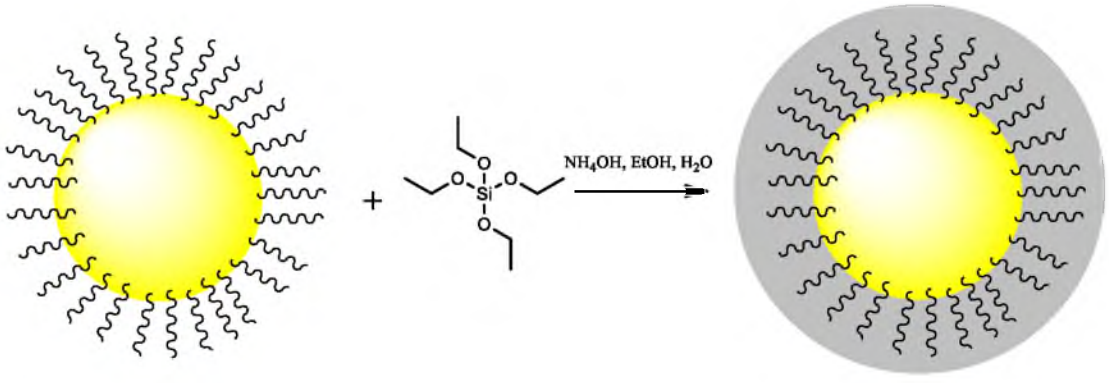


Scheme 1.5: Encapsulation of a nanoparticle using TEOS resulting in a core-shell structure.

superparamagnetic iron oxide and in photothermal therapy drug when gold nanoparticles are encapsulated.

Silica nanoparticles are not limited to encapsulation of fluorophores and other nanoparticles, but can also trap ions, such as heavy metal cations. The cationic metals can interact with the negatively charged silica surface which have proven useful as catalytic support.[84] By modifying the surface of the particles with chelators, metal ions can be permanently trapped. Adding metal chelators to the surface has been suggested as a way to prepare gadolinium carriers for MRI (Scheme 1.6).[85]

## 1.6 ORMOSIL Nanoparticles

Organically modified silica (ORMOSIL) can be defined as the products of hydrolysis and condensation of trialkoxysilanes in the absence of a tetraalkoxy precursor.[86] This new type of silica nanoparticle is very promising, because they possess increased density of organic groups throughout the particle. However, synthesis of nanoparticles from organosilanes has proven to be difficult. This limits the available synthetic methodologies and sometimes requires using small amounts of TEOS precursor to initiate particle formation.

One of the first groups to synthesize successful ORMOSIL nanoparticles was Ottenbrite et al.[86] They used a microemulsion method with a variety of organosilanes

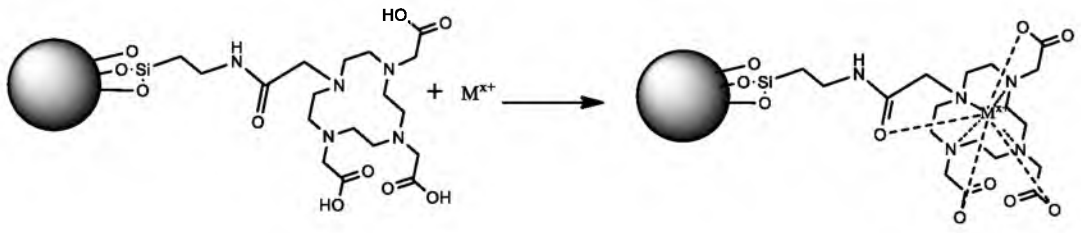


Scheme 1.6: Representation of a metal chelating nanoparticle.

possessing hydrophobic organic groups, which are similar to TEOS, in the presence of aminopropyltriethoxy silane. They demonstrated that the aminopropyltriethoxy silane acted more as a catalyst than a co-condensate and that the resultant 100-500 nm spherical particles were mainly composed of the hydrophobic organosilanes.

Buining et al. further developed the ORMOSIL synthesis. They used either an adapted Stöber method or a micelle-mediated reaction to condense the hydrophobic organosilanes. To synthesize ORMOSIL nanoparticles using the Stöber method, Philipse et al. created silica seeds using a sodium silicate solution (Scheme 1.7). The organosilanes that grew from the silica nuclei had diameters less than 200 nm.[87,88] Although the resulting particles consisted mostly of organosilane, they still required an initial co-condensation with bare silica, which made them pseudo-ORMOSILs.

Baumann et al. demonstrated that a silica seed or a co-condensate organosilane is not required when using a micelle-mediated synthesis. This method results in one of the few examples of ORMOSILs grown from a single organosilane (Scheme 1.8).[89,90] The micelle is produced by placing a cationic surfactant in an aqueous solution. Under the alkaline conditions, the micelle core creates an environment for the organosilane to hydrolyze/condense. The size of these ORMOSIL nanoparticles, like silica nanoparticles, can be adjusted by altering the concentration of the surfactant and the precursor.

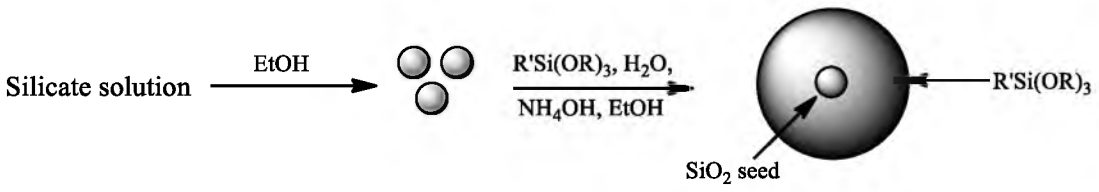


Scheme 1.7: Seed-mediated ORMOSIL particle formation.

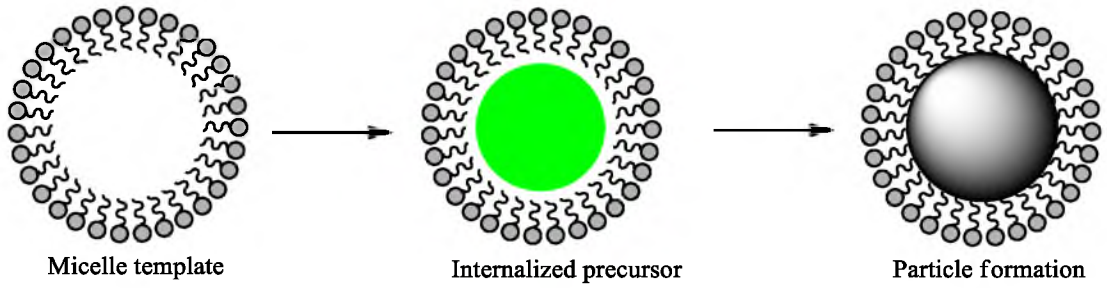


Scheme 1.8: Emulsion-mediated particle growth.

ORMOSIL nanoparticles, in addition to possessing high organic group densities, have a more porous structure when compared to traditional silica nanoparticles. This is caused by the introduction of steric bulk of the organic groups, a transformation that disrupts the compact structure of the silica matrix. The resultant porosity is advantageous because it provides accessibility to the organic groups inside the particle for further reactions.

The porous nature of ORMOSIL nanoparticles can also allow for metal nanoparticle growth inside the matrix by trapping the metal growth nuclei.[91] This prevents the agglomeration-prone metallic particles from aggregating. The metal nanoparticle is then able to impart its functionalities, such as catalytic, fluorescent, or photothermal therapeutic properties, to the overall structure.

## 1.7 Surface-rough Silica Nanoparticles

The density of silanols on spherical silica nanoparticles, and thus organic functionalities, is limited by the available surface area. The surface area can be increased by increasing the sphere size, but the size of the particle can only be increased to a few hundred nanometers. Surface area can also be increased by synthesizing nanoparticles that are not smooth, but surface-rough.

Surface-rough nanoparticles, also referred to as raspberry nanoparticles, possess a larger surface area compared to traditional silica nanoparticles by at least a factor of 2.[59] There are two common methods to produce these types of particles (Scheme 1.9). The first method involves modifying a larger silica particle with smaller silica particles.[65,92] This can be done by attaching aminopropyltriethoxy silane to the surface of the larger particle and then mixing the aminated silica with the smaller, negatively charged silica nanoparticles that bind electrostatically the positively charged aminated particles. The resultant particle has a larger surface area compared to the smooth particles of the same size; however, these particles are often large, with diameters in the micron range.

The other method for creating surface-rough nanoparticles involves etching of silica nanoparticles with a reducing agent, such as sodium borohydride.[64] This has little effect on the size, but leads to more available surface silanols. The new surface-rough particles can then undergo traditional organosilane modification with higher degrees of surface coverage.

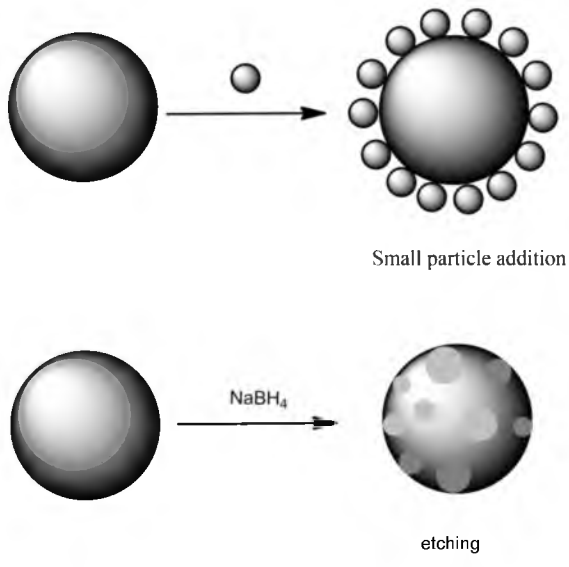


Scheme 1.9: Representation of synthetic strategies to make surface-rough nanoparticles.

Surface-rough silica nanoparticles are of particular interest for the development of antifogging, water-repellent glass chromatographic separations.[65,93,94] To give glass this modality, it has to be processed with an organosilane, typically aminopropyltriethoxy silane, enabling it to bind electro-statically to the nanoparticles prior to any modification step. The hydrophobicity of these particles is attributed to the rough surface and not the hydrophobic groups attached to them.

## 1.8 Mesoporous Silica Nanoparticles

In 1992, mesoporous silica nanoparticles were developed at Mobil Corporation laboratories.[95] These particles have well-defined mesopores and increased surface area. Mesoporous silica nanoparticles have attracted attention as a highly porous molecular sieves[95] and a drug carrier.[96]

Mesoporous silica is synthesized by the hydrolysis and condensation of a silica precursor (e.g. TEOS) in a micellar solution (Scheme 1.10). The micelles act as a template around which the silica precursor polymerizes. The micelles are removed from the final product by calcination or by solvent leaving a porous structure.[97] The mesoporous structure can be synthesized with different pore diameters, varying degrees of pore penetration, and ordered or disordered porous networks by using a diverse array of surfactants.

The late Victor Lin made a major contribution to the development of mesoporous silica nanoparticles. His group prepared mesoporous silica particles that are monodisperse and possess uniformly high levels of porosity. This was done by controlling the interactions between cetyl trimethylammonium bromide (CTAB), a

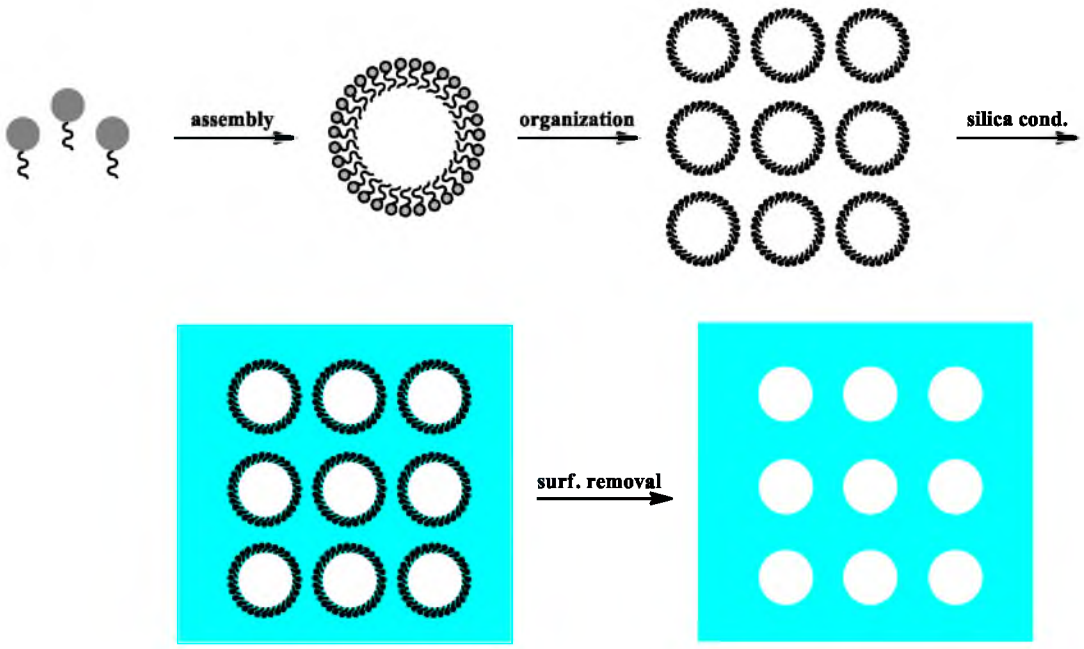


Scheme 1.10: Generation of mesoporous silica from micellar template.

cationic surfactant, and the anionic silica intermediates.[98] Additionally, organosilanes were introduced into these highly porous particles imparting organic functionalities.

When modifying mesoporous silica particles, the same two methods can be applied as with standard silica nanoparticles. The "grafting to" approach provides a well-defined scaffold to modify. However, due to the silanol distribution, there is an uneven distribution of organic groups observed and modifications tends to cause pore blocking.[99] On the other hand, using co-condensation results in even organic group distribution without pore blocking, but increasing the organosilane concentration leads to the loss of mesoporous structure (Scheme 1.11).[100]

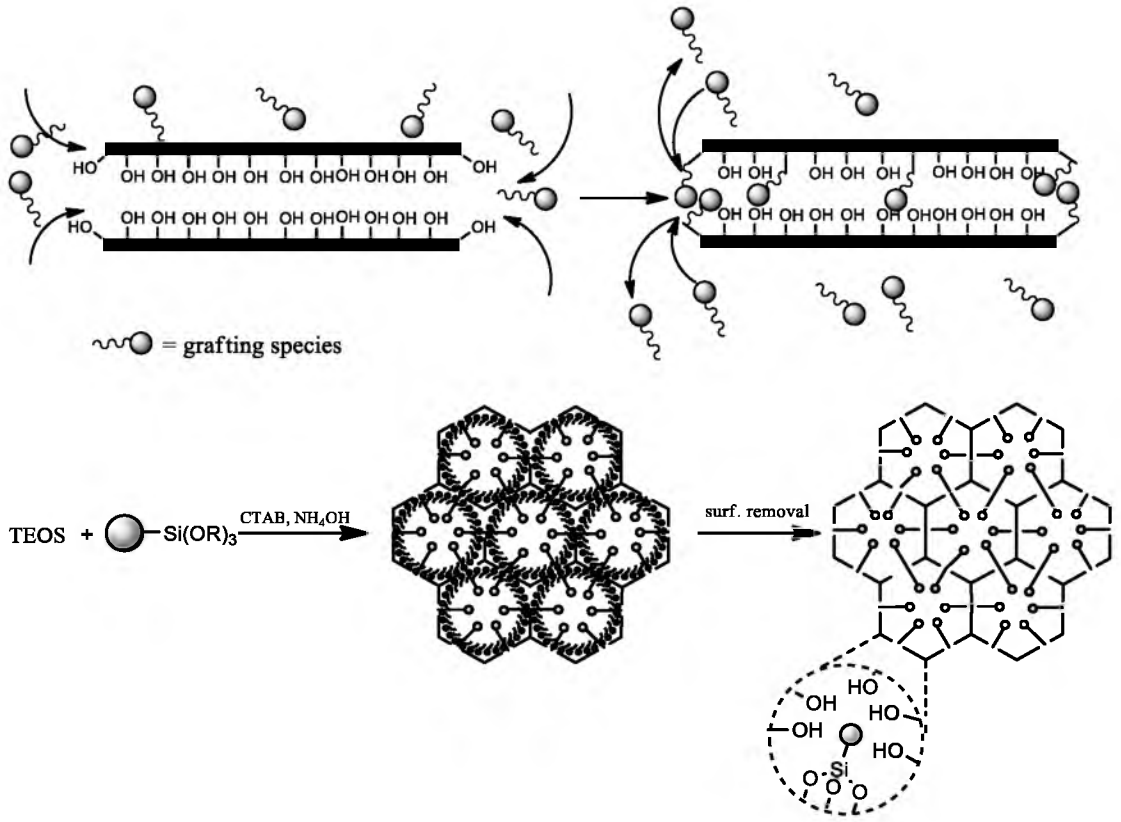


Scheme 1.11: Representation of "grafting to" mesopores and co-condensation.

Applications for mesoporous silica nanoparticles commonly revolve around drug delivery. Because of their porous channels, they can easily uptake and release molecules. Uptake is accomplished by immersing the particles in the cargo molecule solution.[101,102] The molecule can then be trapped by sealing the ends of the pores with either a cleavable plug[103] or environment-responsive polymer (Scheme 1.12).[104] For example, an anticancer drug, DOX, can be loaded into the mesoporous silica and trapped by coating the particle with a polymer containing a disulfide bond.[104] When the particle enters the cell, the antioxidant glutathione cleaves the disulfide bond causing the ejection of the polymer from the surface, thus unblocking the pores and causing DOX to be released inside the cell.[104]

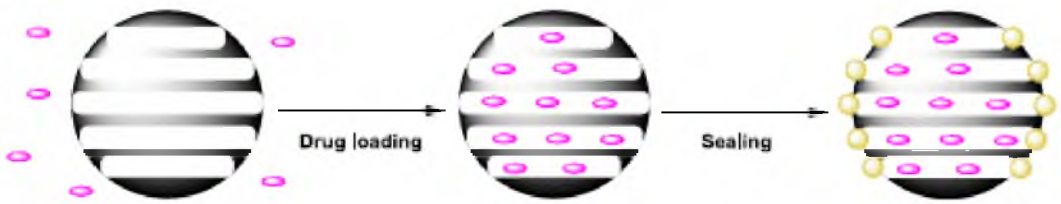


Scheme 1.12: Mesoporous nanoparticle molecule loading and trapping.

## 1.9 Neutron Capture Therapy

In the United States alone, there are about eleven million people with some form of cancer.[105] Since the 1970s, the United States, through the National Cancer Institute (NCI), has put more than two hundred billion dollars into finding treatments and cures for cancer.[106] Presently, treatments are limited to chemotherapy, surgery, radiation therapy, and interferon therapy. The problem with current methods is that none are localized to the tumor itself; even surgery requires damaging healthy tissue. This reduces their effectiveness and increases treatment complications. In 1936, George Locher proposed as a possible solution using boron as a localized cancer therapeutic. His idea is now known as boron neutron capture therapy (BNCT).[107]

Neutron capture therapy is based on the adsorption of slow neutrons in the nuclei of a nonradioactive isotope located inside, or adjacent to, the tumor cell. The adsorption of the neutrons leads to the release of radiation in the form of high linear energy transfer (LET) particles damaging the target cell. In addition to being nonradioactive, the isotope has to have a capture cross-section that is many times greater than that of elements typically found in tissues (Table 1.1) so that the neutrons are absorbed by the therapeutic isotope. A list of capture cross-sections can be seen in Table 1.2. $^{10}B$ (BNCT) is the most

Table 1.1: Thermal Neutron Capture Cross-Section Values of Tissue Elements and Their Percentages.[108]

| Nuclide | Capture Cross-Section (barns) | Weight (% in tissue) | Nuclide | Capture Cross-Section (barns) | Weight (% in tissue) |
|---|---|---|---|---|---|
| H | 0.332 | 10.00 | P | 0.18 | 1.16 |
| C | 0.0034 | 18.0 | S | 0.53 | 0.20 |
| N | 1.82 | 3.0 | Cl | 32.68 | 0.16 |
| O | $1.8 \times 10^{-4}$ | 65.0 | K | 2.1 | 0.20 |
| Na | 0.43 | 0.11 | Ca | 0.4 | 2.01 |
| Mg | 0.053 | 0.04 | Fe | 2.57 | 0.01 |

Table 1.2: Capture Cross-Section Values of Various Nuclides for Thermal Neutrons.[108]

| Nuclide | Capture Cross-Section (barns) | Nuclide | Capture Cross-Section (barns) |
|---|---|---|---|
| $^{6}Li$ | 942 | $^{151}Eu$ | 5800 |
| $^{10}B$ | 3838 | $^{155}Gd$ | 61000 |
| $^{22}Na^{a}$ | 32000 | $^{157}Gd$ | 255000 |
| $^{58}Co^{a}$ | 1900 | $^{164}Dy$ | 1800 |
| $^{113}Co$ | 19800 | $^{184}Os$ | 3000 |
| $^{126}I^{a}$ | 6000 | $^{199}Hg$ | 2000 |
| $^{135}Xe^{a}$ | 2600000 | $^{230}Pa^{a}$ | 1500 |
| $^{148m}Pm^{a}$ | 10600 | $^{235}U^{a}$ | 580 |
| $^{149}Sm$ | 42000 | $^{241}Pu^{a}$ | 1010 |

a: Radioactive

popular isotope due to its low toxicity and chemistry that allows for easy incorporation into a variety of small and macromolecules. $^{157}Gd$ (GdNCT) is the only other proposed potential neutron capture therapeutic because it is nonradioactive and it has the second highest capture cross-section of all elements. The challenges with GdNCT are that gadolinium is toxic and therefore must be tightly bound to the carrier, it has to be located closer to the nucleus to maximize LET damage, and the γ rays it produces are not localized to the target cell.[108]

BNCT is the process in which boron-10 undergoes nuclear fission through an alpha decay pathway by absorbing a thermal neutron (0.025 eV). The fission reaction produces two high LET products, an alpha particle (1.47 MeV) and $^{7}$Li (0.84 MeV). The maximum travel range that these high LET products in tissue is 9 μm.[107,109] Since a typical human cell is 10-30 μm,[110] the radiation is mainly localized to cells containing $^{10}$B, with some possible damage done to immediately adjacent cells.

Although localized treatment is important, there are two requirements that any boron compound must meet to be a plausible BNCT agent. First, the minimum amount of $^{10}$B must be ~$10^{9}$ atoms per cell to provide a greater chance for neutron capture, and second, the tumor-to-normal tissue and tumor-to-blood boron concentration must be greater than 3:1, so as to localize the BNCT reaction to the tumor without doing irreparable damage to the normal tissues.[107,111-114]

There are two boron compounds that have been clinically studied as BNCT agents, mercapto-undecahydro-closo-dodecaborate (BSH) and p-boronophenylalanine (BPA).[107,115,116] In animal testing studies, BSH has a tumor-to-blood ratio of 1.3:1, which is much less than the required ratio. It has been suggested that the tumor-to-tissue ratio is more important than the tumor-to-blood ratio; therefore, if that ratio is increased, the BSH is still a good treatment candidate.[3] BPA meets both requirements. It is, however, selective only to gliomas and melanomas. According to clinical studies of BPA, a minimum dosage of 250 mg/kg body weight is needed to be effective,[117] because only 1 out of every 5 BPA molecules (20% $^{10}$B) could undergo neutron capture. Besides BPA and BSH, boronporphyrins,[118,119] amino acids,[120] polyhedral boranes,[121,122] boronated anti-epidermal growth factor receptor,[123] DNA-binding agents,[124,125] and monoclonal

antibodies[126] have been proposed as alternative boron delivery agents. Presently, increasing the $^{10}B$ capacity to improve the chance of neutron capture has become a focus for modern BNCT agent preparation.

## 1.10 Thesis Overview

It is the goal of this thesis to describe the development of theranostic silica nanoparticles. We report synthetic methodologies that lead to gadolinium-containing mesoporous silica nanoparticles and boron-containing silica nanoparticles. It describes metal-sequestering with silica nanoparticles via organic group modification so that they can chelate gadolinium giving them potential imaging and therapeutic applications, novel mesoporous and surface-rough ORMOSIL nanoparticles, that can be modified to contain large amounts of boron for BNCT, and surface modification of boron nanoparticles with silica to make them biocompatible as potential agents.

## 1.11 References

[1] Ambrogio, M.W.; Thomas, C.R.; Zhao, Y.-L.;Zink, J.I.; Stoddart, J.F. *Acc. Chem. Res.* **2011**, *44*, 903-913.

[2] Liong, M.; Lu, J.; Kovochich, M.; Xia, T.; Ruehm, S.G.; Nel, A.E.; Tamanoi, F.; Zink, J.I. *ACS Nano* **2008**, *2*, 889-896.

[3] Li, Z.; Zhang, Y.; Shuter, B.; Idris, N.M. *Langmuir* **2009**, *25*, 12015–12018.

[4] Rabin, O.; Perez, J.M.; Grimm, J.; Wojtkiewicz, G.; Weissleder, R. *Nature Materials* **2006**, *5*, 118-122.

[5] Al-Jamal, W. T.; Kostarelos, K. *Accounts Chem. Res.* **2011**, *44*, 1094-1104.

[6] Luk, B. T.; Fang, R. H.; Zhang, L. F. *Theranostics* **2012**, *2*, 1117-1126.

[7] Ostrowski, A. D.; Lin, B. F.; Tirrell, M. V.; Ford, P. C. *Mol. Pharm.* **2012**, *9*, 2950-2955.

[8] Petersen, A. L.; Hansen, A. E.; Gabizon, A.; Andresen, T. L. *Adv. Drug Deliv. Rev.* **2012**, *64*, 1417-1435.

[9] Soenen, S. J.; Vande Velde, G.; Ketkar-Atre, A.; Himmelreich, U.; De Cuyper, M. *Wiley Interdiscip. Rev. Nanomed. Nanobiotechnol.* **2011**, *3*, 197-211.

[10] Lo, S.T.; Kumar, A.; Hsieh, J.T.; Sun, X.K. *Mol. Pharm.* **2013**, *10*, 793-812.

[11] Oliveira, J. M.; Salgado, A. J.; Sousa, N.; Mano, J. F.; Reis, R. L. *Prog. Polym. Sci.* **2010**, *35*, 1163-1194.

[12] Lammers, T.; Subr, V.; Ulbrich, K.; Hennink, W. E.; Storm, G.; Kiessling, F. *Nano Today* **2010**, *5*, 197-212.

[13] Lollo, G.; Rivera-Rodriguez, G.; Torres, D.; Alonso, M. J. *An. R. Acad. Nac. Farm.* **2011**, *77*, 76-98.

[14] Nystrom, A. M.; Wooley, K. L. *Accounts Chem. Res.* **2011**, *44*, 969-978.

[15] Ofek, P.; Miller, K.; Eldar-Boock, A.; Polyak, D.; Segal, E.; Satchi-Fainaro, R. *Isr. J. Chem.* **2010**, *50*, 185-203.

[16] Puri, A.; Blumenthal, R. *Accounts Chem. Res.* **2011**, *44*, 1071-1079.

[17] Arosio, D.; Casagrande, C.; Manzoni, L. *Curr. Med. Chem.* **2012**, *19*, 3128-3151.

[18] Kunjachan, S.; Jayapaul, J.; Mertens, M.E.; Storm, G.; Kiessling, F.; Lammers, T. *Curr. Pharm. Biotechnol.* **2012**, *13*, 609-622.

[19] Lammers, T.; Aime, S.; Hennink, W. E.; Storm, G.; Kiessling, F. *Accounts Chem. Res.* **2011**, *44*, 1029-1038.

[20] Lammers, T.; Kiessling, F.; Hennink, W. E.; Storm, G. *Mol. Pharm.* **2010**, *7*, 1899-1912.

[21] Lammers, T.; Kiessling, F.; Hennink, W. E.; Storm, G. *J. Control. Release* **2012**, *161*, 175-187.

[22] Ambrogio, M. W.; Thomas, C. R.; Zhao, Y. L.; Zink, J. I.; Stoddartt, J. F. *Accounts Chem. Res.* **2011**, *44*, 903-13.

[23] Debbage, P.; Jaschke, W. *Histochem. Cell Biol.* **2008**, *130*, 845-875.

[24] Janib, S. M.; Moses, A. S.; MacKay, J. A. *Adv. Drug Deliv. Rev.* **2010**, *62*, 1052-1063.

[25] Iyer, A. K.; He, J.; Amiji, M. M. *Curr. Med. Chem.* **2012**, *19*, 3230-3240.

[26] Svenson, S. *Mol. Pharm.* **2013**, *10*, 848-856.

[27] Anker, J.N.; Hall, W. P.; Lyandres, O.; Shah, N. C.; Zhao, J.; Van Duyne, R. P. *Nat. Mater.* **2008**, *7*, 442−453.

[28] Ambrogio, M.W.; Thomas, C.T.; Zhao, Y.-L.; Zink, J.; Stoddart, F. *Accounts of Chemical Research,* **2011,** *10,* 903-913.

[29] Walker, S. B.; Lewis, J. A. *J. Am. Chem. Soc.* **2012**, *134*, 1419−1421.

[30] Goesmann, H.; Feldmann, C. *Angew. Chem. Int. Ed.* **2010**, *49*,1362−1395.

[31] Michalet, X.; Pinaud, F. F.; Bentolila, L. A.; Tsay, J. M.; Doose, S.; Li, J. J.; Sundaresan, G.; Wu, A. M.; Gambhir, S. S.; Weiss, S. *Science* **2005**, *307*, 538−544.

[32] Dreaden, E. C.; Alkilany, A. M.; Huang, X.; Murphy, C. J.; El-Sayed, M. A. *Chem. Soc. Rev.* **2012**, *41*, 2740−2779.

[33] Glover, R. D.; Miller, J. M.; Hutchison, J. E. *ACS Nano* **2011**, *5*,8950−8957.

[34] Berthod, A. *Journal of Chromatography,* **1991,** *549,* 1-28.

[35] Schepelina, O.; Poth, N.; Zharov, I. *Adv. Funct. Mater.* **2010,** *20,* 1962-1969.

[36] Smith, A. M.; Nie, S. *Acc. Chem. Res.* **2010**, *43*, 190−200.

[37] Murphy, C. J.; Gole, A. M.; Hunyadi, S. E.; Orendorff, C. J. *Inorg. Chem.* **2006**, *45*, 7544−7554.

[38] Wagner, E.; Brünner, H. *Angew. Chem.* 1960, *72*, 744-750.

[39] Stöber, W.; Fink, A.; Bohn, E. *J. Colloid Interface Sci.* **1968**, *26*, 62−69.

[40] P.C. Bird, U.S. Patent 2,244,325 (**1941**).

[41] Bechtold, M.F.; Snyder, O.E. U.S. Patent, 2,574,902 (**1951**).

[42] Alexander, G.B. U.S. Patent 2,750,345 (**1956**).

[43] Alexander, G.B.; McWhorter, J.R. U.S. Patent 2,833,724 (**1958**).

[44] Rule, J.M. U.S. Patent 2,577,484. (**1951**).

[45] Rule, J.M. U.S. Patent 3.012,972 (**1961**).

[46] Albrecht, W.L. U.S. Patent 3,440,174 (**1979**).

[47] Iler, R.K.; Wolter, F.J. U.S. Patent 2,631,134 (**1953**).

[48] Broge, E.C.; Iler, R.K. U.S. Patent 2,680,721 (**1954**).

[49] Bagwe, R. P.; Khilar, K. C. *Langmuir* **1997**, *13*, 6432-6438.

[50] Zhou, J.; Liu, Z.; Li, F. *Chem. Soc. Rev.* **2012**, *41*, 1323−1349.

[51] Tovmachenko, O.G.; Graf, C.; van den Heuvel, D. J.; van Blaaderen, A.; Gerristen, H.C. *Adv. Mater.* **2006**, *18*, 91-95.

[52] Radhakrishnan, B. ; Ranjan, R. ; Brittain, W.J. *Soft Matter* **2006,** *2,* 386-396.

[53] Iler, R. K.; *The Chemistry of Silica,* John Wiley & Sons, NY (1979).

[54] Wyndham, K.D.; O'Gara, J.E.; Walter, T.H,; Glose, K.H.; Lawrence, N.L.; Alden, B.A.; Izzo, G.S.; Hudalla, C.J.; Iraneta, P.C. *Anal. Chem.,* **2003,** *75,* 6781-6788.

[55] Abelow, A.E.; Zharov, I. *Soft Matter* **2008,** *5,* 457-462.

[56] Schmidt, H.; Wolter, H. *J. Non-Cryst. Solids* **1990,** *121,* 428-435.

[57] Ohulchanskyy, T.Y.; Roy, I.; Goswami, L.N.; Chen, Y.; Bergey, E.J.; Pandey, R.K.; Oseroff, A.R.; Prasad, P.M. *Nano Lett.* **2007,** *7,* 2835-2842.

[58] Kim, Y. B.; Kim, Y. A.; Yoon, K. *Macromol. Rapid Commun.* **2006**, *27*, 1247–1253.

[59] Xu, S.; Hartvickson, S.; Zhao, J. X. *ACS Appl. Mater. Interfaces* **2011**, *3*, 1865-1872.

[60] Beck, J.S.; Vartuli, J.C.; Roth, W.J.; Leonowicz, M.E.; Kresge, C.T.; Schmitt, K.D.; Chu, C.T.W.; Olson, D.H.; Sheppard, E.W.; Higgins, S.B.; Schlenkur, J.L. *J. Am. Chem. Soc.*, **1992,** *114,* 10834-10843.

[61] Grün, M.; Lauer, I.; Unger, K. K. *Adv. Mater.* **1997**, *9*, 254–257.

[62] Ambrogio, M.W.; Thomas, C.T.; Zhao, Y.-L.; Zink, J.; Stoddart, F. *Acc. Chem. Res.* **2011,** *10,* 903-913.

[63] Hicks, J. C.; Drese, J. H.; Fauth, D. J.; Gray, M. L.; Qi, G.; Jones, C. W. *J. Am. Chem. Soc.* **2008**, *130*, 2902-2903.

[64] Du, X.; He, J. *ACS Appl. Mater. Interfaces* **2011**, *3*, 1269-1276.

[65] Tsai, H-J.; Lee, Y-L. *Langmuir* **2007**, *23*, 12687-12692.

[66] Coenen, S.; De Kruif, C. J.; *Journal of Colloidal Interface Science,* **1988,** *124,* 104-110.

[67] Hiramatsu, H.; Osterloh, F. E. *Langmuir,* **2003,** *19,* 7003-7011.

[68] Kim, J.M.; Chang, S.M.; Kong, S.M.; Kim, -K.; Kim, I.-H.; Kim, K.-S.; Kim, W.S. *Mol. Cryst. Liq. Cryst.* **2008,** *492,* 245-256.

[69] Iler, R.K.; communication for Small Particles Technology.

[70] Mattsson, and Otterstadt, J.-E. A., unpublished work, from Small Particles Technology.

[71] Otterstedt, J.-E.; Brandreth, D.A. *Small Particle Technology*, Plenum Press, NY, (1998).

[72] Wang, X-D.; Shen, Z-X.; Sang, T.; Cheng, X-B.; Li, M-F.; Chen, L-Y.; Wang, Z-S. *J. Colloid Interface Sci.* **2010**, *341*, 23-29.

[73] Park, J. S.; Hah, H. J.; Koo, S. M.; Lee, Y. S. *Journal of Ceramic Processing Research* **2006**, *7*, 83-89.

[74] Madra, G.; McCoy, B.J. *J. Chem. Phys.* **2003**, *119*, 1683-1693.

[75] Knopp, D.; Tang, D.; Niesser, R. *Anal. Chim. Acta* **2009**, *647*, 14-30.

[76] Xue, L.; Fu, J.; Han, Y. *Colloids Surf, A* **2009**, *338*, 15-19.

[77] Jin, Y.; Li, A.; Hazelton, S. G.; Liang, S.; John, C. L.; Selid, P. D.; Pierce, D. T.; Zhao, J. X. *Coor. Chem. Rev.* **2009**, *253*, 2998-3014.

[78] Brauer, F.; Gläsel, H-J.; Decker, U.; Ernst, H.; Freyer, A.; Hartmann, E.; Sauerland, V.; Mehnert, R. *Progress in Organic Coatings* **2003**, *47*, 147-153.

[79] Bladeren, A.V.; Vrij, A. *Langmuir* **1992**, *8*, 2921-2931.

[80] Bottrill, N.; Green, M. *Chem. Comm.***2011,** *47,* 7039-7050.

[81] Smith, J.E.; Medley, C.D.; Tang, Z.; Shangguan, D.; Lofton, C.; Tan, W. *Anal. Chem.* **2007,** *79,* 3075-3082.

[82] Zhao, X.; Tapec-Dytioco, R.; Tan, W.; *J. Am. Chem. Soc.* **2003,** *125,* 11474-11475.

[83] Selvan, S.T.; Patra, P.K.; Ang, C.Y.; Ying, J.Y. *Angew. Chem. Int. Ed.* **2007,** *46,* 2448-2452.

[84] Zidki, T.; Zhang, L.; Shafirovich, V.; Lymar, S. V. *J. Am. Chem. Soc.* **2012**, *134*, 14275-14278.

[85] Feldmann, V.; Engelmann, J.; Gottschalk, S.; Mayer, H. A. *J. Colloid Interface Sci.* **2012**, *366*, 70-79.

[86] Ottenbrite, R.M.; Wall, J.S.; Siddiqui, J.A. *J. Am. Ceram. Soc.* **2000,** *83,* 3214-3215.

[87] Arkhireeva, A.; Hay, J. N. *J. Mater. Chem.* **2003,** *13,* 3122-3127.

[88] Buining, P.A.; Liz-Marzan, L.M.; Philipse, A.P. *J. Colloid Interface Sci.* **1996,** *227,* 318-321.

[89] Arkireeva, A.; Hay, J.N.; Oware, W. *Journal of non-Crystalline Solids,* **2005,** *351,* 1688-1695.

[90] Baumann, F.; Schmidt, M.; Deubzer, B.; Geck, M.; Dauth, J. *Macromolecules,* **1994,** *27,* 6102-6105.

[91] Kim, Y. B.; Kim, Y. A.; Yoon, K. *Macromol. Rapid Commun.* **2006**, *27*, 1247–1253.

[92] Wang, C.; Yan, J. Cui, X.; Wang, H. *J. Colloid Interface Sci.* **2011**, *354*, 94-99.

[93] Li, X.; He, J. *ACS Appl. Mater. Interfaces* **2012** dx.doi.org/10.1021/am3002082.

[94] Ahmed, A.; Forster, M.; Clowes, R.; Bradshaw, D.; Myers, P.; Zhang, H. *J. Mater. Chem. A* **2013**, *1*, 3276-3286.

[95] Beck, J.S.; Vartuli, J.C.; Roth, W.J.; Leonowicz, M.E.; Kresge, C.T.; Schmitt, K.D.; Chu, C.T.W.; Olson, D.H.; Sheppard, E.W.; Higgins, S.B.; Schlenkur, J.L. *J. Am. Chem. Soc.,* **1992,** *114,* 10834-10843.

[96] Vivero-Escoto, J. L.; Slowing, I. I.; Trewyn, B. G.; Lin, V. S-Y. *Small* **2010**, *6*, 1952-1967.

[97] Tang, F.; Li, L.; Chen. D. *Adv. Mater.* **2012** dx.doi.org/10.1002/adma.201104763.

[98] Lai, C.-Y.; Trewyn, B.G.; Jeftinija, D,M.; Jeftinija, K.; Xu, S.; Jeftinija, S.; Lin, V.S.-Y. *J. Am. Chem. Soc.* **2003,** *125,* 4451-4459.

[99] Macquarrie, D. J.; Jackson, D. B.; Mdoe, J. E. J.; Clark, J. H. *New J. Chem.* **1999**, *23*, 539-544.

[100] Walcarius, A.; Delacôte, C. *Chem. Mater.* **2003**, *15*, 4181-4192.

[101] Cho, Y.; Shi, R.; Borgens, R. B.; Ivanisevic, A. *Nanomedicine* **2008**, *3*, 507-519.

[102] Charnay, C.; Bégu, S.; Tourné-Péteilh, C.; Nicole, L.; Lerner, D. A.; Devoisselle, J.M. *European Journal of Pharmaceutics and Biopharmaceutics* **2004**, *57*, 533-540.

[103] Lai, C.Y.; Trewyn, B.G.; Jeftinija, D.M.; Jeftinija, K.; Xu, S.; Jeftinija, S.; Lin, V.S. *J. Am Chem. Soc.* **2003,** *125,* 4451-4459.

[104] Chang, B.; Chen, D.; Wang, Y.; Chen, Y.; Jiao, Y.; Sha, X.; Yang, W. *Chem. Mater.* **2013** dx.dio.org/10.1021/cm3037197.

[105] SEER Cancer Statistics Review. 2010. 1 Jan 2007 Surveillance Research Program, NCI. <http://www.seer.cancer.gov>.

[106] How much money is spent on cancer research. 2010. 2 Feb 2010 <nanomedicinecenter.com>.

[107] Coderre, J.A.; Morris, G.M. *Radiat. Res.* **1999**, *151*, 1-18.

[108] Soloway, A.H.; Tjarks, W.; Barnum, B.A.; Rong, F.-G.; Barth, R.F.; Codogni, I.M.; Wilson, J.G. *Chem. Rev.* **1998**, *98*, 1515-1562.

[109] Barth, R.F.; Coderre A.; Vicente, M.; Blue, T. E. *Clin. Cancer Res.* **2005,** *11*, 3987-4002.

[110] The National Institute of General Medical Sciences. Inside the Cell. 2005.

[111] Hawthorne, M. F. *Angew. Chem. Int. Ed.* **1993**, *32*, 950-984.

[112] Valliant, J. F.; Guenther, K. J.; King, A. S.; Morel, R.; Schaffer, P.; Sogbein, O. O.; Stephenson, K. *A. Coord. Chem. Rev.* **2002**, *232*, 173- 230.

[113] Javid, M.; Brownell, G.L.; Sweet, W.H. *J. Clin. Invest.* **1952,** *31,* 604.

[114] Tolpin, E.I.; Wellum, G.R.; Dophan, F.C., Jr.; Kornblith, P.L.; Zamenhof, R.G. *Oncology* **1975,** *32,* 223.

[115] Hatanaka, H.A. *J. Neurol.* **1975**, *209*, 81–94.

[116] Mishima, Y.; Ichihashi, M.; Tsui, M.; et al. *Lancet* **1989**, *2*, 388–389.

[117] Coderre, J.A.; Hopewell, J.W.; Turcotte, J.C.; Riley, K.J.; Binns, P.J.; Kiger III, W.S.; Harling, O.K. *Appl. Radiat. Isot.* **2004**, *61*, 1083-1087.

[118] Isaac, M. F.; Khal, S. B. *J. Organomet. Chem.* **2003**, *680,* 232-243.

[119] Ceberg C.P.; Brun A.; Kahl S.B.; Koo M.S.; Persson B.R.; Salford L.G. *J. Neurosurg.* **1995**, *83,* 86-92.

[120] Kabalka, G.W.; Yao, M.L. *Synthesis* **2003,** *18,* 2890-2893.

[121] Diaz, A.; Stelzer, K.; Laramore, G.; Wiersema, R. *Research and Development in Neutron Capture Therapy*; Monduzzi Editore: Bologna, **2002**, pp. 993-999.

[122] Kueffer, P.J.; Maitz, C.A.; Khan, A.A.; Schuster, S.A.; Shlyakhtina, N.I.; Jalisatgi, S.S.; Brockman, J.D.; Nigg, D.W.; Hawthorne, F. *Proc. Natl. Acad. Sci.* **2013**, *110*, 6512-6517.

[123] Yang, W.; Wu, G.; Barth, R.F.; et al. *Cancer Res.* **2008**, *14,* 883-891.

[124] Tietze, L.F.; Griesbach, U.; Bothe, U.; Nakamura, H.; Yamamoto, Y. *Chembiochem* **2002**, *3*, 219-225.

[125] Woodhouse S.L.; Rendina L.M., *Chem. Commun.* **2001,** 2464-2465.

[126] Nakamura, H.; Miyajima, Y.; Takei, T.; Kasaoka, S.; Maruyama, K. *Chem. Commun.* **2004**, 1910-1911.

# CHAPTER 2

# MESOPOROUS METAL-CHELATING SILICA NANOPARTICLES

## 2.1 Introduction

Nanoparticles that can bind metals have potential applications in medical treatment for diseases that involve the buildup of metals in the body, such as Alzheimer's and Parkinson's disease,[1] in metal sequestering for water treatment,[2] fluorescent enhancement,[3,4] and as carriers for MRI contrasting agents.[4-6] Most of these metal-binding nanoparticles utilize thiols or polyamino carboxylic acids to chelate metals. [2,4,5,8] Silica nanoparticles, because of their uniform sizes, inert nature, and low toxicity may act as useful supports for metal chelator functionalities.

Recently, many metal-chelating nanoparticles have been synthesized using thiol, or amino-containing silanes.[3,8,9] In the case of amino-containing silanes, a second step is required to convert them to polyamino carboxylic acid functionalities. The number of organic functionalities on the silica nanoparticle is dependent on the available silanols on its surface. Potentially larger amounts of metals can be chelated if the number of the silica nanoparticle's available organic groups are increased. This can be accomplished by increasing the surface area of the silica nanoparticle.

Silica particle surface area can be increased by creating channels (2-50 nm in diameter) in the silica nanoparticle.[10] This results in mesoporous silica nanoparticles (MSNs) that have a larger surface area while maintaining the same particle volume,

compared to nonporous silica particles of identical size. MSNs can thus provide more available silanols for organosilane modification.

There are two main methodologies in attaching an organosilane to the surface of MSNs. The "grafting to" approach provides a well-defined structure (e.g. MCM-41), but can give a nonuniform distribution of the organosilane and potentially block the pores.[11] The other method involves the co-condensation of both the organosilane and the tetraalkoxy silane, e.g. TEOS (Scheme 2.1). This "one-pot" synthesis provides a uniform distribution of the organosilane with no pore blocking. However, the higher the concentration of the organosilane used the more the mesoporous structure degrades.[12]

Recently, it has been demonstrated that nanoparticles with large gadolinium loading have greater $r_1$ and $r_2$ relaxivities compared to single-molecule gadolinium carriers for MRI applications.[4,6,13,14] The synthesis of these gadolinium-containing nanoparticles involves the treatment of 3-trimethoxysilylpropyl diethylenetriamine

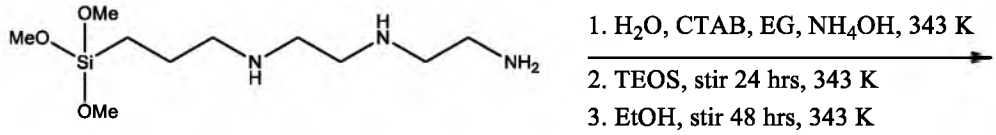


N1-(3-Trimethoxysilylpropyl)diethylenetriamine (DETA)

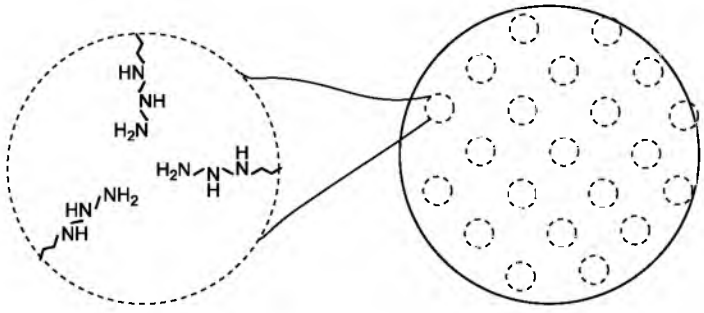


Scheme 2.1: Co-condensation of SiDETA with TEOS in CTAB solution resulting in mesoporous nanoparticles.

(SiDETA) with bromoacetic acid under basic conditions (Scheme 2.2) to create a polyaminocarboxylic acid containing silane, diethylenetriametetraacetic acid (SiDTTA). Typically, gadolinium ions are then chelated by the resultant SiDTTA prior to modifying the surface of the solid silica or mesoporous silica nanoparticles. These methods may hinder access to gadolinium by creating multilayers (post-modification of solid silica), blocking the pores (post-modification of MSNs), or incorporating SiDTTA-Gd within the MSN matrix and not on the surface (co-condensation of SiDTTA-Gd with TEOS). The potential inaccessibility of gadolinium, specifically to water, can greatly reduce the effectiveness of these particles as MRI contrast agents.

Additionally, gadolinium has a potential use in neutron capture therapy of cancer, as mentioned in Chapter 1. $^{157}Gd$ has been suggested as a neutron capture therapeutic because of its large neutron capture cross-section, which reduces the amount of gadolinium needed to be an effective NCT agent.[15] A nanoparticle that contains gadolinium, therefore, can potentially image and treat tumor cells simultaneously. The only theranostic aspect that these "as is" particles lack is cell targeting which can easily

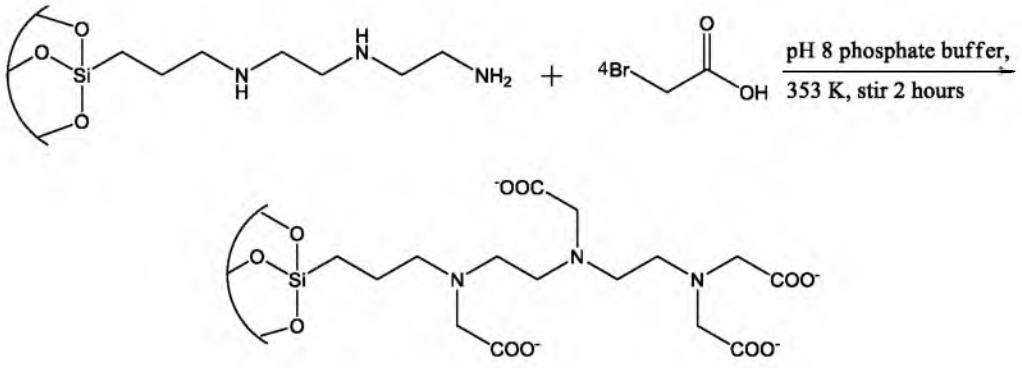


3-aminopropyl(trimethoxysilyl)diethylenetriamine tetraacetic acid (SiDTTA)

Scheme 2.2: Conversion of DETA to DTTA using bromoacetic acid under basic conditions.

be added by modifying the silica surface with an organosilane (e.g. 3-aminopropyl-triethoxysilane) that can be attached to a targeting ligand.

This chapter presents a synthetic method to create mesoporous silica nanoparticles that contain the polyamino carboxylic acid DTTA. This is achieved by co-condensation of TEOS and DETA followed by treating the particles with bromoacetic acid at pH 8. This opens up the possibility of using these nanoparticles to chelate a variety of metals, thus creating potential applications in metal sequestering and neutron cancer therapy. Additionally, because gadolinium is chelated post-synthesis, the gadolinium ions are chelated by accessible DTTA molecules only. This should result in every chelated gadolinium ion being accessible to water, which is particularly important in MRI applications.

## 2.2 Experimental Section

### 2.2.1 Materials

Tetraethoxy siliane (TEOS, Alfa Aesar), 3-trimethoxysilylpropyl dietheylenetriamine (SiDETA, Sigma-Alrich), Bromoacetic acid (BrAA, Sigma Aldrich), Ammonium hydroxide ($NH_4OH$), Hexadecyltrimethylammonium bromide (CTAB, Sigma Aldrich), Ethylene glycol (EG), 200 proof ethanol, MilliQ water, Dibasic sodium phosphate ($Na_2HPO_4$), Monobasic sodium phosphate ($NaH_2PO_4$, Mallinckrodt), Disodium ethylenetriaminetetraacetic acid dihydrate ($Na_2EDTA \cdot 2H_2O$, Mallinckrodt), Calcium chloride anhydrous ($CaCl_2$, Mallinckrodt ), Cupric chloride dihydrate ($CuCl_2 \cdot 2H_2O$, J.T. Baker), Cobalt chloride ($CoCl_2$, Sigma-Aldrich 97%), Gadolinium chloride hexahydrate ($GdCl_3 \cdot 6H_2O$, Sigma-Aldrich), Murexide (Sigma-Aldrich), and Eriochrome Black T (Mallinckrodt).

### 2.2.2 Instruments

Transmission electron microscopy (TEM, FEI Techna $G^2$ T-12), Thermogravimetric analysis (TGA, TA Instruments 2950 Thermogravimetric Analyzer), Infrared spectroscopy (IR, Bruker Tensor 37), Dynamic light scattering (DLS, NICOMP 380 ZLS), and Nitrogen adsorption-desorption (BET analysis, Micrometrics ASAP 2020).

### 2.2.3 Co-condensation of SiDETA and TEOS

90 mL MilliQ water, 0.5868 g CTAB, 15 mL EG, and 3.6 mL 25% $NH_4OH$ are added to a 250 mL round bottom flask and stirred at 70 °C. After 25 minutes, 207 µL of SiDETA and 715 µL TEOS are added to the solution (32% w/w) followed by the addition of 43 mL ethanol after 24 hours. The solution is stirred for an additional 48 hours to ensure complete mesoporous nanoparticle formation and maximum incorporation of SiDETA. The particles are collected by centrifugation and washed 3 times with ethanol. The CTAB is removed from the pores by transferring the mesoporous DETA nanoparticles to a 100 mL round bottom flask containing 30 mL of a 1 M HCl ethanol solution, heated to 80 °C, and allowing it to sit for 14 hours. The particles are then collected and washed 3 times with ethanol to remove the free CTAB and HCl (Scheme 3.1).

### 2.2.4 Conversion of DETA mesoporous silica nanoparticles to DTTA mesoporous silica nanoparticles

A 6:1 mole ratio of BrAA and DETA are added to a 25 mL round bottom flask. 10 mL of a 0.1 M phosphate buffer (pH 8) are added to the flask followed by the

dropwise addition of 1M NaOH until the solution reaches a pH of 8. The solution is then stirred and heated to 80 °C for 2 hours. The DTTA containing mesoporous silica nanoparticles are then collected via centrifugation and washed 3 times with water to remove any excess BrAA. The particles are then dried under air (Scheme 3.2).

### 2.2.5 Calcium solution

A 0.04 M calcium standard is made by adding 1.1098 g $CaCl_2$ (0.01 mol) to a 150 mL beaker. 25 mL MilliQ water is added to the beaker. Then concentrated HCl is added to the beaker until the $CaCl_2$ solid is dissolved. Two additional drops concentrated HCl are added to the solution. The solution is then transferred to a 250 mL volumetric flask that is filled with MilliQ water.

### 2.2.6 Phosphate buffer solution

A 0.1 M phosphate buffer is made by adding 12.6931 g $Na_2HPO_4$ and 0.3657 g $NaH_2PO_4$ to a 250 mL volumetric flask and filled with MilliQ water. The pH of the solution is the adjusted to 8 if needed. This solution is used to maintain the solution pH for DETA to DTTA conversion and for copper(II) and cobalt(II) titrations.

### 2.2.7 EDTA standard solution

3.8 g of $Na_2EDTA{\cdot}2H_2O$ (10.21 mmol) and 0.1 g of $MgCl_2$ are added to a 1 L volumetric flask. The flask is filled with MilliQ water (if the solution stays murky, 1 M NaOH is added dropwise before water is filled to mark). The solution is then filtered using Buchner funnel and vacuum. The stock solution is standardized by titrating the $Ca^{2+}$ solution with Eriochrome Black T. The stock solution should be about 0.01 M. A 100 mL aliquot of the EDTA stock solution is then placed in a clean 1 L volumetric flask

and diluted with MilliQ water adjusting the pH to 8, and standardized by titrating $Ca^{2+}$. This solution is used for testing the metal chelation of the nanoparticles.

### 2.2.8 Copper solution

A 0.04 M copper(II) solution is made by adding 1.7048 g $CuCl_2 \cdot 2H_2O$ (0.01 mol) to a 250 mL volumetric flask. The flask is filled with water but not to the marker. Ammonia is added dropwise to the solution as an auxiliary complexing agent until the royal blue color persists. The solution is then adjusted to pH 8 and water added to the marker. Aliquots of the solution are then added to flasks containing 7 mL pH 8 phosphate buffer. 2 drops of Murexide indicator (1 mg Murexide per mL $H_2O$) are added to each flask and the contents standardized with EDTA solution.

### 2.2.9 Cobalt solution

A 0.04 M cobalt(II) solution is made by adding 1.2984 g $CoCl_2$ (0.01 mol) to a 250 mL volumetric flask. The flask is filled with water but not to the marker. Ammonia is added dropwise to the solution as an auxiliary complexing agent until a darkish pink is observed. The solution is then adjusted to pH 8 and water added to the marker. Aliquots of the solution are then added to flasks containing 7 mL pH 8 phosphate buffer. 2 drops of Murexide indicator (1 mg Murexide per mL $H_2O$) are added to each flask and the contents standardized with EDTA solution.

### 2.2.10 Gadolinium solution

A 0.04 M gadolinium(III) solution is made by adding 3.717 g $GdCl_3 \cdot 6H_2O$ (0.01 mol) to a 250 mL volumetric flask. The flask is filled with water and the solution is

adjusted to pH 7. This solution is used for TGA measurements and not for titration so it is not standardized.

### 2.2.11 Copper and cobalt chelation

A known mass of the DTTA-containing nanoparticles (5-20 mg) is added to a flask. Then an excess of copper or cobalt solution (0.25-0.75 mL) is added followed by the addition of 7 mL phosphate buffer. The solution is sonicated for 30 minutes and allowed to sit for 1.5 hours. 2 drops of Murexide solution are added to the solution immediately followed by EDTA titration. The difference between the initial moles of the metal ion and moles of EDTA used results in the moles being chelated by the DTTA.

### 2.2.12 Gadolinium chelation

100 mg of DTTA-containing nanoparticles are added to 6 mL of gadolinium solution and sonicated for 2 hours. The particles are then collected via centrifugation and washed 3 times with EDTA solution to remove free or loosely bound metal. The particles are then washed 3 times with water to remove EDTA and dried.

### 2.2.13 Fluorescent tag addition

Dansyl chloride is used as the fluorescent tag, because it reacts quickly with primary amines. 4 mg of dansyl chloride in 5 mL dry acetonitrile is added to the DTTA-containing nanoparticles and gadolinium chelating nanoparticles. The particles are washed with acetonitrile until the supernatant no longer fluoresces. A UV lamp is used to observe fluorescence.

## 2.3 Results and Discussion

A co-condensation method was implemented in the synthesis of DETA-containing mesoporous silica nanoparticles. This approach was expected to prevent any pore blockage and also produce a more homogeneous distribution of organic functionalities.[12] Figure 2.1 shows the particles obtained using a 32% w/w of SiDETA to TEOS in the presence of the surfactant CTAB. These mesoporous DETA-containing silica nanoparticles (DETA-MSNPs) are uniform in size (111±4 nm) and have mesopores easily observed by TEM (Figure 2.1). Using nitrogen isotherm analysis (Figure 2.2a), a type IV isotherm with a hysteresis loop was observed for DETA-MSNPs, which is representative for mesoporous structures (Figure 2.3a).[16] The measured pore size of these mesoporous particles, based on the isotherm data, is 2.6 nm (Figure 2.3b). The particles

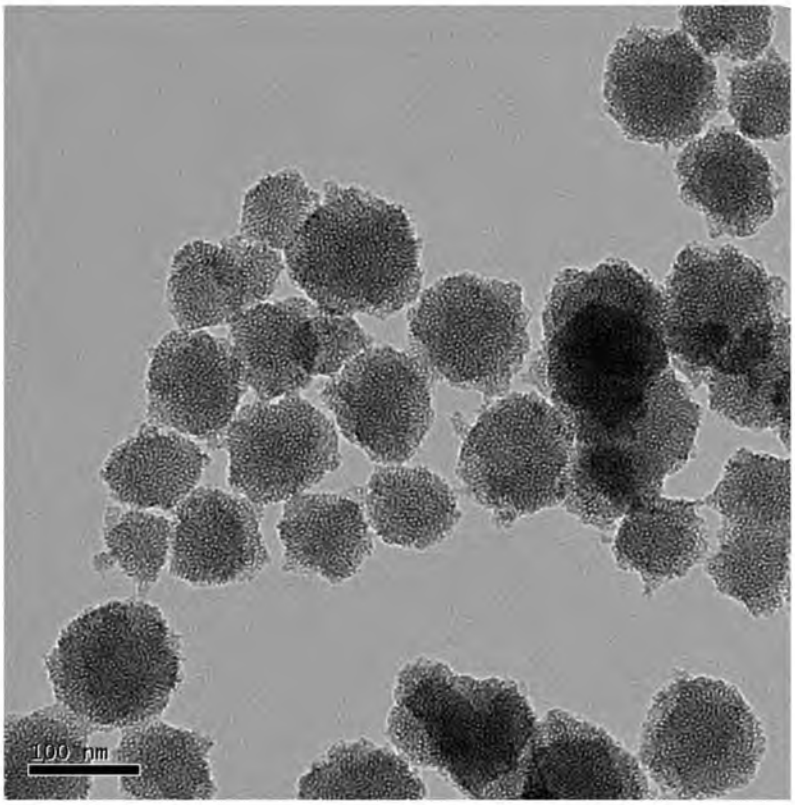


Figure 2.1: TEM image of DETA-MSNPs.

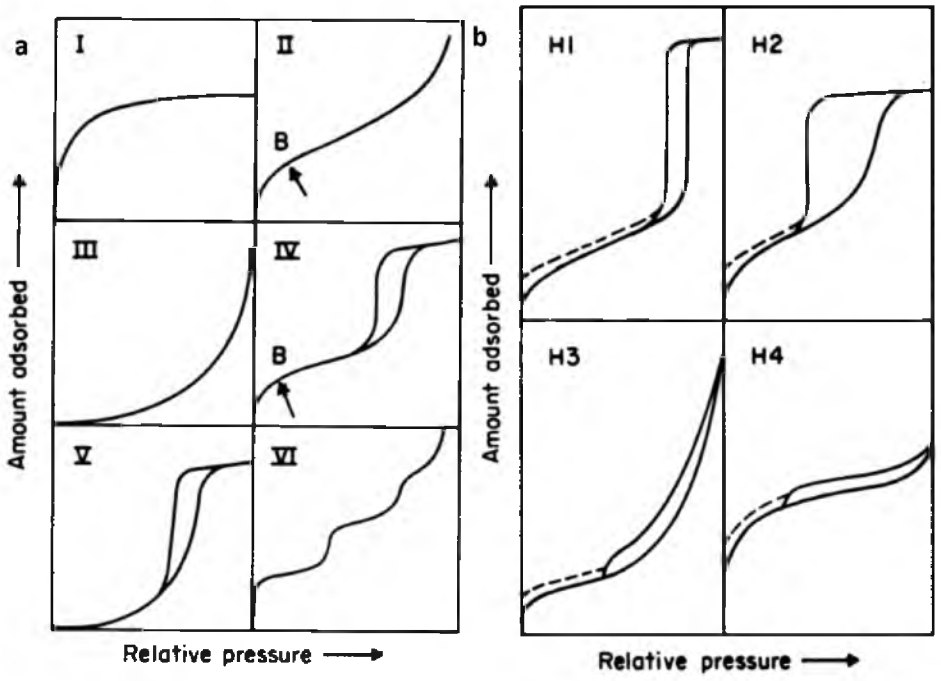


Figure 2.2: Representations of adsorption-desorption isotherms and hysteresis loops. a) Types of isotherms (type IV and type V are considered isotherms for mesoporous materials) b) Types of hysteresis loops.[16]

have a calculated surface area of 664 $m^2/g$, which is much larger than the solid spherical silica nanoparticles' (~200 nm) surface area (17 $m^2/g$). After the conversion of DETA to DTTA to make DTTA-containing mesoporous silica particles (DTTA-MSNPs), the same type IV isotherm was observed with pore sizes of 2.2 nm (Figures 2.4a-b). However, the surface area decreased to 572 $m^2/g$. We speculate that this decrease is caused by some pore blockage. The average diameter of DTTA-MSNPs remained virtually unchanged at 108 ± 4 nm (Figure 2.5), compared to DETA-MSNPs.

The conversion of DETA to DTTA was confirmed using IR spectroscopy (Figure 2.6). The spectrum of DETA-MSNPs shows a broad peak at 3400 $cm^{-1}$ representing N-H

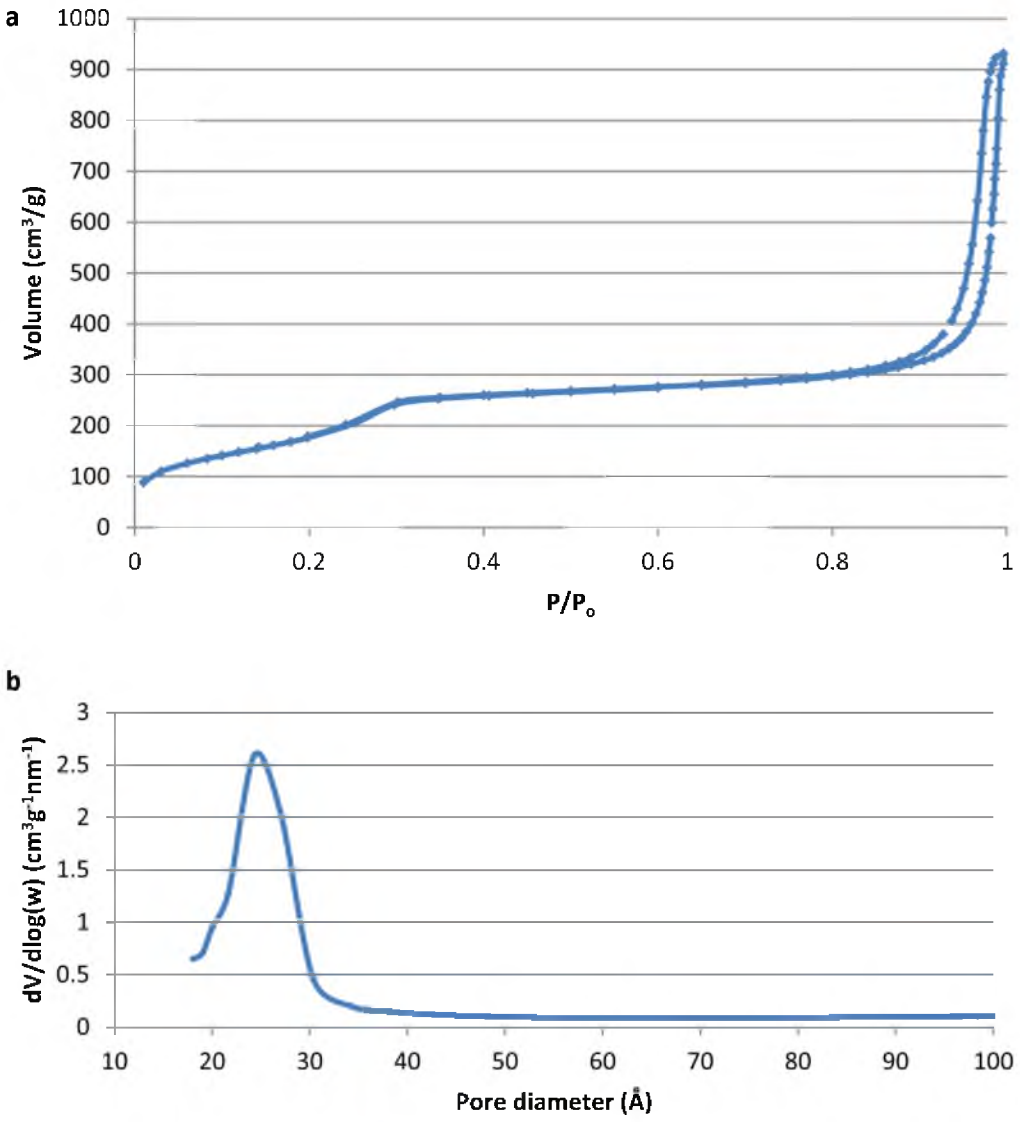


Figure 2.3: Nitrogen adsorption-desorption analysis of DETA-MSNPs. a) Nitrogen adsorption-desorption isotherm of DETA-MSNPs. b) Pore size distribution for DETA-MSNPs with a peak at 2.6 nm.

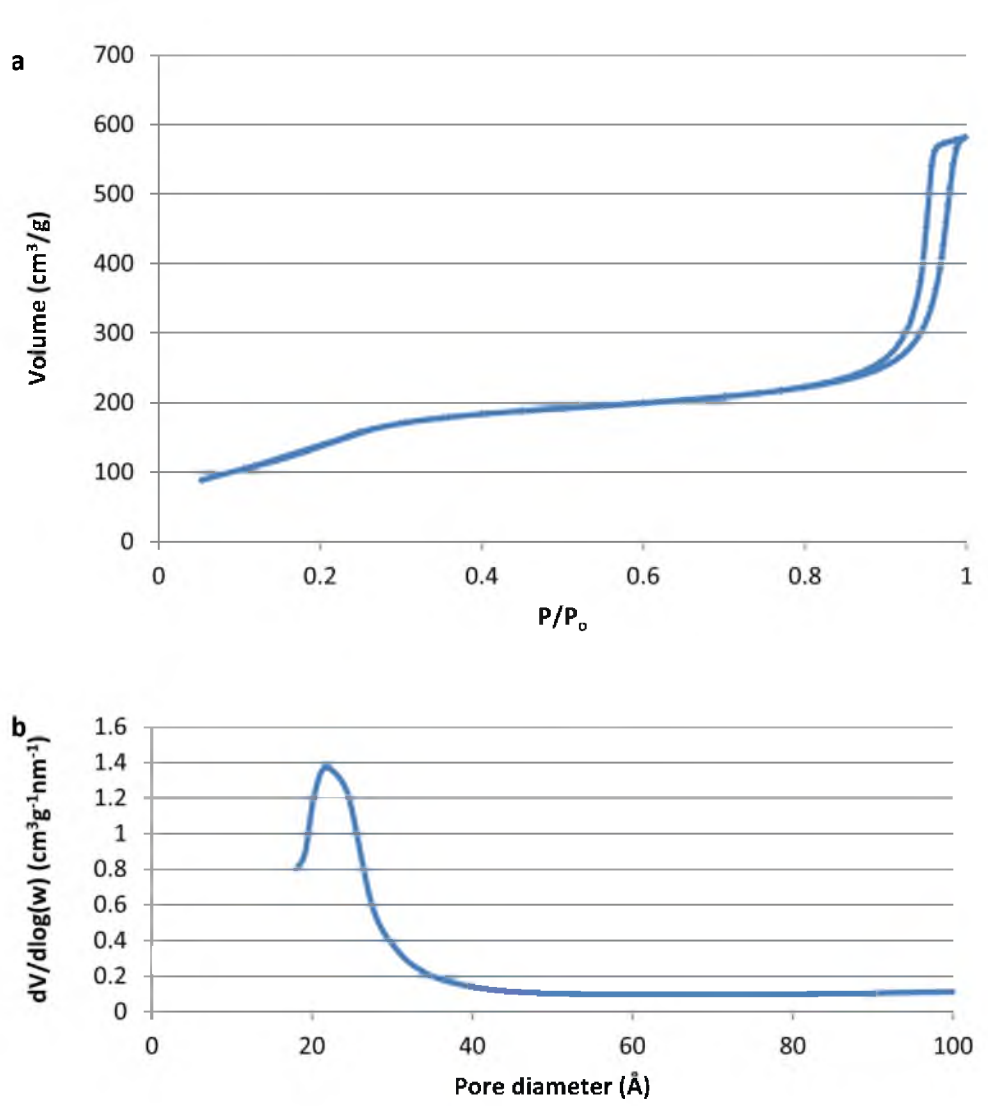


Figure 2.4: Nitrogen adsorption-desorption analysis of DETA-MSNPs. a) Nitrogen adsorption-desorption isotherm of DTTA-MSNPs. b) Pore size distribution for DTTA-MSNPs with a peak at 2.2 nm.

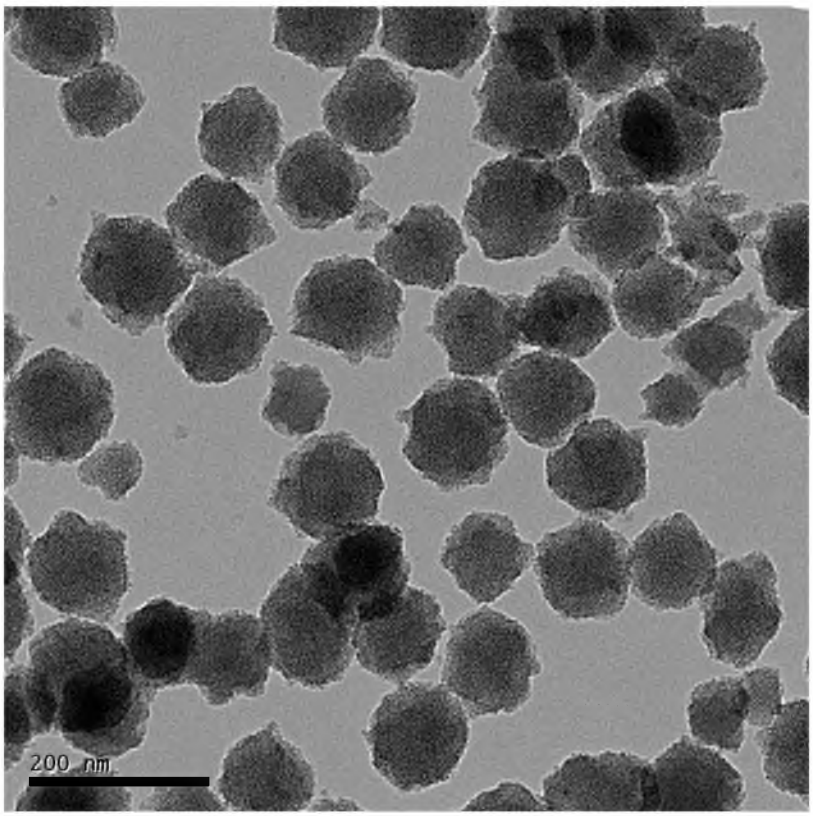


Figure 2.5: TEM image of DTTA-MSNPs.

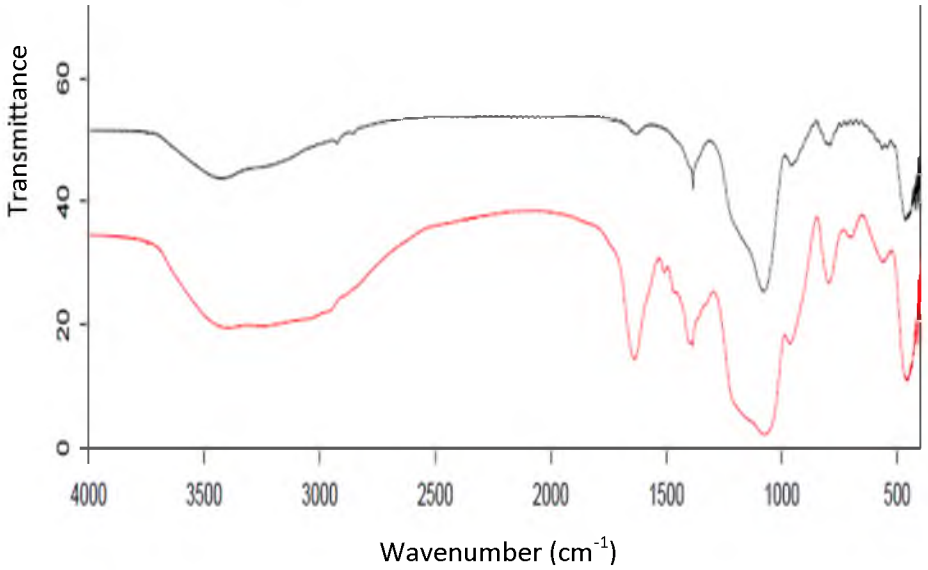


Figure 2.6: IR spectra of DETA-MSNPs (black) and DTTA-MSNPs (red).

and silanol O-H stretches. After DETA is converted into DTTA, two intense peaks are observed at about 1650 $cm^{-1}$, representing the C=O stretch, and at 1380 $cm^{-1}$, which is probably a combination of O-H bends and C-O stretching. There is also a distinct broadening of the 3400 $cm^{-1}$ peak for the DTTA-MSNPs caused by the presence of O-H stretching from the carboxylic acid.

Another indication that the DETA-MSNPs have being converted to DTTA-MSNPs is that their zeta potentials are different. The zeta potential for DETA-MSNPs is +53.1 mV but after DETA conversion to DTTA, a negative potential of -29.3 mV is observed.

Using TGA, a weight loss of the DETA-MSNPs organic groups was observed between 300 and 800 °C, with the loss of 11.12 % (Figure 2.7). It should be noted that TGA plots for DETA-MSNPs contain a weight loss that is greater than DTTA-MSNPs, which is the opposite of what is expected since the DTTA-MSNPs have a greater organic molecular weight. This can be attributed to the combustion of CTAB that is remaining with the DETA-MSNP sample. This theory is supported by the stepwise weight loss at 300-375 °C disappearing during DTTA-MSNP analysis which is believed to happen because of the additional washing steps removing the remnant CTAB. Although the

CTAB may prevent some DETA from being converted to DTTA, it may also preserve some advantageous primary amines, as will be discussed below.

After converting DETA to DTTA, a weight loss of 17.66 % was observed (Figure 2.7). From these data, the conversion of DETA to DTTA inside the mesoporous silica particles is approximately 22.8% (Eq. 2.1-2.3). The low conversion of the total DETA functionalities is most likely caused by the DETA functionalities being incorporated

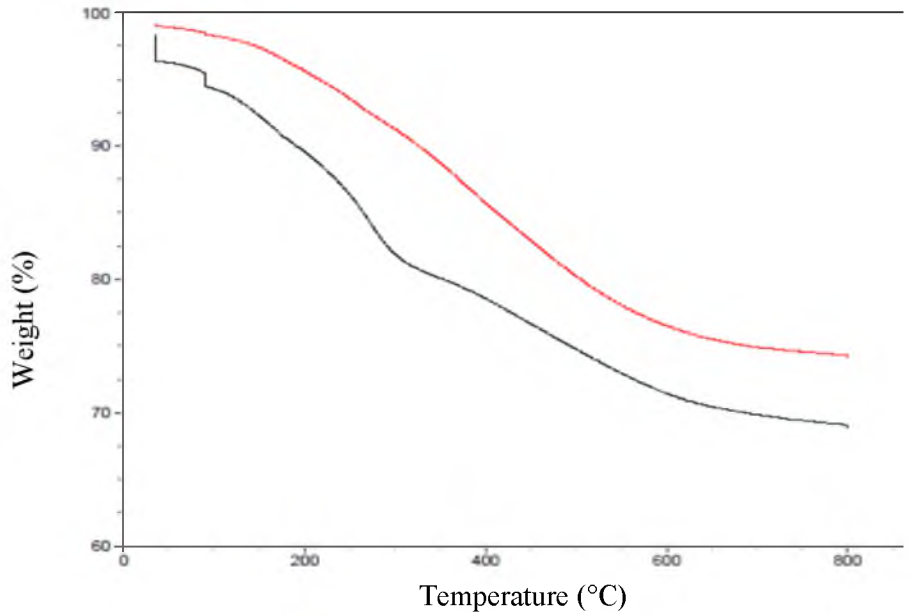


Figure 2.7: TGA weight losses of DETA-MSNPs (black) and DTTA-MSNPs (red).

$$\frac{\rho \cdot \frac{4}{3} \cdot \pi \cdot r_{(cm)}{}^{3} \cdot \%W_{loss_{DETA-MSNP}}}{100 \cdot MW_{DETA}} = \frac{\text{mol DETA}}{\text{particle}}$$

Eq. 2.1: Determining the moles DETA per particle based on TGA weight loss: ρ is the particle density in $g \cdot cm^{-3}$ (~1.46), r is the particle radius, $MW_{DETA}$ is the molecular weight of DETA, and $\%W_{loss}$ is the measured weight loss of the DETA-MSNPs according to TGA.

$$\frac{\rho \cdot \frac{4}{3} \cdot \pi \cdot r_{(cm)}{}^{3} \cdot (\%W_{loss_{DTTA-MSNP}} - \%W_{loss_{DETA-MSNP}})}{100 \cdot MW_{DTTA}} = \frac{\text{mol DTTA}}{\text{particle}}$$

Eq. 2.2: Determining the moles DTTA per particle based on TGA data: ρ is the particle density in $g \cdot cm^{-3}$(~1.46), r is the particle radius, $MW_{DTTA}$ is the molecular weight of DTTA, and $\%W_{loss}$ is the measured weight loss of the mesoporous nanoparticle according to TGA.

$$\frac{\text{mol DTTA}}{\text{particle}} \div \frac{\text{mol DETA}}{\text{particle}} \times 100 = \text{mol \% DETA conversion}$$

Eq. 2.3: Determining the percentage of moles DETA converted to moles DTTA.

inside the silica nanoparticles, in addition to being incorporated onto the surface, during co-condensation.[6] This is supported by calculating the number of DETA functionalities of the mesoporous nanoparticle surface using the measured surface area (664 $m^2/g$). By assuming a DETA surface coverage of 1 molecule DETA per $nm^2$, the total percentage of DETA on the surface is determined to be ~16% of the total DETA functionalities throughout the silica nanoparticle body. This indicates that all surface DETA functionalities are being converted into DTTA functionalities and that the CTAB remaining with the DETA-MSNPs is not preventing conversion inside the pores.

Next, we studied the metal chelation ($Cu^{2+}$, $Co^{2+}$, and $Gd^{3+}$) by DTTA-MSNPs. We used EDTA titration with a Murexide indicator for $Cu^{2+}$ and $Co^{2+}$ solutions before and after the chelation with the nanoparticles to determine the extent of the metal uptake. Because DTTA binds metal cations more strongly than EDTA, while DETA groups do not, it may be possible to determine the extent of DETA to DTTA conversion using EDTA titration. This was observed when titrating DETA-MSNPs and DTTA-MSNPs treated with the copper(II) solution. The number of moles EDTA used for the titration of copper(II) in the presence of DETA-MSNPs was equal to the starting moles of copper(II) (this is also observed by the loss of blue color from the particles). However, during the titration copper(II) in the presence of DTTA-MSNPs, fewer moles of EDTA were used to complete titration, indicating that the number of DTTA groups may be equivalent to the untitrated moles of copper(II). Furthermore, an additional correction is made for the initial weight of DTTA-MSNPs titrated by calculating the theoretical weight percentage of DTTA functionalities in a particle (Eq. 2.4-2.6; 63.6%) and multiplying that value to

the weight of the particles titrated to get a theoretical maximum value of moles DTTA present in a given sample.

$$\frac{\%W_{SiDETA} \div MW_{SiDETA} \cdot MW_{SiO_{1.5}DETA}}{\%W_{SiDETA} \div MW_{SiDETA} \cdot MW_{SiO_{1.5}DETA} + \%W_{TEOS} \div MW_{TEOS} \cdot MW_{SiO_2}} = \%W_{SiO_{1.5}DETA}$$

Eq. 2.4: Determining the percent weight composition of $SiO_{1.5}DETA$ in a particle sample: $\%W_{SiDETA}$ is the percent of the organosilane used (32%).

$$\frac{\%W_{SiO_{1.5}DETA}}{MW_{SiO_{1.5}DETA}\left(\%W_{SiO_{1.5}DETA} / MW_{SiO_{1.5}DETA} + \%W_{SiO_2} / MW_{SiO_2}\right)} = \%mol_{SiO_{1.5}DETA}$$

Eq. 2.5: Theoretical mol percentage of DETA in a particle sample.

$$\frac{\%mol_{SiO_{1.5}DETA} \cdot MW_{DTTA}}{\%mol_{SiO_{1.5}DETA} \cdot MW_{SiO_{1.5}DTTA} + (100 - \%mol_{SiO_{1.5}DETA}) \cdot MW_{SiO_2}} = \%W_{DTTA}$$

Eq. 2.6: Theoretical weight composition of DTTA of the particles if all DETA groups are converted to DTTA.

The EDTA titration data for $Cu^{2+}$ and $Co^{2+}$ are shown in Figures 2.8 and 2.9, respectively. The slopes of the two lines represent the mole percent of the metal chelated by the DTTA-MSNPs, 16.9 ± 1% for $Cu^{2+}$ and 19.7 ± 2% for $Co^{2+}$. These mole percents correspond closely with the calculated 22.8% DETA/DTTA conversion value from the TGA data and the theoretical surface coverage of DETA (~16%), supporting the theory that EDTA titration can be used to determine the percentage of DETA converted. By accounting for the 22.8% in the titration data, instead of the theoretical weight percent, we conclude that ~50-60% of the DTTA participate in metal chelating. This implies that some DTTA moieties are hindered, perhaps by adjacent chelated metals causing a charge-charge repulsion.

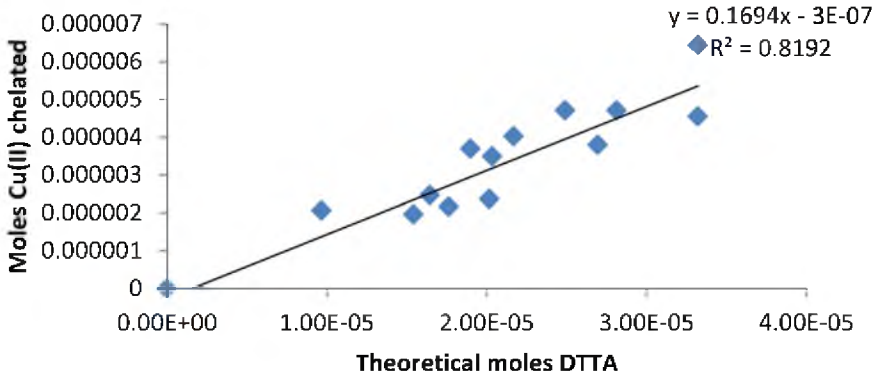


Figure 2.8: Moles of copper chelated by DTTA-MSNPs. With a slope that represents the moles of DETA converted.

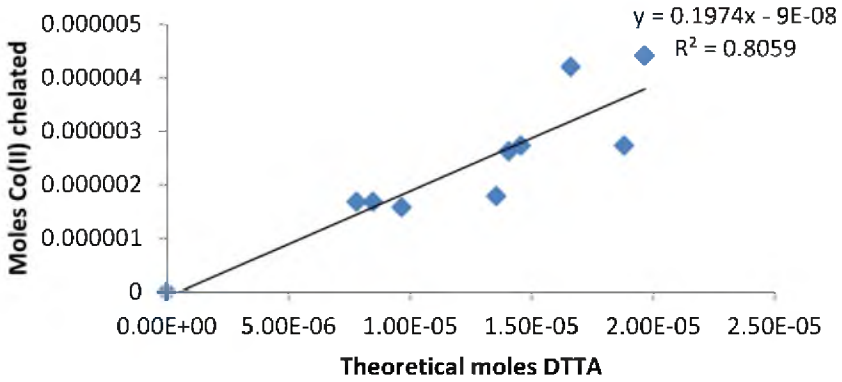


Figure 2.9: Mole of cobalt chelated by DTTA-MSNPs. With a slope that represents the moles of DETA converted.

$Gd^{3+}$ is difficult to titrate because it precipitates during the titration with the alkaline EDTA solution. Thus, we used TGA to determine the percentage of $Gd^{3+}$ that is chelated by the DTTA-MSNPs. Samples were prepared by soaking the DTTA-MSNPs in a solution containing large excess of $Gd^{3+}$. The particles were then collected by centrifugation and washed twice with EDTA solution then twice with water. TGA analysis of the dried particles gave weight losses of 17.7 and 16.4% for DTTA-MSNPs and DTTA-MSNPs-Gd, respectively (Figure 2.10). This means that a 1.3% weight of

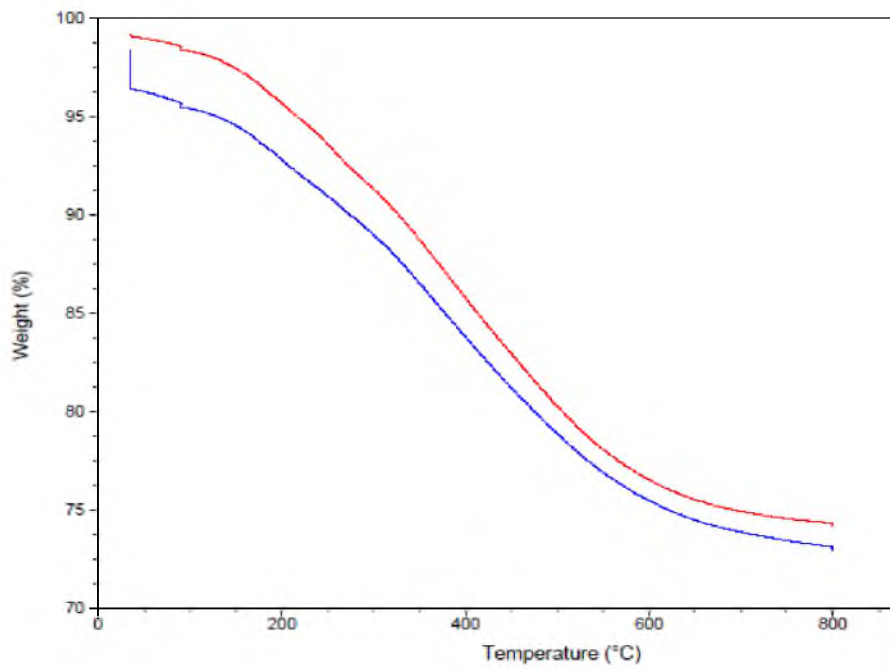


Figure 2.10: TGA weight losses of DTTA-MSNPs(red) and DTTA-MSNPs-Gd (blue).

gadolinium is being chelated (~45% of available DTTA molecules chelating Gd), which corresponds to a gadolinium loading of ~7.1 x $10^{19}$ Gd atoms/$cm^3$ using Eq. 2.7-2.8.

For comparison, Rieter et al.[13] prepared solid silica nanoparticles coated with SiDTTA-Gd with an average diameter of 37 nm containing 2.4 × $10^{20}$ Gd/$cm^3$. Taylor et al.[6] synthesized mesoporous Gd-containing silica particles (T-mDTTA-Gd), with an average diameter of 75 nm, and surface area approximately 5 times higher than that of our DTTA-MSNPs. They grafted SiDTTA-Gd to mesoporous silica and obtained a maximum gadolinium loading of 3.3 × $10^{20}$ Gd/$cm^3$. Although the T-mDTTA-Gd particles had a much larger surface area (1470 $m^2$/g), the "grafting to" approach reduced their pore size from 2.4 nm for the starting mesoporous silica to 0.9-1 nm for T-mDTTA-Gd. This change from mesoporous to microporous structure was not observed for our DTTA-MSNPs.

$$\rho_{m\,DTTA} \cdot \frac{4}{3} \cdot \pi \cdot r^3 \cdot \frac{10^{-21}\text{cm}^3}{\text{nm}^3} = W_{SP}$$

Eq. 2.7: Mass of a single DTTA-MSNP.

$$\frac{\%W_{Gd} \cdot W_{sp} \cdot N_A}{100 \cdot MW_{Gd} \cdot \frac{4}{3} \cdot \pi \cdot r_{cm}^3} = \frac{\text{atoms Gd}}{\text{cm}^3}$$

Eq. 2.8: Number of gadolinium atoms per particle volume based on TGA data.

Furthermore, designs for gadolinium-carrying particles usually involve the incorporation of a fluorophore to give the particle a dual imaging modality. This typically requires another silane, commonly APTES, for fluorophore attachment. With our DTTA-MSNPs, there are free primary amines from the unreacted DETA molecules. To confirm their presence, we treated DTTA-MSNPs with dansyl chloride. Figure 2.11 shows the fluorescence of the resulting dansylated DTTA-MSNPs and DTTA-MSNP-Gd particles.

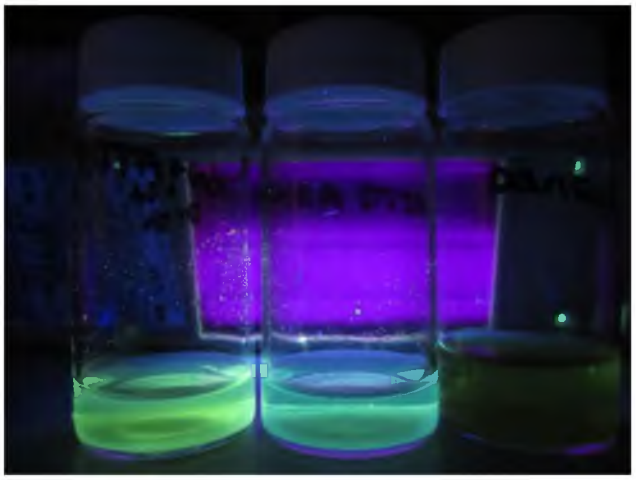

Figure 2.11: Fluorescence of dansyl chloride modified DTTA-MSNPs-Gd (**Left**) and DTTA-MSNPs (**Center**). To the right is a solution of dansyl chloride in acetonitrile with no amines present.

## 2.4 Conclusions

A new procedure to synthesize mesoporous metal-chelating silica nanoparticles has been developed. These nanoparticles are prepared by co-condensation of TEOS and diethylenetriametetraacetic acid under basic conditions in the presence of CTAB, followed by the conversion of DETA to DTTA. These particles maintain the large surface area after the DETA conversion and keep their pore sizes in the mesoporous range, which is not typically observed for "grafted to" mesoporous analogs. These particles can chelate a variety of metals, such as gadolinium, copper, and cobalt, giving them potential applications in a variety of fields, such as MRI, neutron capture therapy, and metal sequestering.

Despite the fact that other silica nanoparticles using chelation to bind gadolinium have been suggested as MRI contrast agents, our new synthetic strategy has the potential to maximize gadolinium access to water by maintaining mesopore diameters and chelating gadolinium to exposed DTTA functionalities, while providing an additional organic handle for fluorescent tag attachment to impart dual imaging modality. Moreover, DTTA-MSNPs can act as theranostic agents with MRI diagnostic and neutron capture therapeutic modalities, and if desired, with additional fluorescent imaging and targeting modalities.

## 2.5 References

[1] Cui, Z.; Lockman, P.R.; Atwood, C.S.; Hsu, C-H.; Gupte, A.; Allen, D.D.; Mumper, R.J. *European Journal of Pharmaceutics and Biopharmaceutics*. **2005**, *59*, 263–272.

[2] Yantasee, W.; Warner, C.L.; Sangvanich, T.; Addleman, R.S.; Carter, T.G.; Wiacek, R.J.; Fryxell, G.E.; Timchalk, C.; Warner, M.G. *Environ. Sci. Techno*l. **2007**, *41*, 5114-5119.

[3] Deng W.; Jin, D. ; Drozdowicz-Tomsia, K.; Yuan, J.; Wu, J.; Goldys, E.M. *Proc. of SPIE* Vol. 7909 79090Z-2.

[4] Li, Z.; Zhang, Y.; Shuter, B.; Idris, N.M. *Langmuir* **2009**, *25*, 12015–12018.

[5] Feldmann, V.; Engelmann, J.; Gottschalk, S.; Mayer, H.A. *J. Colloid Interface Sci.* **2012**, *366*, 70-79.

[6] Taylor-Pashow, K.M.L.; Rocca, J.D.; Lin, W. *Nanomaterials* **2012**, *2*, 1-14.

[7] Hamid, A.; Tripp, C.; Bruce, A.; Bruce, M. *Res. Chem. Intermed.* **2011** *37*, 791-810.

[8] Neouze, M-A.; Schubert, U. *Monatsh. Chem.* 2008, *139*, 183–195.

[9] Zhang, Y.; Yu, X.; Wang, X.; Shan, W.; Yang, P.; Tang, Y. *Chem. Commun.* **2004**, 2882-2883.

[10] Rouquerol, J.; Avnir, D.; Fairbridge, C.W.; Everett, D.H.; Haynes, J.H.; Pernicone, N.; Ramsay, J.D.F.; Sing, K.S.W.; Unger, K.K. *Pure & Appl. Chem.* **1994**, *66*, 1739-1758.

[11] Macquarrie, D.J.; Jackson, D.B.; Mdoe, J.E.J.; Clark, J.H. *New J. Chem.* **1999**, *23*, 539-544.

[12] Walcarius, A.; Delacôte, C. *Chem. Mater.* **2003**, *15*, 4181-4192.

[13] Rieter, W. J.; Kim, J. S.; Taylor, K. M. L.; An, H.; Lin, W.; Tarrant, T.; Lin, W. *Angew. Chem. Int. Ed.* **2007**, *46*, 3680-3682.

[14] Taylor, K. M. L.; Kim, J. S.; Rieter, W. J.; An, H.; Lin, W. *J. Am. Chem. Soc.* **2008**, *130*, 2154-2155.

[15] Soloway, A.H.; Tjarks, W.; Barnum, B.A.; Rong, F.-G.; Barth, R.F.; Codogni, I.M.; Wilson, J.G. *Chem. Rev.* **1998**, *98*, 1515-1562.

[16] Sing, K.S.W.; Everett, D.H.; Haul, R.A.W.; Moscou, L.; Pierotii, R.A.; Rouquérol, J.; Siemieniewska, T. *Pure & Appl. Chem.* **1985**, *57*, 603-619.

# CHAPTER 3

# THE SYNTHESIS OF LARGE SURFACE AREA VINYL ORMOSIL NANOPARTICLES

## 3.1 Introduction

The chemical and thermal stability and hydrophilic properties of silica nanoparticles make them useful carriers for fluorophores and other inorganic nanoparticles. These silica nanoparticle carriers have potential applications in the fields of optics, imaging, and therapeutics.[1] Although silica is relatively inert, when modified with organosilanes, silica nanoparticles gain advantageous organic functionalities. For example, organosilanes can change the surface charge or polarity of the silica nanoparticles, and/or can be further modified by traditional synthetic techniques.

Silica nanoparticles can be modified with an organosilane by "grafting to" or co-condensation methods.[1] The "grafting to" approach adds organic functionalities to the surface of an already synthesized silica nanoparticle. When dealing with a monolayer, the organosilane surface coverage becomes highly dependent on the surface silanols of the particle and steric interactions between organic functionalities. When a multilayer is formed by the condensation of the organosilane with itself, the number of organic groups increases, but so does the size of the particle. Additionally, the multilayer may prevent access to organic functionalities located closer to the core of the particle.

The co-condensation approach provides organic functionalities throughout the silica nanoparticle body. Although this method results in a greater number of organic functionalities, the core groups are relatively inaccessible for further modification and typically need to be modified prior to co-condensation (e.g. covalent encapsulation of a fluorophore).[2] For both methods, the accessibility and apparent number of organic functionalities is mostly limited to those on the silica surface.

Recently, methods that increase the surface area to volume ratio of silica nanoparticles and thus increase the number and/or accessibility of the organic functionalities have been developed. These methods involve the synthesis of surface-rough[3] or mesoporous structures.[4] Even though both structures have a greater surface area than solid silica nanoparticles, their applications are very different.

Surface-rough silica nanoparticles are synthesized by etching the silica particles[5] or by adding smaller silica spheres to the surface of a larger silica spheres.[3] When modified with hydrophobic organosilanes, these surface-rough silica nanoparticles possess superhydrophobic properties and have been used in producing water-repellent glass.[6]

Mesoporous nanoparticles are made using a micellar solution where the silica precursor condenses around the micelles. This creates a greater surface area and more silanols for further surface modification. The mesoporous structure allows for a greater accessibility to organic functionalities via the pores. Mesoporous silica nanoparticles have found applications in drug delivery[7] and imaging[8] because they are able to trap drug molecules, or imaging species, in their porous channels. Since silica nanoparticles often need to incorporate organic functionalities to make them useful, it would be beneficial to

synthesize silica nanoparticles that are made solely from the organosilane that provides the desired functionality.

Organically modified silica (ORMOSIL) nanoparticles are relatively new to the field of silica chemistry. These particles are synthesized by the hydrolysis and condensation of an organosilane in the absence of a tetraalkoxy silane. The advantage that an ORMOSIL nanoparticle has over a solid modified silica nanoparticle is a greater number of organic functionalities throughout its body. The organic functionalities are also more accessible because the silica matrix is distorted by the loss of a silicon-oxygen bond and steric effects, which create a degree of porosity.[9] As with traditional silica nanoparticles, increasing the surface area of the ORMOSIL nanoparticles is thought to increase the number and accessibility of the organic functionalities.

ORMOSILs synthesized with vinyl-containing silanes are of interest because the vinyl groups can be modified to contain boric acids through hydroboration chemistry.[9] As discussed in Chapter 1, nanoparticles that contain large amounts of boron have the potential to be effective boron neutron capture therapy (BNCT) agents. Additionally, the silica matrix provides a modifiable structure to which additional silanes can be attached.

This chapter describes two new synthetic methodologies for preparing large surface area vinyl ORMOSIL structures. These methodologies use micellar solutions to create mesoporous and surface-rough structures. Additionally, organic transformations are performed for the vinyl groups and the results are compared to "solid" vinyl ORMOSIL particles to determine the extent of vinyl modification and to create a boron carrier that can be potentially used in BNCT.

## 3.2 Experimental Section

### 3.2.1 Materials

Vinyltrimethoxy silane (VTMS, Gelest Inc.), Hexadecyltrimethylammonium bromide (CTAB, 99.0%, Sigma-Aldrich), Mesitylene (97%, 1,3,5-Trimethylbenzene, TMB, Sigma-Aldrich), Ethylene glycol (EG, Macron Chemicals), Ammonium hydroxide (28-30%, Sigma-Aldrich), 1 M Borane tetrahydrofuran ($BH_3THF$, Sigma-Aldrich), Bromine ($Br_2$, Sigma-Alrich), and Potassium permanganate ($KMnO_4$, 99%, Sigma-Aldrich).

### 3.2.2 Instruments

Transmission electron microscopy (TEM, FEI Techna $G^2$ T-12), Infrared spectroscopy (IR, Bruker Tensor 37), Nitrogen adsorption-desorption (BET analysis, Micrometrics ASAP 2020), and Thermogravimetric analysis (TGA, Instruments 2950 Thermogravimetric Analyzer).

### 3.2.3 Mesoporous vinyl silica nanoparticle synthesis

A solution consisting of 0.5868 g CTAB, 90 mL MilliQ water, 43 mL ethanol, 15 mL EG, and 3.6mL 25% $NH_4OH$ is stirred rapidly in a 250 mL round bottom flask at 70 °C for 25 minutes. 0.690 mL of VTMS is then added to the solution and stirred for 72 hours. The particles are collected by centrifugation and washed 3 times with ethanol. The particles are then added to a 100 mL round bottom flask containing 30 mL of a 1 M HCl ethanolic solution and heated at 80 °C for 12 hours to remove the CTAB. The particles are collected and then washed 3 times with ethanol.

### 3.2.4 Surface-rough vinyl silica nanoparticle synthesis

A solution consisting of 0.5868 g CTAB, 0.66 mL TMB (2.95:1 TMB:CTAB), 90 mL MilliQ water, 43 mL ethanol, 15 mL EG, and 3.6mL 25% $NH_4OH$ is stirred rapidly in a 250 mL round bottom flask at 70 °C for 25 minutes. 0.690 mL of VTMS is then added to the solution and allowed to stir for 72 hours. The particles are then collected by centrifugation and washed 3 times with ethanol. The particles are then added to a 100 mL round bottom flask containing 30 mL of 1 M HCl ethanolic solution and heated at 80 °C to remove the CTAB. The particles are collected and then washed 3 times with ethanol.

### 3.2.5 Bromination of vinyl silica particles

0.1 g of the vinyl silica nanoparticles (vSNPs, 1.25 mmol) are placed in a scintillation vial containing 10 mL of dichloromethane and sonicated until the particles are dispersed throughout the solution. Three equivalents of bromine (0.19 mL, 3.75 mmol) are added to the solution and then briefly sonicated. The solution is allowed to sit overnight to ensure complete reaction of the bromine (Scheme 3.1). The particles are collected via centrifugation and washed five times with dichloromethane to completely remove all bromine.

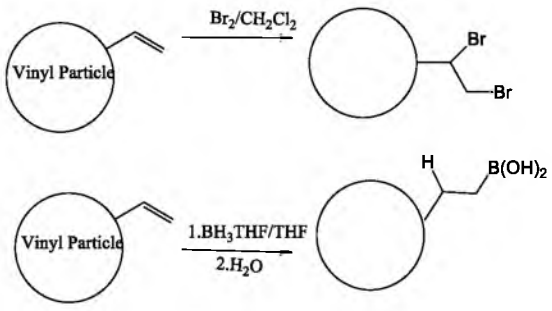


Scheme 3.1: Representation of bromination and hydroboration of vSNPs.

### 3.2.6 Hydroboration of vinyl silica particles

0.1 g of the vSNPs is placed in a 25 mL round bottom flask. An excess of 1 M $BH_3THF$ (5 mL) and 6 mL of THF is added to the flask and stirred under nitrogen. After 3 hours, the flask is sonicated to disperse the particles and then stirred again overnight. The particles are then washed with THF 3 times to remove excess $BH_3THF$, washed with a 9:1 ethanol-water mixture followed by sonication in MilliQ water to complete the conversion to boric acids, and then washed twice with MilliQ water (Scheme 3.1).

### 3.2.7 Potassium permanganate oxidation of vinyl silica particles

0.1 g of vSNPs are dispersed in 10 mL of ethanol. The solution is transferred to a 25 mL round bottom flask and stirred. 2 mL of a 5% w/v $KMnO_4$ solution is added dropwise to the flask. The solution is stirred for 24 hours then collected via centrifugation and washed twice with ethanol. Concentrated $H_2SO_4$ and water is added to the brown precipitate and allowed to react for 3 hours or until the brown color disappears. The solution is then centrifuged to collect the white particles and washed once with dilute $H_2SO_4$ then 3 times with water.

## 3.3 Results and Discussion

### 3.3.1 Synthesis of vinyl silica nanoparticles

Presently, there are a few organosilane precursors that can form ORMOSIL nanoparticles.[10] The vinyltrimethoxy silane (VTMS) precursor is one organosilane that not only forms ORMOSIL nanoparticles but can also provide a reactive organic group susceptible to bromination, hydroboration, hydroxylation, and oxidation. The other

advantage to using VTMS is that it can undergo hydrolysis and condensation using the simple Stöber method.

Solid vinyl silica nanoparticles (svSNPs) were initially made to act as a baseline for surface area comparisons. These particles were made using the same synthetic procedure as mesoporous vinyl silica nanoparticles (mvSNPs), described below, except that CTAB was not used. These particles are large in diameter (592 ± 18 nm) and non-porous (Figure 3.1). Nitrogen absorption-desorption isotherm analysis on the svSNPs gave a BET surface area of 8.48 $m^2 \cdot g^{-1}$. It should also be noted that the svSNPs absorb little nitrogen (~ 13 $cm^3 \cdot g^{-1}$ STP) and exhibit a type II isotherm (Figure 3.2), which is indicative of nonporous materials (Figure 3.3a).[11]

Factors such as ethylene glycol and the concentration of water and ethanol play an important role in the formation of mesoporous vinyl silica nanoparticle (mvSNP). The purpose of ethylene glycol is to provide high viscosity to the solution, which creates more silica nuclei for particle formation, and helps control the particle size and uniformity.[12]

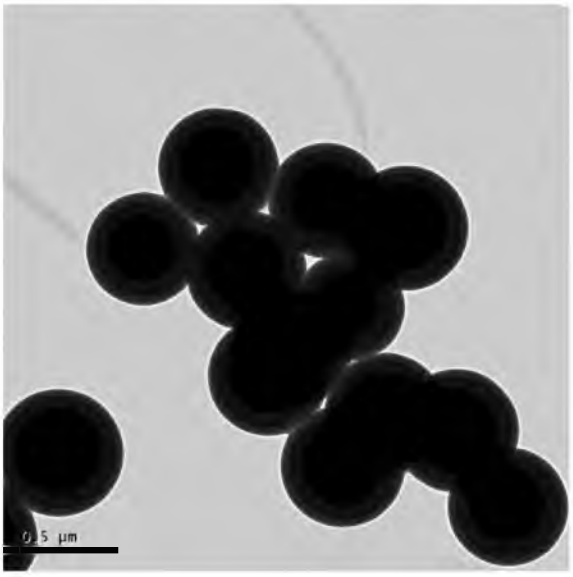


Figure 3.1: TEM image of svSNPs.

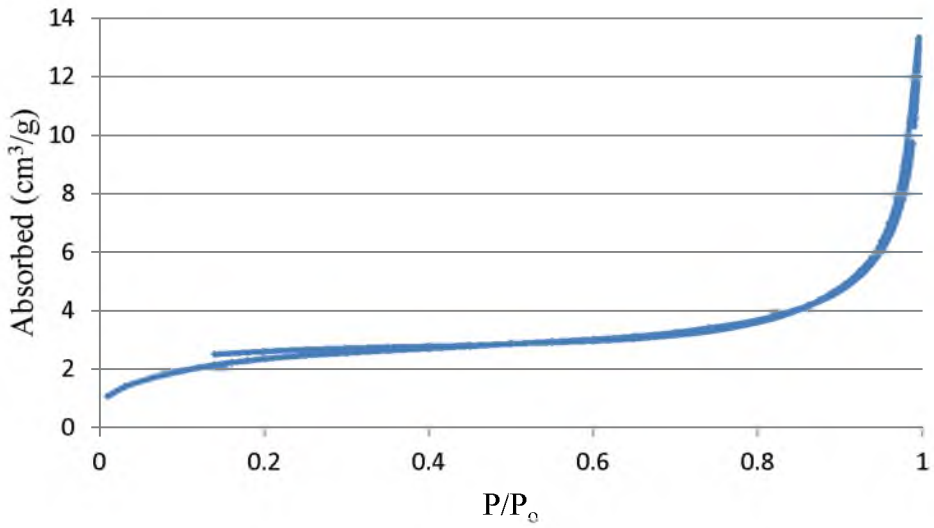


Figure 3.2: Nitrogen adsorption-desorption isotherm of svSNPs.

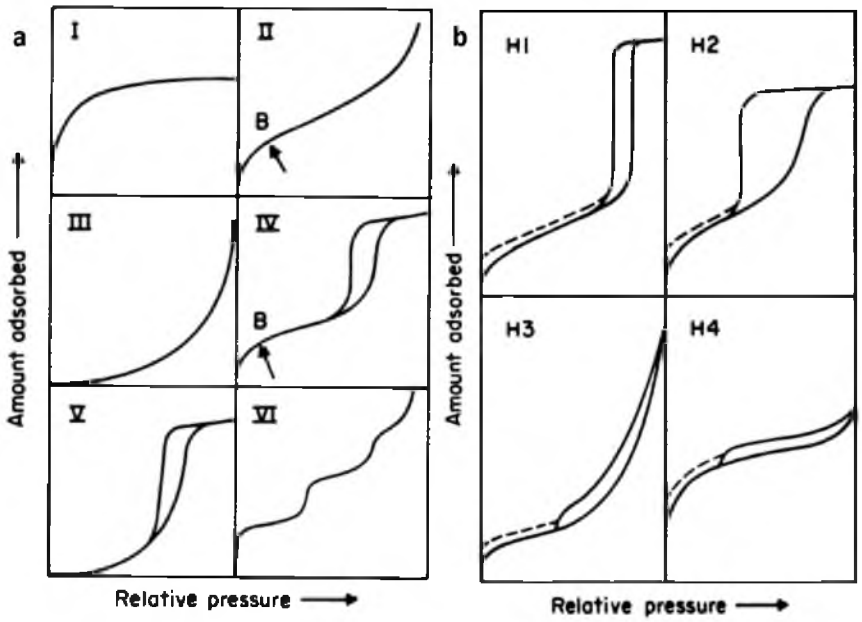


Figure 3.3: Representations of adsorption-desorption isotherms and hysteresis loops. a) Types of isotherms (type IV and type V are considered isotherms for mesoporous materials) b) Types of hysteresis loops.[11]

Several factors inhibit the mvSNP formation. When VTMS is added to a micellar CTAB solution that contains only water or ethanol, or if the ethanol:water ratio is lower than described in the procedure, the solution does not turn opaque, indicating that particles are not formed. The reaction can also result in a gel network when the concentration of ethanol is increased, when it is added after VTMS, or if the reaction time is less than 72 hours (Figure 3.4a). If the solution temperature falls below 50 °C, the loss of porosity is observed (Figure 3.4b). It should be noted that the mvSNP synthetic method has a lower yield than the respective yield of svSNPs.

Distinct porous spherical structures were observed by TEM for the mvSNPs with an average particle size of 137 ± 8 nm (Figure 3.5a-b). These pores appear to have different sizes and are randomly distributed throughout the ORMOSIL body. The pore size variations may be caused by some of the hydrophobic VTMS precursor entering the hydrophobic micelle core and causing the micelle to swell. This may also be the explanation for the low product yield, especially if the pores are interconnecting during synthesis. An example of the mvSNPs nitrogen sorption isotherm is shown in Figure

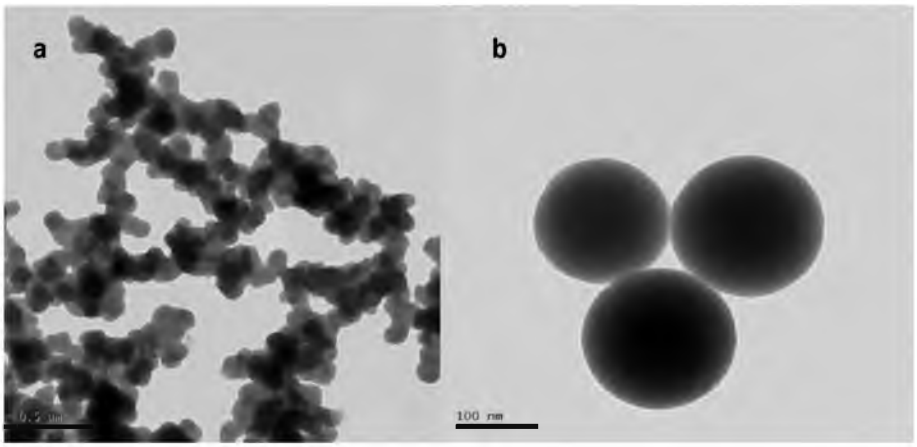


Figure 3.4: TEM images of a) Vinyl gel network produced b) nonporous particles observed below 50 °C.

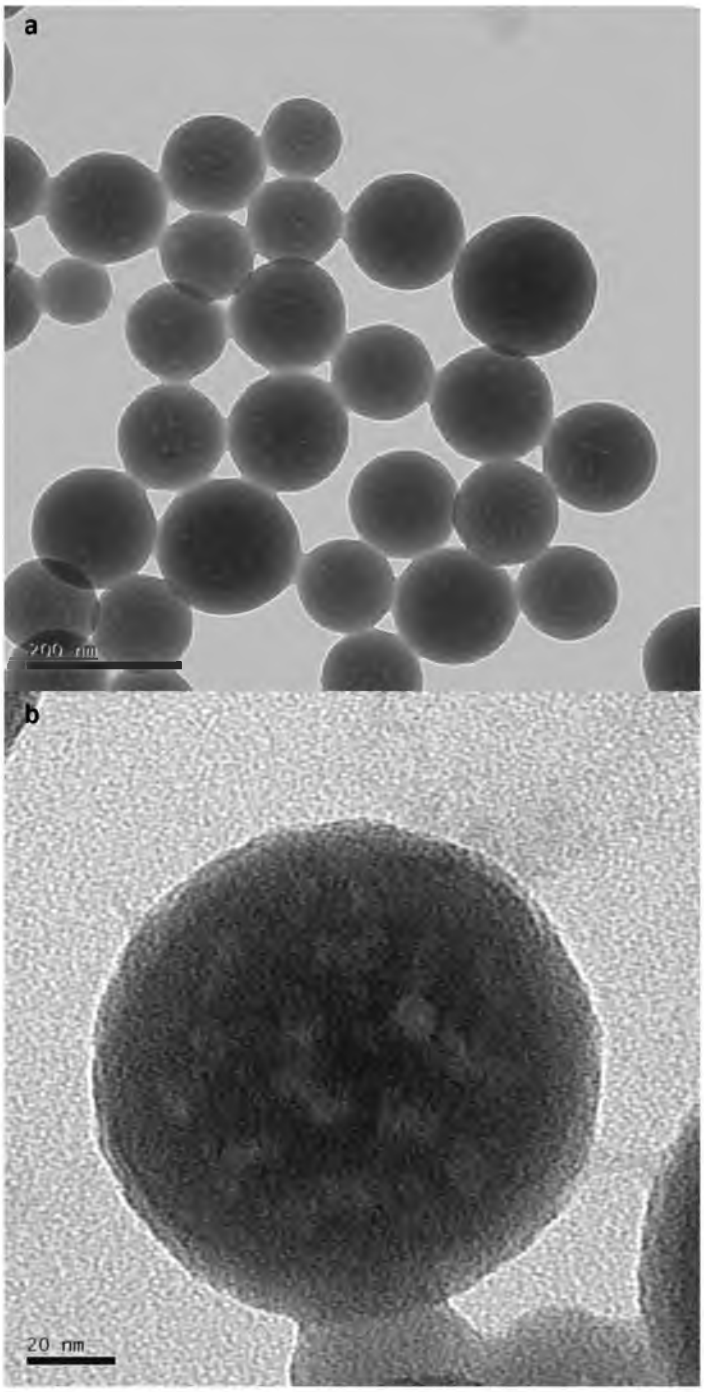


Figure 3.5: TEM images of mvSNPs synthesized at 70°C.

3.6a. This isotherm has an expected large nitrogen absorption (~260 $cm^3 \cdot g^{-1}$ STP) and appears to be type II (Figure 3.3a). However, it has an H1 hysteresis loop (Figure 3.3b) between 0.92 to 1 $P/P_o$, indicating mesoporosity, and therefore, it is probably a type IV without the noticeable plateau, which is not uncommon for mesoporous materials.[13,14]

Although the large nitrogen absorption and hysteresis loop are indicative of a mesoporous material, the pore diameter measurement has a wide distribution of sizes from the 2 nm to 300 nm. This broad size range can be explained by a combination of micropores (< 2 nm), mesopores (2- 50 nm), some of which may be connected, and voids created by particle aggregation. Figure 3.6b shows the pore size distribution up to 50 nm to emphasize the periodic pore size maxima from 2 nm to ~ 30 nm (2, 7, 12, 18, and 23 nm) demonstrating that the mesopores are not uniform in size. According to BJH calculations, the mvSNP samples have the average pore sizes between 36.8 and 50.4 nm, which roughly corresponds to the large pore sizes observed by TEM and the highest pore size from Figure 3.6b, and a pore volume of 0.32 $cm^3 \cdot g^{-1}$. For comparison, svSNPs have a "pore volume" of 0.02 $cm^3 \cdot g$. Additionally, BET analysis of the mvSNP samples gave surface areas that lie between 30.32 and 43.96 $m^2 \cdot g^{-1}$, which means that these particles have a surface area 3.5 to 5 times larger than svSNPs. This surface area is lower than that expected based on other large pore particles.[14] This is likely due to the mvSNPs pore density being lower than that of typical mesoporous particles.

We expected that when the swelling agent TMB is added to the micellar CTAB solution prior to VTMS condensation, the VTMS particles will possess larger pores than the mvSNPs described above. However, this was not the case. When the product of this reaction was imaged with TEM, a surface-rough structure was observed with an average

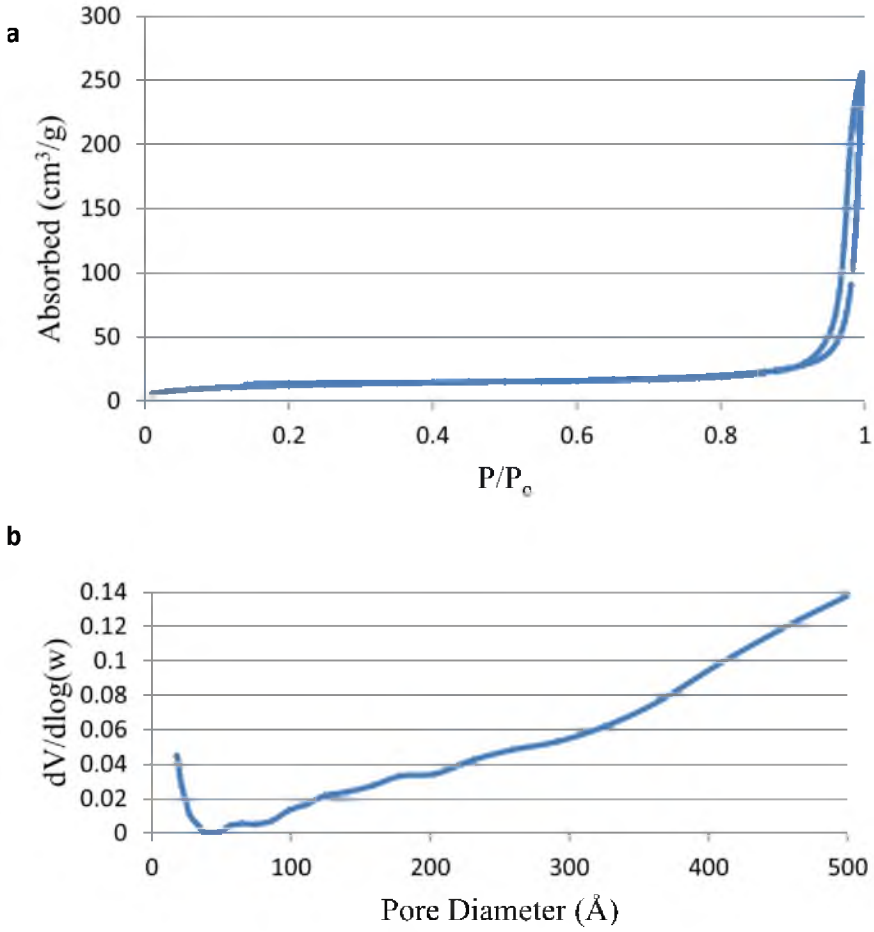


Figure 3.6: Nitrogen adsorption-desorption analysis of mvSNPs. a)Nitrogen adsorption-desorption isotherm of mvSNPs. b) Pore size distribution of mvSNPs between 0 and 50 nm.

size of 97 ± 6 nm (Figure 3.7a-b). This structure may be due to VTMS not being able to condense fully around the swollen micelles. However, the yield of the surface-rough particles was higher compared to mvSNPs, which is likely caused by TMB replacing some of the VTMS in the micelles, or causing the micelles to be "leaky" allowing for VTMS to enter and exit. The isotherm of these surface-rough vinyl silica nanoparticles (rvSNPs), as with the mvSNPs, has a larger nitrogen adsorption (~450 $cm^3 \cdot g^{-1}$) than that of svSNPs. The main difference between the rvSNPs and mvSNP nitrogen sorption

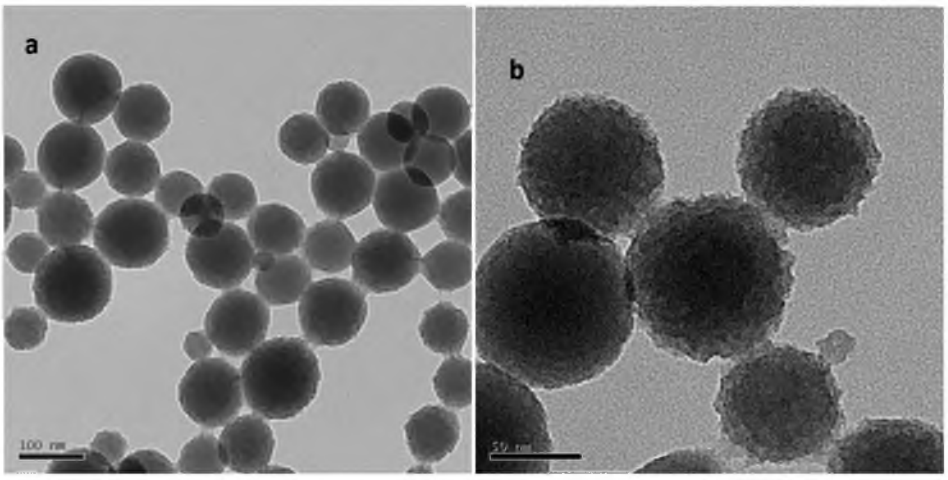


Figure 3.7: TEM images of rvSNPs.

isotherms is that the rvSNP's hysteresis does not have a "loop" like that of the mvSNPs (Figure 3.8). This implies that they contain porous areas that do not allow nitrogen to exit. According to BJH calculations, these rvSNPs have pores that are smaller than those of the mvSNPs (18.5 nm) with volumes of 0.65 $cm^3 \cdot g^{-1}$. This observation is likely due to the cavities created by the rough surface. If there were "through-and-through" pores of this calculated size, they would be visible by TEM. Even though there may be a degree of porosity, these vinyl silica particles have an obvious rough surface. These rvSNPs have a

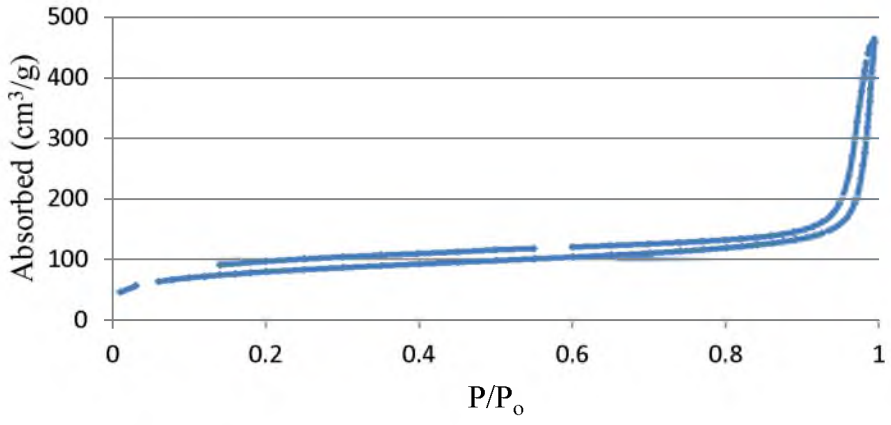


Figure 3.8: Nitrogen adsorption-desorption isotherm of rvSNPs.

BET surface area of 278.70 $m^2 \cdot g^{-1}$, which is much larger than the surface area of either the mvSNPs or the svSNPs.

### 3.3.2 Bromination of vinyl silica nanoparticles

Bromination was performed first because $Br_2$ reacts readily with alkene groups. We expected that brominating the vinyl particles will allow us to determine the extent of vinyl accessibility. The treatment of the vinyl particles with bromine produced an off-white colored powder. When brominated particles were examined using IR, a loss of the vinyl stretch at 960 $cm^{-1}$ and a diminishment of the 1602 $cm^{-1}$ stretch were observed. This suggests that the alkenes have indeed reacted. The small bands appearing at the 875 and 650 $cm^{-1}$ range, along with the peak spitting at 760 $cm^{-1}$, are characteristic of C-Br stretching (Figure 3.9).

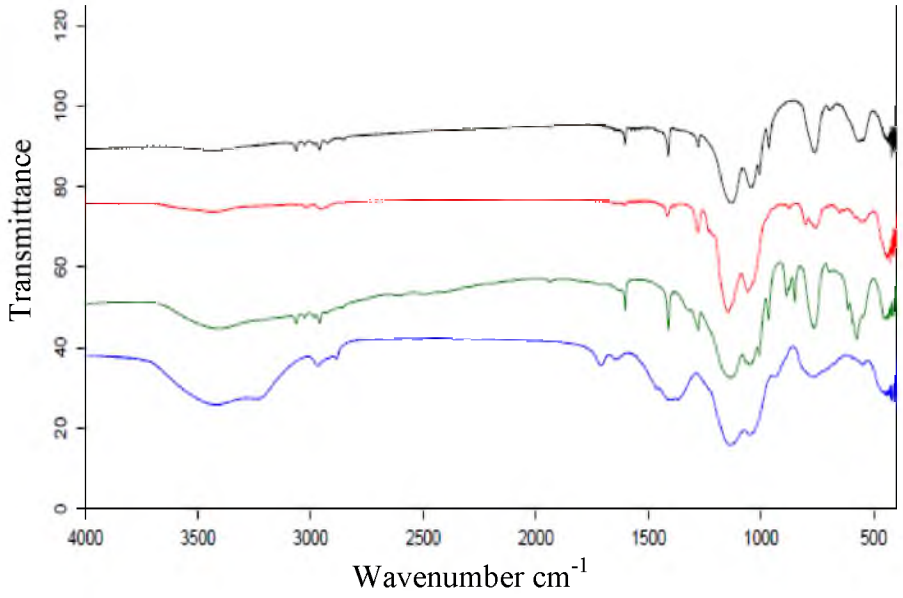


Figure 3.9: IR spectra of vinyl (black), brominated vinyl (red), oxidized vinyl (green), and hydroborated vinyl (blue) nanoparticles.

TGA gave information about the extent of vinyl conversion via bromination. Brominated svSNP, rvSNPs, and mvSNPs exhibit similar weight losses of ~60%. This is much greater than the weight loss observed for the "solid" vinyl particles (~9%) (Figure 3.10-3.12). Despite their surface areas which implies the amount of vinyl functionalities that are accessible, the vinyl nanoparticles have similar mole conversion percentages of ~85% (Eq. 3.1-3.3). This result supports the idea of inherent ORMOSIL porosity and implies that these particles, with the exception of their surface areas, are not very different from each other in terms of reactivity. This was not the case for hydroborated samples.

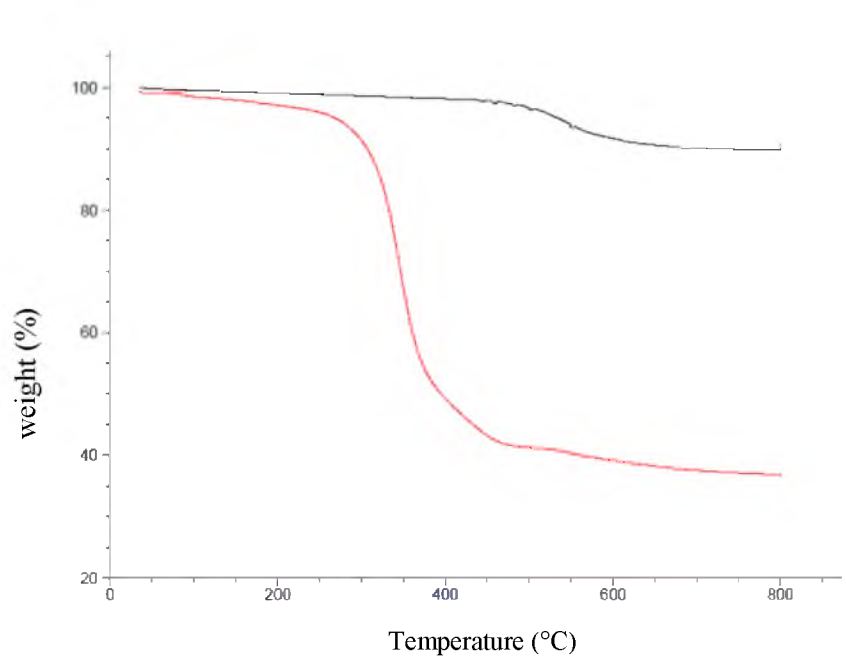


Figure 3.10: TGA weight losses of svSNPs (black) and brominated svSNPs (red).

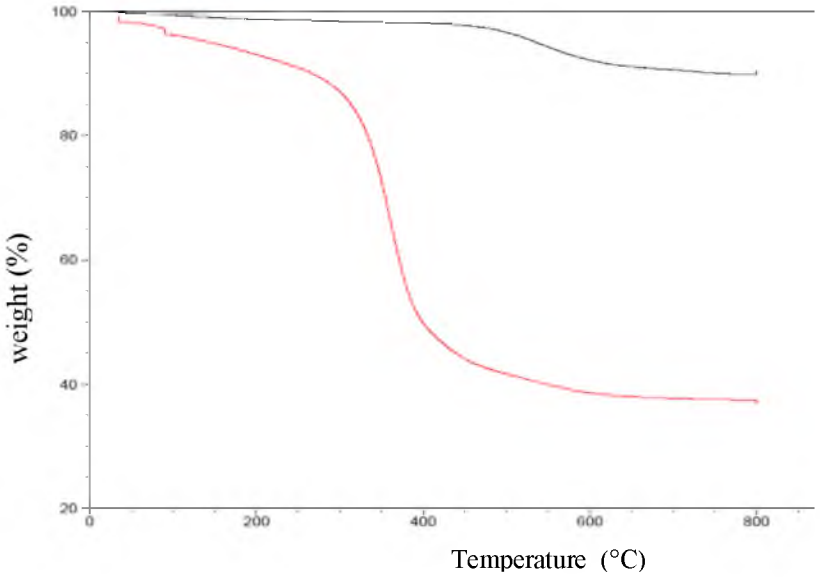


Figure 3.11: TGA weight losses of rvSNPs (black) and brominated rvSNPs (red).

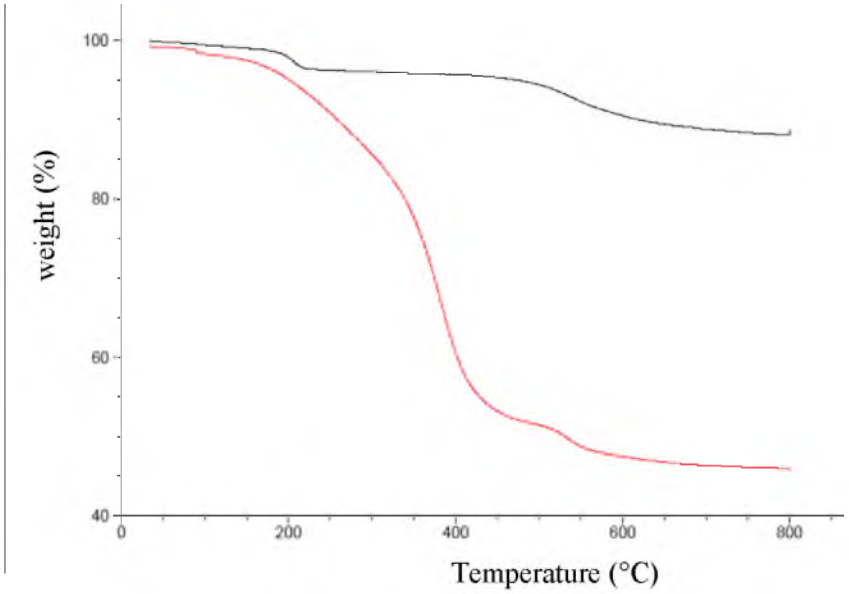


Figure 3.12: TGA weight losses of mvSNPs (black) and brominated mvSNPs (red).

$$\frac{\rho \cdot \frac{4}{3} \cdot \pi \cdot r_{(cm)}{}^{3} \cdot \ \%W_{loss_{vSNP}}}{100 \cdot MW_{vinyl}} = \frac{\text{mol vinyl}}{\text{particle}}$$

Eq. 3.1: Determining the moles vinyl per particle based on TGA data: ρ is the particle density in $g \cdot cm^{-3}$(~1.35), r is the particle radius, $MW_{vinyl}$ is the molecular weight of vinyl, and $\%W_{loss}$ is the measured weight loss of the vSNPs according to TGA.

$$\frac{\rho \cdot \frac{4}{3} \cdot \pi \cdot r_{(cm)}{}^{3} \cdot (\%W_{loss_{VNP+X}} - \%W_{loss_{VNP}})}{100 \cdot MW_{X}} = \frac{\text{mol X}}{\text{particle}}$$

Eq. 3.2: Determining the moles of bromine or boric acid in reacted vinyl particles: ρ is the particle density in $g \cdot cm^{-3}$(~1.35), r is the particle radius, $MW_X$ is the molecular weight of bromine or boric acid, and $\%W_{loss}$ is the measured weight loss of the nanoparticle according to TGA.

$$\frac{\text{mol X}}{\text{particle}} \div \frac{\text{mol vinyl}}{\text{particle}} \times 100 = \text{mol \% conversion}$$

Eq. 3.3: Determining the percentage of vinyls reacted during bromination or hydroboration.

### 3.3.3 Hydroboration of vinyl silica nanoparticles

Since one of the desired uses for these particles is to act as a boron carrier for BNCT, determining the amount of boron that each particle can carry is important. Initially, IR spectroscopy was used to determine if hydroboration has taken place. According to the IR spectrum (Figure 3.10), the vinyl nanoparticles have a Si-C stretch around 1410 $cm^{-1}$ which broadens after hydroboration due to the presence of B-O vibrations. There is a band at 770 $cm^{-1}$ representative of O-B-O and/or B-C stretches. The broad band at 3500 $cm^{-1}$ is indicative of the presence of hydroxyl groups created when borohydride is converted into boric acid. Additionally, there is a new band at 1712 $cm^{-1}$, which is characteristic of a C-B-C stretch. All of this indicates that vinyl groups were indeed converted to boric acid inside the vinyl nanoparticles. The hydroborated particles

were placed into a hexane water mixture. While the vinyl particles remain in hexane, the hydroborated particles disperse into the aqueous layer (Figure 3.13).

Since other svSNPs have been synthesized and hydroborated,[9] we used them to compare the extent of hydroboration for our vinyl nanoparticles and the amount of boron they carry per unit volume. Calculating the number of boron atoms per unit volume was used to avoid the confusion presented by the different particle sizes for the different vinyl particles. For svSNPs, TGA results show a weight loss of ~9.7% and the hydroborated svSNPs have a weight loss of ~19.0% (Figure 3.14). Using Eq. 3.4, the number of boron atoms per volume was calculated to be $1.69 \times 10^{21}$ B·cm$^{-3}$ ($1.8 \times 10^{8}$ B per particle). The mole conversion of the svSNP's vinyl groups by hydroboration was determined to be ~58%.

$$\frac{\frac{\text{mol B(OH)}_2}{\text{particle}} \cdot \frac{1\ \text{mol B}}{1\ \text{mol B(OH)}_2} \cdot N_A}{\frac{4}{3} \cdot \pi \cdot r_{(cm)}{}^3} = \frac{\#B}{cm^3}$$

Eq. 3.4: Determining the number of borons atoms per unit volume in each vSNP.

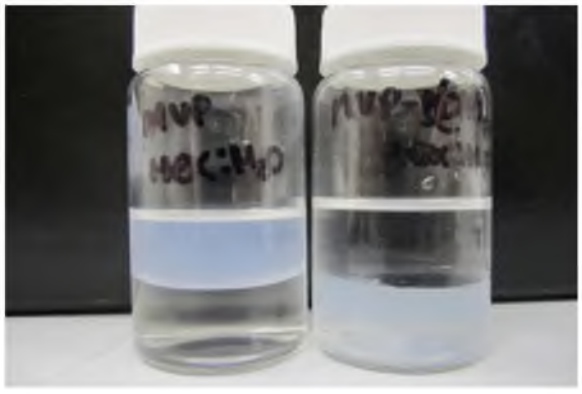

Figure 3.13: The hydrophobic mvSNPs are located in the hexane layer of the vial (**Left**). The hydroborated mvSNPs are located in the aqueous layer (**Right**).

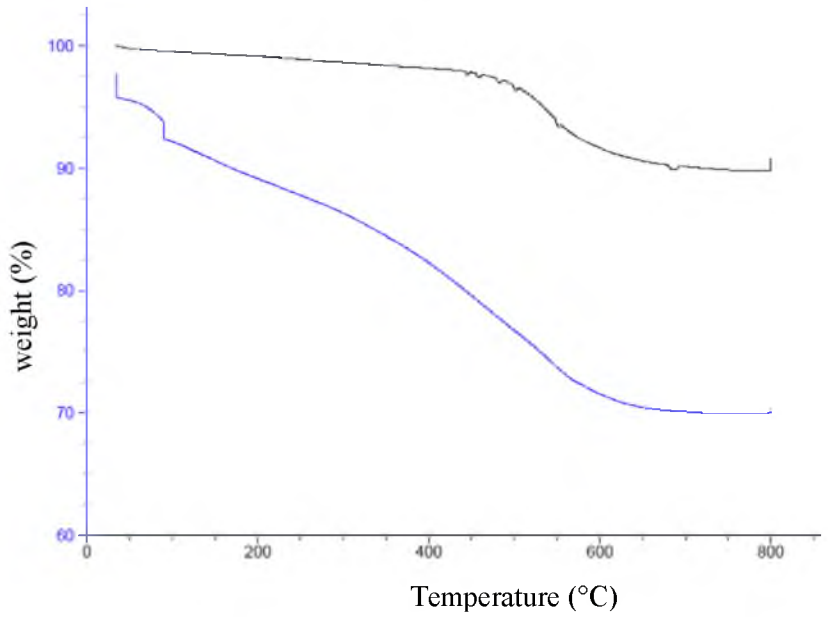


Figure 3.14: TGA weight losses of svSNPs (black) and hydroborated svSNPs (blue).

The rvSNPs showed a weight loss of ~9.3% and, after hydroboration, a weight loss of ~17.9% (Figure 3.15). This corresponds to the conversion of vinyl groups and boron atoms per volume similar to those of svSNPs, 55.7% and $1.56 \times 10^{21} B \cdot cm^{-3}$ ($7.2 \times 10^5$ B per particle), respectively. Although the rvSNPs have a larger surface area, and presumably a greater number of surface vinyl groups than the svSNPs, the difference was negated because of the inherent porosity of svSNPs. The mvSNPs show an improvement to the hydroboration of the vinyl groups. A vinyl weight loss of ~8.4% along with a boronated weight loss of ~20.9% were observed (Figure 3.16). This gives a $2.3 \times 10^{21}$ $B \cdot cm^{-3}$ ($3.1 \times 10^6$ B per particle) and a mole conversion of ~89.8% for vinyl groups, which is about 1.5 times greater than that for svSNPs or rvSNPs. This increase is most likely caused by the larger pores creating better access to the core vinyl functionalities.

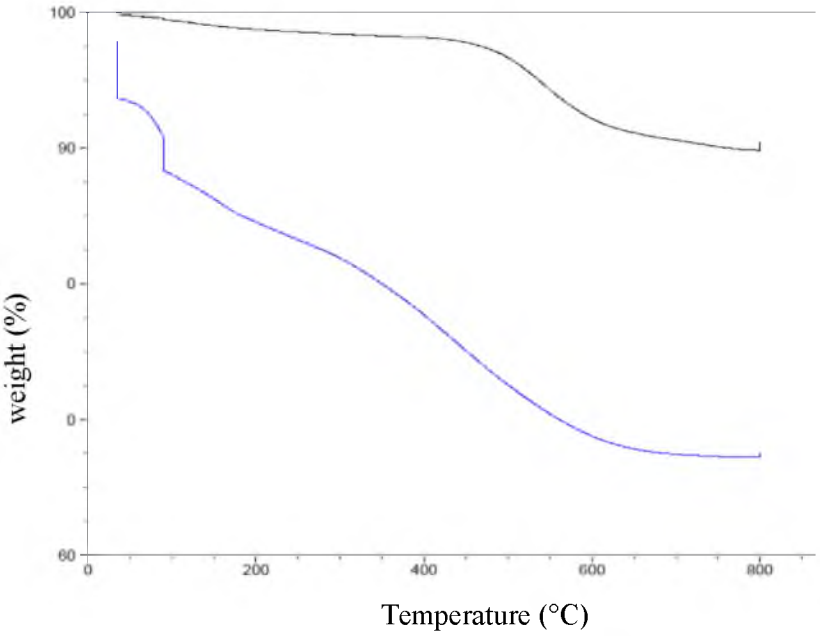


Figure 3.15: TGA weight losses of rvSNPs (black) and hydroborated rvSNPs (blue).

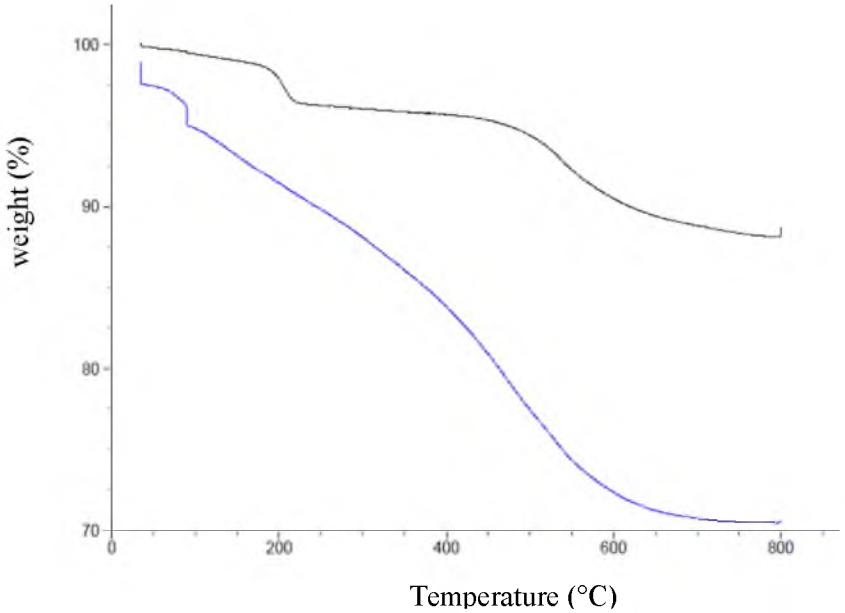


Figure 3.16: TGA weight losses of mvSNPs (black) and hydroborated mvSNPs (blue).

### 3.3.4 Oxidation of vinyl nanoparticles

The data for vinyl oxidation is not complete, but there are some positive preliminary results for a svSNP oxidation based on IR (Figure 3.9) and TGA analysis (Figure 3.17). The IR spectrum shows little loss of C-H stretches as is seen with bromination and hydroboration, but the broad peak appearing at 3400 $cm^{-1}$ representing O-H stretching indicates the oxidation of the alkene. Additionally, a small peak appears between the doublet at 1000-1200 $cm^{-1}$ that may represent a C-O stretch (~1100 $cm^{-1}$). Since there is no peak at 1700 $cm^{-1}$, this IR spectrum indicates the conversion of the alkene into a diol instead of a carboxylic acid. It should be noted that there is a peak between 800 and 900 $cm^{-1}$ that is probably caused by a S-O stretch from sulfuric acid contamination during oxidation.

When these oxidized svSNPs are measured with TGA, a weight loss of ~14%, between 200 and 800 °C is observed (Figure 3.17) indicating that the vinyl has been

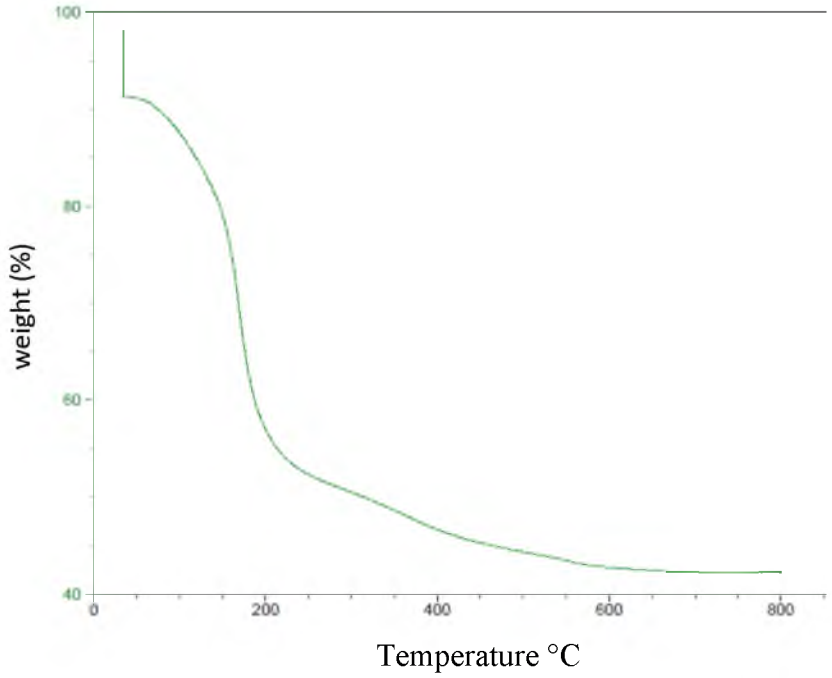


Figure 3.17: TGA analysis of oxidized svSNPs.

converted into a heavier organic compound. Assuming that the vinyl is being converted to a diol, a vinyl conversion of ~20% is calculated. The low percent of conversion may explain why IR peaks attributed to alkenes are still observed. The next process will be to determine the extent of vinyl oxidation for mvSNPs. These results will be used to compare the vinyl conversions of the svSNPs and mvSNPs to determine if the mvSNPs demonstrate a greater conversion of vinyl groups, as observed with the hydroboration data.

## 3.4 Conclusions

The syntheses of two new types of large surface area vinyl ORMOSIL nanoparticles have been presented. First, we used CTAB to create a micellar solution, producing large pore mesoporous vinyl particles. Secondly, we prepared surface-rough rough vinyl particles by adding the swelling agent TMB to the micellar solution. These particles may have an increased number of surface vinyl groups that could prove useful in making hydrophobic surfaces. Additionally, we demonstrated that vinyl ORMOSIL nanoparticles, specifically the mesoporous ones, could become excellent carriers for large amounts of boron, approximately $10^6$ boron atoms per particle, to act as BNCT agents.

## 3.5 References

[1] Jin, Y.; Li, A.; Hazelton, S.G.; Liang, S.; John, C.L.; Selid, P.D.; Pierce, D.T.; Zhao, J.X. *Coor. Chem. Rev.* **2009**, *253*, 2998-3014.

[2] Wang, L.; Tan, W. *Nano Lett.* **2006**, *6*, 84-88.

[3] Wang, C.; Yan, J. Cui, X.; Wang, H. *J. Colloid Interface Sci.* **2011**, *354*, 94-99.

[4] Beck, J.S.; Vartuli, J.C.; Roth, W.J.; Leonowicz, M.E.; Kresge, C.T.; Schmitt, K.D.; Chu, C.T.W.; Olson, D.H.; Sheppard, E.W.; Higgins, S.B.; Schlenkur, J.L. *J. Am. Chem. Soc.*, **1992,** *114,* 10834-10843.

[5] Du, X.; He, J. *ACS Appl. Mater. Interfaces* **2011**, *3*, 1269-1276.

[6] Li, X.; He, J. *ACS Appl. Mater. Interfaces* **2012** dx.doi.org/10.1021/am3002082.

[7] Vivero-Escoto, J. L.; Slowing, I. I.; Trewyn, B. G.; Lin, V. S-Y. *Small* **2010**, *6*, 1952-1967.

[8] Feldmann, V.; Engelmann, J.; Gottschalk, S.; Mayer, H. A. *J. Colloid Interface Sci.* **2012**, *366*, 70-79.

[9] Brozek, E.M.; Zharov, I. *Chem. Mater.* **2009**, *21*, 1451-1456.

[10] Ottenbrite, R.M.; Wall, J.S.; Siddiqui, J.A. *J. Am. Ceram. Soc.* **2000,** *83,* 3214-3215.

[11] Sing, K.S.W.; Everett, D.H.; Haul, R.A.W.; Moscou, L.; Pierotii, R.A.; Rouquérol, J.; Siemieniewska, T. *Pure & Appl. Chem.* **1985**, *57*, 603-619.

[12] Gu, J.; Fan, W.; Shimojima, A.; Okubo, T. *Small* **2007**, *3*, 1740-1744.

[13] Wang, C.; Yan, J. Cui, X.; Wang, H. *J. Colloid Interface Sci.* **2011**, *354*, 94-99.

[14] Hartono, S.B.; Gu, W.; Kleitz, F.; Liu, J.; He, L.; Middelberg, A.P.J.; Yu, C.; Lu, G.Q.; Qiao, S.Z. *ACS Nano* **2012**, *6*, 2104-2117.

# CHAPTER 4

# SYNTHESIS OF SILICA SHELL/BORON CORE ($B@SiO_2$) NANOPARTICLES

## 4.1 Introduction

In the United States alone there are about eleven million people with some form of cancer.[1] Since the 1970s, the United States, through the National Cancer Institute (NCI), has put more than two hundred billion dollars into finding treatments and cures for cancer.[2] Presently, treatments are limited to chemotherapy, surgery, radiation therapy, and interferon therapy. The problem with current methods is that none are localized to the tumor itself; even surgery requires damaging healthy tissue. This reduces their effectiveness and increases treatment complications. In 1936, George Locher proposed as a possible solution using boron as a localized cancer therapeutic. His idea is now known as boron neutron capture therapy (BNCT).[3]

Neutron capture therapy is based on the adsorption of slow neutrons in the nuclei of a nonradioactive isotope located inside, or adjacent to, the tumor cell. The adsorption of the neutrons leads to the release of radiation in the form of high linear energy transfer (LET) particles damaging the target cell. In addition to being nonradioactive, the isotope has to have a capture cross-section that is many times greater than that of elements typically found in tissues (Table 4.1) so that the neutrons are absorbed by the therapeutic isotope. A list of capture cross-sections can be seen in Table 4.2. $^{10}B$ (BNCT) is the most

Table 4.1: Thermal Neutron Capture Cross-Section Values of Tissue Elements and Their Percentages.[4]

| Nuclide | Capture Cross-Section (barns) | Weight (% in tissue) | Nuclide | Capture Cross-Section (barns) | Weight (% in tissue) |
|---|---|---|---|---|---|
| H | 0.332 | 10.00 | P | 0.18 | 1.16 |
| C | 0.0034 | 18.0 | S | 0.53 | 0.20 |
| N | 1.82 | 3.0 | Cl | 32.68 | 0.16 |
| O | $1.8 \times 10^{-4}$ | 65.0 | K | 2.1 | 0.20 |
| Na | 0.43 | 0.11 | Ca | 0.4 | 2.01 |
| Mg | 0.053 | 0.04 | Fe | 2.57 | 0.01 |

Table 4.2: Capture Cross-Section Values of Various Nuclides for Thermal Neutrons.[4]

| Nuclide | Capture Cross-Section (barns) | Nuclide | Capture Cross-Section (barns) |
|---|---|---|---|
| $^{6}$Li | 942 | $^{151}$Eu | 5800 |
| $^{10}$B | 3838 | $^{155}$Gd | 61000 |
| $^{22}$Na[a] | 32000 | $^{157}$Gd | 255000 |
| $^{58}$Co[a] | 1900 | $^{164}$Dy | 1800 |
| $^{113}$Co | 19800 | $^{184}$Os | 3000 |
| $^{126}$I[a] | 6000 | $^{199}$Hg | 2000 |
| $^{135}$Xe[a] | 2600000 | $^{230}$Pa[a] | 1500 |
| $^{148m}$Pm[a] | 10600 | $^{235}$U[a] | 580 |
| $^{149}$Sm | 42000 | $^{241}$Pu[a] | 1010 |

a: Radioactive

popular isotope due to its low toxicity and chemistry that allows for easy incorporation into a variety of small and macromolecules. $^{157}$Gd (GdNCT) is the only other proposed potential neutron capture therapeutic because it is nonradioactive and it has the second highest capture cross-section of all elements. The challenges with GdNCT are that gadolinium is toxic and therefore must be tightly bound to the carrier, it has to be located closer to the nucleus to maximize LET damage, and the γ rays it produces are not localized to the target cell.[4]

BNCT is the process in which boron-10 undergoes nuclear fission through an alpha decay pathway by absorbing a thermal neutron (0.025 eV). The fission reaction produces two high LET products, an alpha particle (1.47 MeV) and $^{7}$Li (0.84 MeV). The maximum range that these high LET products travel in tissue is 9 μm.[3,5] Since a typical human cell is 10-30 μm,[6] the radiation is mainly localized to cells containing $^{10}$B, with some possible damage done to immediately adjacent cells.

Although localized treatment is important, there are two requirements that any boron compound must meet to be a plausible BNCT agent. First, the minimum amount of $^{10}$B must be ~$10^{9}$ atoms per cell to provide a greater chance for neutron capture, and second, the tumor-to-normal tissue and tumor-to-blood boron concentration must be greater than 3:1, so as to localize the BNCT reaction to the tumor without doing irreparable damage to the normal tissues.[3,7-10]

There are two boron compounds that have been clinically studied as BNCT agents, mercapto-undecahydro-closo-dodecaborate (BSH) and p-boronophenylalanine (BPA).[3,11,12] In animal testing studies, BSH has a tumor-to-blood ratio of 1.3:1, which is much less than the required ratio. It has been suggested that the tumor-to-tissue ratio is more important than the tumor-to-blood ratio; therefore, if that ratio is increased, the BSH is still a good treatment candidate.[3] BPA meets both requirements. It is, however, selective only to gliomas and melanomas. According to clinical studies of BPA, a minimum dosage of 250 mg/kg body weight is needed to be effective,[13] because only 1 out of every 5 BPA molecules (20% $^{10}$B) could undergo neutron capture. Besides BPA and BSH, boronporphyrins,[14,15] amino acids,[16] polyhedral boranes,[17,18] boronated anti-epidermal growth factor receptor,[19] DNA-binding agents,[20,21] and monoclonal

antibodies[22] have been proposed as alternative boron delivery agents. Presently, increasing the $^{10}B$ capacity to improve the chance of neutron capture has become a focus for modern BNCT agent preparation.

Recently, boron nanoparticle hybrids (e.g. boron carbide) have been suggested as possible boron neutron capture therapy (BNCT) agents because of their high boron content.[23] Elemental boron nanoparticles (BNPs) also have a high calculated boron content (~$10^7$ boron atoms per 50 nm particle).[24] Even though the studies of elemental boron nanoparticles focused on their fuel applications,[25] if the particles were made water-dispersible and thus could be used in biological media, they would also have potential as a boron neutron capture therapeutic. How to make them water-dispersible is a problem that may be solved using silica coating. As discussed in Chapter 1, silica is highly advantageous as an inorganic nanoparticle carrier for physiological uses, because it provides a modifiable, hydrophilic shell.

## 4.2 Experimental Section

### 4.2.1 Materials

Elemental boron powder (95-97%, Sigma-Aldrich), Undecenoic acid (UND acid, 95%, Sigma-Aldrich), Triethoxy silane (95%, Sigma-Aldrich), Tetraethoxy silane (TEOS, 99.999+%, Alfa Aesar), Ammonium hydroxide (28-30%, Sigma-Aldrich), 3-aminopropyltriethoxy silane (APTES, 98%, Sigma-Aldrich), Dansyl chloride (99%, Sigma-Aldrich), Curcumin (Sigma-Aldrich), Speier's catalyst, $H_2PtCl_6 \cdot 6H_2O$ (99.9%, Sigma Aldrich).

### 4.2.2 Instruments

Transmission electron microscopy (TEM, FEI Techna $G^2$ T-12), UV/Vis spectrophotometer (Mikropack DH-2000 UV-Vis-NIR), Scanning transmission electron microscopy with energy dispersive x-ray spectroscopy (STEM-EDS, FEI Titan 80-300).

### 4.2.3 Air stable boron nanoparticle preparation

The BNPs are made[26,27] using 2 g of microscale elemental boron powder that is ground in a Retsch PM400 planetary mill with tungsten carbide in a milling jar at an 80:1 charge ratio (ball and powder ratio). To protect boron surfaces from oxidation, 1 mL of undecenoic acid (UND acid) is added to the boron and 15mL hexane mixture prior to milling. The resultant particles are washed 3 times in hexane to remove excess fatty acid and redispersed in 200 proof ethanol. TEM is used to analyze morphology and size distribution of BNPs.

### 4.2.4 Hydrosilylation reaction

Triethoxy silane is added to the surface of the UND-modified BNPs by redispersing 0.0798 g of dry BNPs in dry acetonitrile (15 mL). 1mL of triethoxy silane is added to the reaction flask and stirred for 24 hours in the presence of a Speier's catalyst, $H_2PtCl_6 \cdot 6H_2O$ (7.0 mg). The particles are then washed twice with acetonitrile and 3 times with ethanol to remove any excess triethoxy silane. The particles (0.049 g) are redispersed in ethanol (13 mL).

### 4.2.5 Coating of BNPs with silica

The Stöber method[28] is implemented to complete the silica shell formation around the BNPs. Ammonium hydroxide (0.116 mL), tetraethoxy silane (0.25 mL, TEOS),

MilliQ water (0.791 mL), and absolute ethanol (3 mL) are added to 2 mL of the triethoxy silane BNP solution and stirred for 24 hours. The particles are washed with ethanol 5 times to remove free TEOS and pure silica nanoparticles, leaving a black powder. If a white silica layer persists, the centrifuged particles are left in ethanol overnight to allow the pure silica nanoparticles to slowly disperse in the solution. This is then followed by the removal of the supernatant so that only the black silica coated BNPs are present. Size and morphology are observed by TEM. The particles are also added to water to determine if they are water-dispersible.

### 4.2.6 APTES modification

The silica-coated BNPs (B@SiO2 NPs) are dried and redispersed in dry acetonitrile (5 mL). 2% v/v of 3-aminopropyltriethoxy silane (APTES) is added to the solution and stirred for 17 hours. The APTES solution is then washed 5 times with dry acetonitrile, to remove any excess APTES, and redispersed in ethanol.

### 4.2.7 Fluorescent tag addition

Dansyl chloride is used as the fluorescent tag, because it reacts quickly with primary amines. 4 mg of dansyl chloride, in 5 mL dry acetonitrile, is added to the B@SiO2 NPs and the APTES modified B@SiO2 NPs. The particles are washed with acetonitrile until the supernatant no longer fluoresces. A UV lamp is used to observe fluorescence.

### 4.2.8 Curcumin study

The curcumin study requires four solutions to be made prior to mixing with boron, 1) an acetic acid buffer, 2) sulfuric-glacial acetic acid reagent, 3) curcumin, and 4)

100 ppm boric acid stock solution. The solutions are prepared following the procedure described by Liu and Lee.[29] 1 L of the acetic acid buffer is made by mixing 135 mL of glacial acetic acid with 180 g of ammonium acetate (Merck) in 90 mL of ethanol and diluted to 1 L with MilliQ water. The sulfuric-glacial acetic acid solution is made by mixing a 1:1 ratio by volume of concentrated sulfuric acid and glacial acetic acid to a total volume of at least 20 mL. The curcumin solution is made by taking 0.125 g of the curcumin powder and adding it to 100 mL glacial acetic acid. The boron stock solution (100 ppm) is prepared by dissolving 0.5717 g boric acid to a final volume of 1 L in MilliQ water. All solutions are kept in nalgene bottles to avoid boron contamination from glassware.

To obtain a standards curve, five boric acid solutions (1-5 ppm) are made from the 100 ppm stock solution. 500 μL of each boric acid solution are taken and added to a 50 mL nalgene bottle. Subsequently, 3 mL of acetic anhydride is added, to avoid water contamination that can interfere with curcumin, and let sit for 20 minutes. 3 mL of the curcumin solution and sulfuric acid/glacial acetic acid solution are added to the bottle and allowed to react for 70 minutes to ensure complete reaction. Then each solution is quenched with 20 mL of the acetic acid buffer to remove any of the interfering curcumin-proton complex and their absorbance is measure at 543 nm. The BNPs and B@SiO2 NPs curcumin tests are done in the same fashion.

Another calibration curve is made using a 1 M KOH in ethanol solution. The calibration procedure is done the same way, except 1 mL of acetic anhydride is replaced by 1 mL of the KOH solution. The boric acid standards are added to the KOH and let sit

overnight before the test is performed. The B@SiO2 NPs are also placed in KOH, but prior to sitting overnight, they are sonicated for 8 hours.

## 4.3 Results and Discussion

The BNPs made by the surfactant-assisted ball milling method in the presence of oleic acid are air stable,[27] because the surface fatty acids prevent the oxidation to boron oxide ($B_2O_3$). However, the fatty acids cause them to be hydrophobic, preventing them from being used in biological applications. Coating BNPs with silica would make them hydrophilic and would also allow for easy surface modifications.

UND acid was chosen as the surfactant for the ball milling method, as opposed to the original oleic acid ligand in the literature, [26,27] because it contains a terminal alkene group. The alkene can react with silanes through a hydrosilylation reaction.[30-33] By treatment with triethoxy silane, the surface of the BNPs acquires a layer of $Si(OEt)_3$. It is expected that the initial ethoxysilane layer will react with TEOS under the Stöber conditions,[28] to fully encapsulate the BNPs in a silica layer (Scheme 4.1).

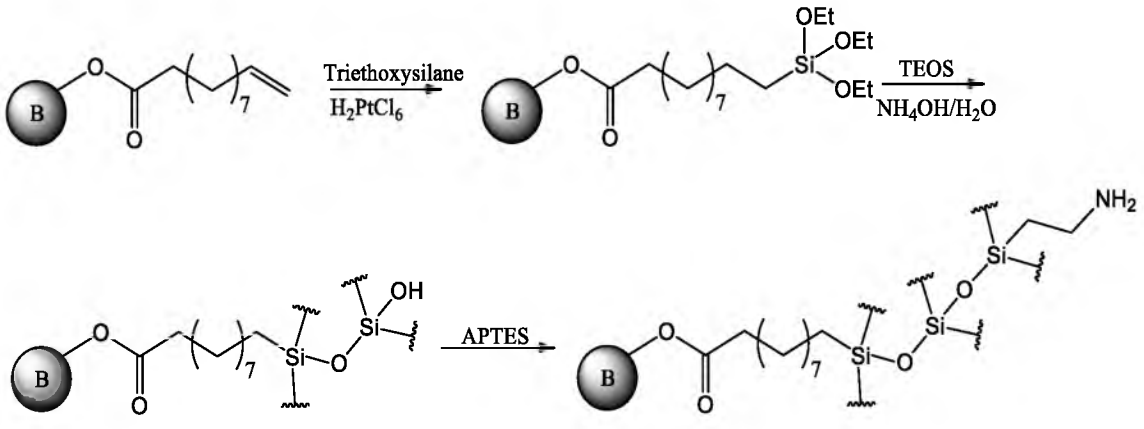


Scheme 4.1: Coating fatty acid boron nanoparticles with silica.

Previously, we reported that UND-BNPs have a size distribution ranging from 11 to 70 nm with the average size of 38 nm.[24] After the treatment with triethoxy silane and TEOS, the resulting particles appear spherical, homogeneous in size (64 ± 3 nm), and distinctly separated as seen in TEM images (Figure 4.1a). This implies that a silica shell of 26 nm in thickness is forming around the BNPs. These particles are distinctly different from the amorphous BNPs (Figure 4.1b), but no core-shell structure is observed to indicate boron encapsulation. This is likely due to the lower density of boron compared to silica, which results in the electron beam penetrating higher to lower density nanoparticles. The absence of amorphous material and the presence of spherical particles suggest that boron is indeed encapsulated by silica. Because the core-shell structure cannot be imaged, a colorometric study and STEM-EDS were used to confirm their structure.

The molecules that can form complexes with boron and be measured spectrophotometrically are 1,1- dianthrimide,[34] carmine,[35] azomethine-H,[36] and curcumin.[37] Curcumin, often used to determine boron concentrations in water and soil, complexes with boron to form rosocyanine, which has an orange to red color. Figure 4.2 shows the linear dependence of boron-curcumin complex absorbance on boron concentration at 543 nm. Curcumin can react with micron-sized boron powder;[38] therefore, we expected that the BNPs will form a complex with curcumin, but the silica-coated BNPs will not because of their protective shell.

Because the weight added by silica is unknown but is expected to be small, BNP and B@$SiO_2$ NP samples were prepared with equal concentrations (~3800 ppm) on the assumption that all sample mass is elemental boron. Even though the sample

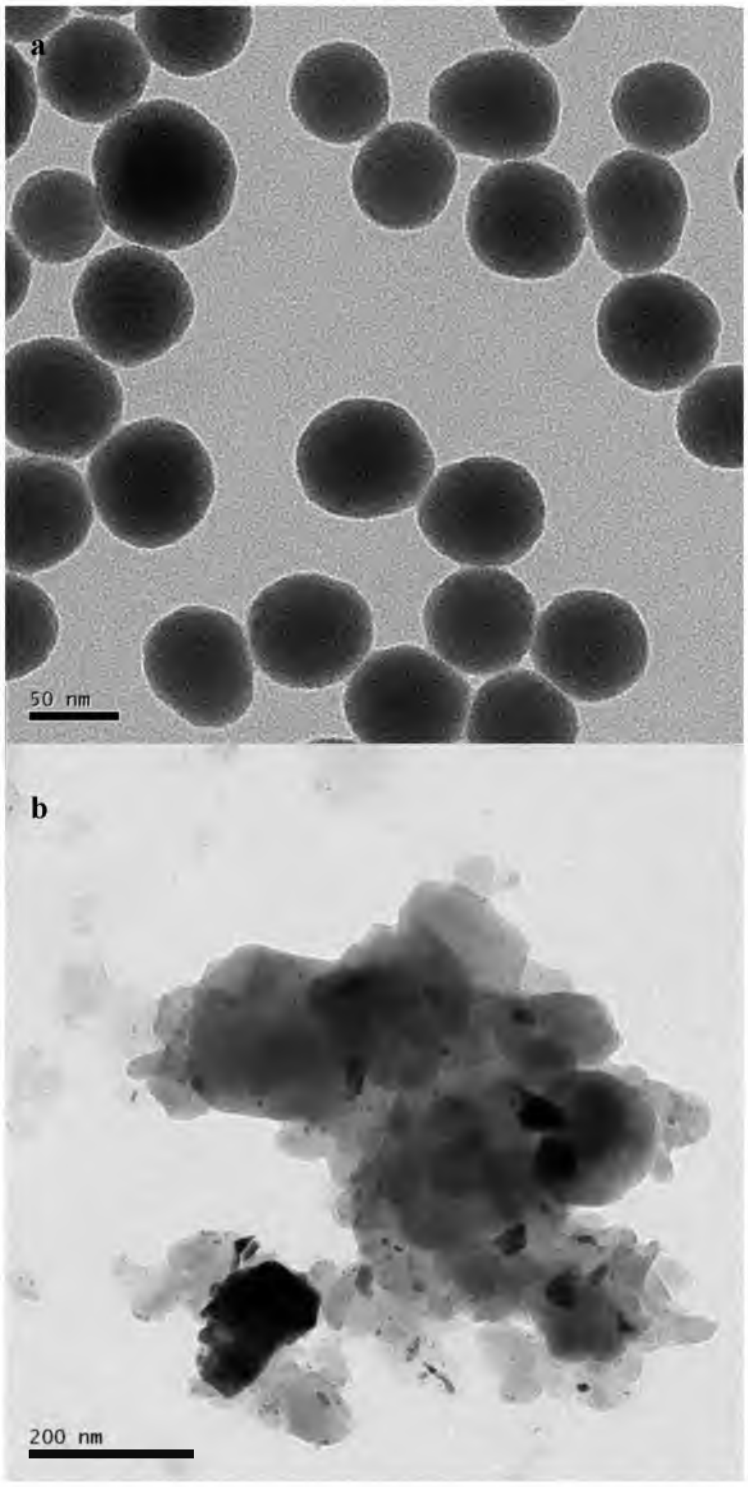


Figure 4.1: TEM images of a) Silica coated boron nanoparticles b) amorphous boron nanoparticles.

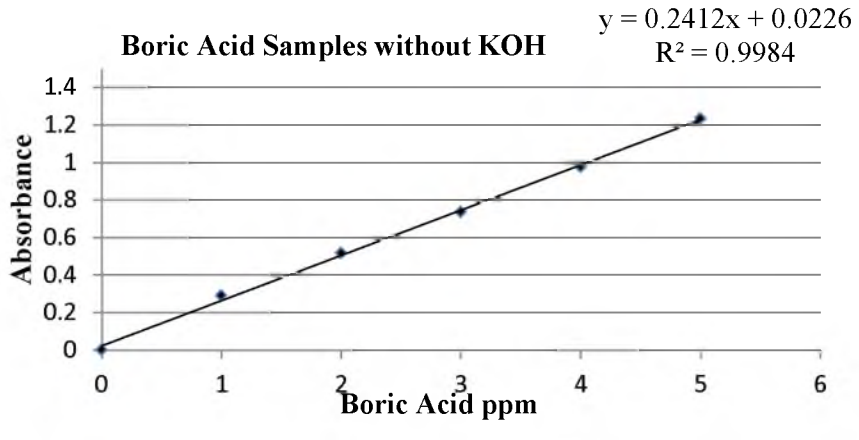


| Boric Acid | 0 ppm | 1 ppm | 2 ppm | 3 ppm | 4 ppm | 5 ppm |
|---|---|---|---|---|---|---|
| Absorbance | 0 | 0.29 | 0.59 | 0.74 | 0.98 | 1.23 |

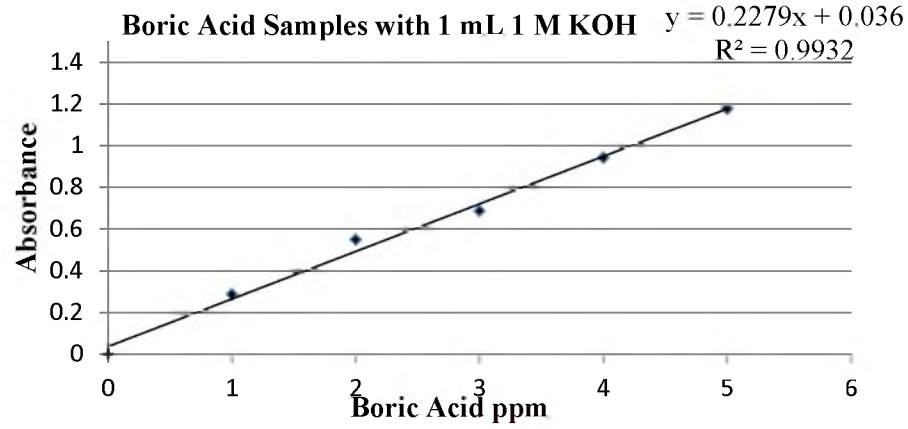


| Boric Acid | 0 ppm | 1 ppm | 2 ppm | 3 ppm | 4 ppm | 5 ppm |
|---|---|---|---|---|---|---|
| Absorbance | 0 | 0.29 | 0.55 | 0.68 | 0.94 | 1.18 |

Figure 4.2: Calibration curves for curcumin study.

concentration used was higher than the concentration of the standards, it was demonstrated that for micron-sized boron powder, curcumin will react with the surface only.[37] This results in measured boron concentrations that are between 0.05-0.1 % of the total boron concentration.[38] BNPs in curcumin have a much higher absorbance at 543 nm compared to B@$SiO_2$ NPs (Table 4.3). This indicates that BNPs complex with the curcumin, despite the surface ligand, and that the silica shell is protecting the boron core

Table 4.3: Absorbance Measurements of Boron Samples.

| | Absorbance | Boron detected (ppm) |
|---|---|---|
| BNPs | 1.383 | 5.91 |
| $B@SiO_2$ | 0.099 | 0.32 |
| $B@SiO_2$ in KOH | 0.560 | 2.30 |

from curcumin. Since the B@SiO2 NPs did give a low absorbance, it is likely that some BNPs are not fully encapsulated, the silica shell is slightly porous, or some boric acid is present on the surface of $B@SiO_2$ NPs.

If $B@SiO_2$ NPs are indeed formed, dissolving the silica should expose the boron to the curcumin and a significantly larger absorbance should be observed. The two common reagents used to dissolve silica are hydrofluoric acid (HF) or sodium/potassium hydroxide (NaOH/KOH). We used HF first to dissolve the silica shell because of the expected high rate of its reaction with silica. However, when the resulting samples were studied, the absorbance was similar to that for the $B@SiO_2$ NPs. This may be the result of HF forming fluoroborates, which are very volatile and may be released into the atmosphere during sample preparation, or, although fluoroborates are made, the curcumin could not chelate them because of the strong B-F bond.[37] The use of KOH was more successful because the resulting boron particles reacted with curcumin and the presence of KOH had little to no effect on the calibration curve (Figure 4.2). After stirring the $B@SiO_2$ NPs in KOH solution for 24 hours and performing the curcumin procedure, we observed a 6 fold increase in absorbance and therefore, in boron concentration (Table 4.3), compared to that of untreated $B@SiO_2$ NPs. Thus, this qualitatively confirms that the boron is encapsulated by a silica shell (Figure 4.3). The lower concentration of boron

Figure 4.3: B@$SiO_2$ NPs in curcumin without KOH (left) and B@$SiO_2$ NPs in curcumin after dissolving silica shell (right).

detected in B@$SiO_2$ NPs (by a factor of ~2.5) after the silica shell is dissolved compared to that of the BNPs is likely due to the silica shell providing a more significant weight to the BNPs than initially assumed, resulting in a lower effective boron concentration.

The elemental analysis of the BNPs and B@$SiO_2$ NPs was performed using STEM-EDS. For the BNPs, STEM-EDS spectrum exhibits an intense peak at 0.187 keV corresponding to boron atoms (Figure 4.4). The B@$SiO_2$ NPs STEM-EDS spectrum exhibits a boron peak and also a peak at 1.75 keV, corresponding to silicon (Figure 4.5). This demonstrates that both silica and boron are present in the same particle. The elemental composition of the BNPs includes a large amount of boron outweighed only by oxygen (Table 4.4). When elemental analysis of the B@$SiO_2$ NPs is performed, the weight ratio of silica to boron is calculated to be 1.05:1 (Table 4.5). This explains why the measured boron concentration of dissolved B@$SiO_2$ NPs is about half that of the BNPs. The silica shell thickness can be calculated based on the determined weight ratio.

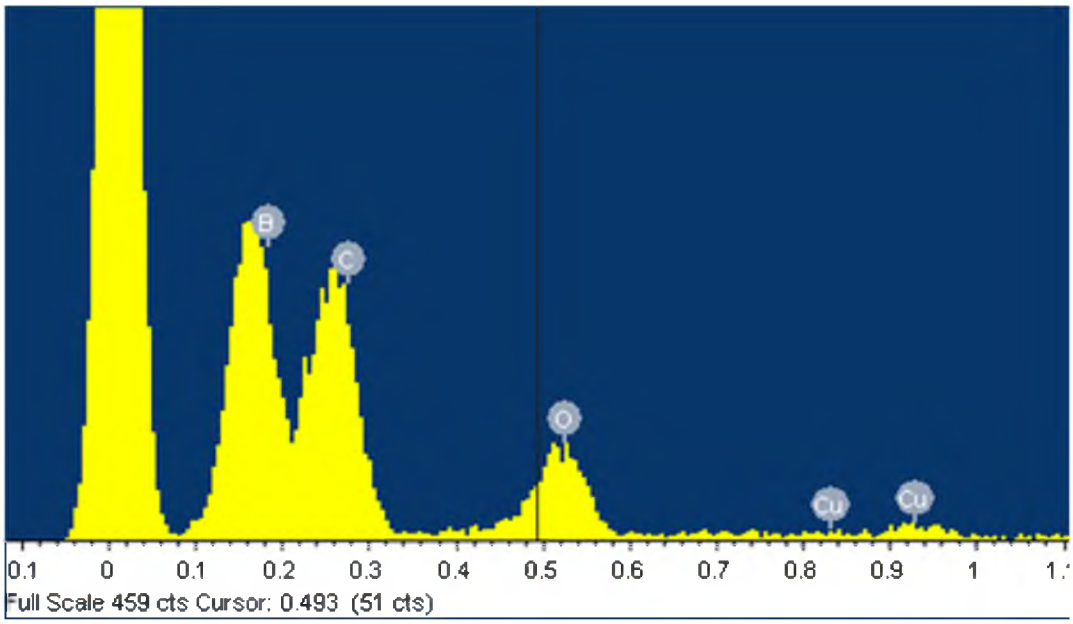


Figure 4.4: STEM-EDS spectrum of boron nanoparticles.

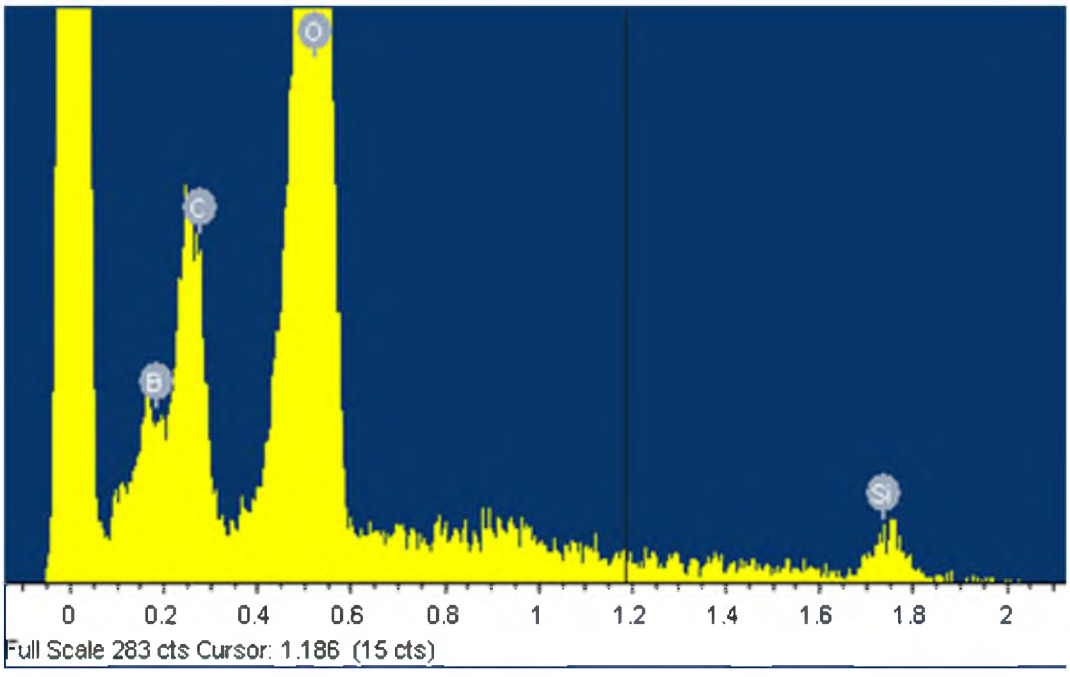


Figure 4.5: STEM-EDS spectrum of B@$SiO_2$ NPs.

Table 4.4: Elemental Analysis of Boron Nanoparticles.

| Element | Weight% | Atomic% | Compd% | Formula |
|---|---|---|---|---|
| B K | 17.84 | 24.09 | 57.45 | B2O3 |
| C K | 10.50 | 12.76 | 38.46 | CO2 |
| Cu L | 3.26 | 0.75 | 4.08 | CuO |
| O | 68.40 | 62.40 | | |
| Totals | 100.00 | | | |

Table 4.5: Elemental Analysis of B@$SiO_2$ NPs.

| Element | Weight% | Atomic% | Compd% | Formula |
|---|---|---|---|---|
| B K | 0.83 | 1.13 | 2.68 | B2O3 |
| C K | 26.32 | 32.18 | 96.44 | CO2 |
| Si K | 0.41 | 0.21 | 0.87 | SiO2 |
| O | 72.44 | 66.48 | | |
| Totals | 100.00 | | | |

$$\frac{\rho_{B@SiO_2} \cdot \frac{4}{3} \cdot \pi \cdot (r_{SiO_2} + r_{BNP})^3}{\rho_{BNP} \cdot \frac{4}{3} \cdot \pi \cdot r_{BNP}^3} = \frac{W_{SiO_2} + W_B}{W_B}$$

Eq. 4.1: Determining silica shell thickness: ρ is the density of the particle, $r_{SiO2}$ is the unknown thickness of the silica shell, $r_{BNP}$ is the determined radius of the boron nanoparticle, and $W_{SiO2}$ and $W_B$ are the EDS weight percentages of silica and boron.

This is done by using Eq. 2.1 and assuming the densities of the BNPs and the B@$SiO_2$ NPs are similar. The silica shell thickness is calculated to be 10 nm, which is not significantly different from the 26 nm value calculated from the average particle sizes of B@$SiO_2$ NPs and BNPs. It should be noted that the absolute amount of boron detected in the B@$SiO_2$ NPs sample is much smaller than that observed for the BNPs sample. This can be attributed to the presence of the silica shell, but it more likely results from the presence of adventitious carbon.

To make B@$SiO_2$ NPs more suitable for BNCT, the silica shell was modified with APTES to provide primary amines to the surface. With primary amine functionalities, targeting ligands and fluorophores can be attached to the surface of the B@$SiO_2$ NPs. Treating these aminated particles with an amine-reactive fluorophore is an additional method to confirm the formation of the silica shell. Thus, dansyl chloride was used with APTES-modified B@$SiO_2$ NPs because it reacts rapidly with primary amines and forms a fluorescent species. When dansyl chloride was added to the APTES-modified particles, a blue-green fluorescence was observed, which was absent for unmodified B@SiO2 NPs treated with dansyl chloride (Figure 4.6). This qualitatively demonstrated that the B@$SiO_2$ NPs can be modified with primary amines.

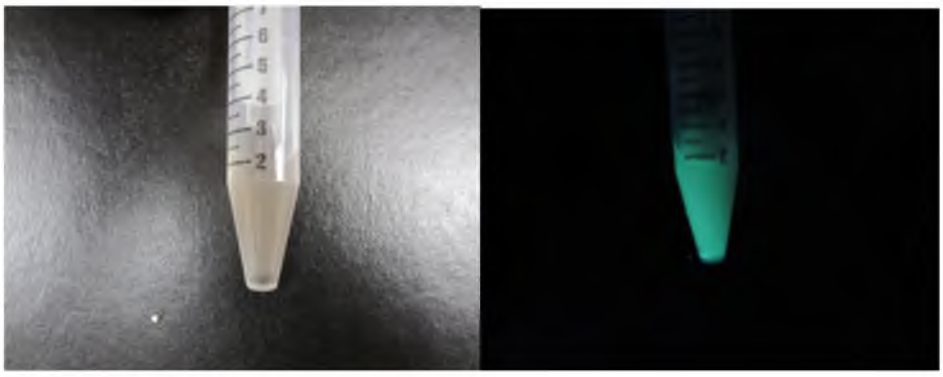

Figure 4.6: Dansylation of APTES modified B@$SiO_2$ NPs.

## 4.4 Conclusions

Boron nanoparticles contain a large amount of boron compared to most other BNCT agents. The challenge in using them therapeutically is to make boron nanoparticles water-dispersible. We demonstrated that boron nanoparticles can be encapsulated in a silica shell to make water-dispersible boron/silica core-shell nanoparticles. Silica encapsulates the boron to produce spherical nanoparticles with the average 64 nm diameter and 3 nm dispersity, and with the silica shell thickness estimated to be between 10 and 26 nm. The presence of boron was confirmed by the curcumin complexation studies and STEM-EDS analysis. Furthermore, we were able to modify the silica shell surface with primary amines that allow for the attachment of a fluorophore and, potentially, of targeting ligands.

## 4.5 References

[1] SEER Cancer Statistics Review. 2010. 1 Jan 2007 Surveillance Research Program, NCI. <http://www.seer.cancer.gov>.

[2] How much money is spent on cancer research. 2010. 2 Feb 2010 <nanomedicinecenter.com>.

[3] Coderre, J.A.; Morris, G.M. *Radiat. Res.* **1999**, *151*, 1-18.

[4] Soloway, A.H.; Tjarks, W.; Barnum, B.A.; Rong, F.-G.; Barth, R.F.; Codogni, I.M.; Wilson, J.G. *Chem. Rev.* **1998**, *98*, 1515-1562.

[5] Barth, R.F.; Coderre A.; Vicente, M.; Blue, T. E. *Clin. Cancer Res.* **2005,** *11*, 3987-4002.

[6] The National Institute of General Medical Sciences. Inside the Cell. 2005.

[7] Hawthorne, M. F. *Angew. Chem. Int. Ed.* **1993**, *32*, 950-984.

[8] Valliant, J. F.; Guenther, K. J.; King, A. S.; Morel, R.; Schaffer, P.; Sogbein, O. O.; Stephenson, K. *A. Coord. Chem. Rev.* **2002**, *232*, 173- 230.

[9] Javid, M.; Brownell, G.L.; Sweet, W.H. *J. Clin. Invest.* **1952,** *31,* 604.

[10] Tolpin, E.I.; Wellum, G.R.; Dophan, F.C., Jr.; Kornblith, P.L.; Zamenhof, R.G. *Oncology* **1975,** *32,* 223.

[11] Hatanaka, H.A. *J. Neurol.* **1975**, *209*, 81–94.

[12] Mishima, Y.; Ichihashi, M.; Tsui, M.; et al. *Lancet* **1989**, *2*, 388–389.

[13] Coderre, J.A.; Hopewell, J.W.; Turcotte, J.C.; Riley, K.J.; Binns, P.J.; Kiger III, W.S.; Harling, O.K. *Appl. Radiat. Isot.* **2004**, *61*, 1083-1087.

[14] Isaac, M. F.; Khal, S. B. *J. Organomet. Chem.* **2003**, *680,* 232-243.

[15] Ceberg C.P.; Brun A.; Kahl S.B.; Koo M.S.; Persson B.R.; Salford L.G. *J. Neurosurg.* **1995**, *83,* 86-92.

[16] Kabalka, G.W.; Yao, M.L. *Synthesis* **2003,** *18,* 2890-2893.

[17] Diaz, A.; Stelzer, K.; Laramore, G.; Wiersema, R. *Research and Development in Neutron Capture Therapy*; Monduzzi Editore: Bologna, **2002**, pp. 993-999.

[18] Kueffer, P.J.; Maitz, C.A.; Khan, A.A.; Schuster, S.A.; Shlyakhtina, N.I.; Jalisatgi, S.S.; Brockman, J.D.; Nigg, D.W.; Hawthorne, F. *Proc. Natl. Acad. Sci.* **2013**, *110*, 6512-6517.

[19] Yang, W.; Wu, G.; Barth, R.F.; et al. *Cancer Res.* **2008**, *14,* 883-891.

[20] Tietze, L.F.; Griesbach, U.; Bothe, U.; Nakamura, H.; Yamamoto, Y. *Chembiochem* **2002**, *3*, 219-225.

[21] Woodhouse S.L.; Rendina L.M., *Chem. Commun.* **2001,** 2464-2465.

[22] Nakamura, H.; Miyajima, Y.; Takei, T.; Kasaoka, S.; Maruyama, K. *Chem. Commun.* **2004**, 1910-1911.

[23] Mortensen, M. W.; Björkdahl, O.; Sørensen, P. G.; Hansen, T.; Jensen, M. R.; Gundersen, H. J. G.; Bjørnholm, T. *Bioconjugate Chem.* **2006**, *17*, 284-290.

[24] Gao, Z.; Walton, N.I.; Malugin, A.; Ghandehari, H.; Zharov, I. *J. Mater. Chem.* **2012**, *22*, 877-882.

[25] Bellot, J. B.; Noh, W.; Nuzzo, R. G.; Girolami, G. S. *Chem. Commun.* **2009**, *22*, 3214-3215.

[26] Devener, B.V.; Perez, J. P. L.; Anderson S.L. *J. Mater. Res.* **2009**, *24*, 2462-2464.

[27] Devener B.V.; Perez J. P. L.; Jankovich J.; Anderson S.L. *Energy Fuels* **2009**, *23*, 6111-6120.

[28] Stöber, W.; Fink, A.; Bohn, E. *J. Colloid Interface Sci.* **1968**, *26*, 62-69.

[29] Liu, Y.M.; Lee, K. *Mar. Chem.* **2009**, 115, 110-117.

[30] Dávila-Ibáñez, A.B.; López-Auintela, A.; Rivas, J.; Salgueirino V. *J. Phys. Chem. C* **2010**, *114*, 7743-7750.

[31] Coletti, C.; Marrone, A.; Giorgi, G.; Sgamellotti, A.; Cerofonlini, G.; Re, N. *Langmuir* **2006**, *22*, 9949-9956.

[32] Ying, B.; Jiajian, P.; Yingqian, H.; Jiayun, L.; Huayu, Q.; Guoqiao,L. *Chin. J. Chem. Eng.* **2009**, *17*, 1038-1042.

[33] Yao, J.Z.; Chen, Y.Y.; Tian, B.S. *J. Organomet. Chem.* **1997**, *534*, 51-56.

[34] Ellis, G.H.; Zook, E.G.; Baudisch, O. *Anal. Chem.* **1949**, *21*, 1345-1348.

[35] Hatcher, J.T.; Wilcox, L.V. *Anal. Chem.* **1950**, *22*, 567-569.

[36] Demir, B.S.; Serindağ, O. *Eurasian J. Anal. Chem.* **2006**, *1*, 11-18.

[37] Thangavel, S.; Dhavile, S.M.; Chaurasia, S.C. *Anal. Chim. Acta.* **2004**, 502, 265-270.

[38]Grotheer, E.W. *Anal. Chem.* **1979**, *51*, 2402-2403.

# CHAPTER 5

# CONCLUSIONS AND FUTURE DIRECTIONS

## 5.1 Conclusions

Silica nanoparticles can act as carriers for fluorophores, organic functionalities, and other nanoparticles. Silica nanoparticles provide an inert, hydrophilic structure that does not react with their cargo. Organosilanes impart organic functionalities to the surface of the silica nanoparticles, making the particles multifunctional. This work demonstrated different synthetic methodologies for the production of internally functionalized silica nanoparticle.

To demonstrate the utility of internally functional silica particles, we developed a synthetic strategy to produce metal-chelating mesoporous nanoparticles using co-condensation of TEOS with an organosilane (SiDETA) which is presented. This provides a porous network with the organosilane included throughout the mesoporous nanoparticle body. The DETA functionality can be modified with bromoacetic acid to produce the EDTA analog DTTA, which imparts the metal-chelating functionality to mesoporous nanoparticles.

Gadolinium was chelated by the mesoporous DTTA-containing nanoparticles that may find applications as MRI contrast agents. The amount of gadolinium chelated by theses nanoparticles is 46500 Gd atoms per particle. Because all gadolinium atoms are chelated by surface DTTA groups, they are accessible to water, which is the main

requirement for MRI. Additionally, gadolinium has been proposed as a neutron capture therapeutic. Thus, our gadolinium-chelating nanoparticles combine imaging and therapeutic modalities.

To increase the accessibility of the functional groups inside the silica nanoparticles, we synthesized, for the first time, mesoporous and surface-rough organically modified silica (ORMOSIL) nanoparticles. The ORMOSILs are synthesized using vinyltrimethoxy silane in a micellar CTAB solution. The mesoporous vinyl nanoparticles synthesized in the micellar solution have larger surface areas than the solid vinyl particles. The surface-rough vinyl nanoparticles have a surface area larger than the solid vinyl and mesoporous vinyl particles. When brominated or hydroborated, however, the rvSNPs show no significant difference in the percentage vinyls converted when compared to reacted svSNPs.

The mesoporous vinyl nanoparticles have a smaller surface area than the surface-rough particles, but because of their additional pores, the extent of hydroboration is almost double that of the other ORMOSILs. This means that our mesoporous particles, on a per volume basis, carry more boron atoms than the solid or surface-rough particles. Both the mesoporous and surface-rough particles have excellent potential as a BNCT agents because of their boron loading and particle diameter.

To further increase the amount of boron atoms delivered to cancer cells for BNCT and to make biocompatible theranostic anticancer agents, we developed the synthesis of boron-core-silica-shell nanoparticles. We prepared these particles by forming the hydrophilic silica shell on the surface of suitably modified boron nanoparticles. These core-shell nanoparticles were characterized using STEM-EDS and curcumin titration (as

a colorimetric indicator). These characterization steps confirmed that boron has being encapsulated inside the silica shell. Additionally, the silica shell was modified with 3-aminopropyltriethoxysilane to place primary amines on the silica surface. A variety of species (fluorophores, targeting ligands) can then be attached to the surface and give the core-shell particle imaging and therapeutic properties.

## 5.2 Future Directions

Even though silica nanoparticles have been continuously studied since the 1960s, they are still being improved and developed for a variety of applications. The new field of ORMOSIL chemistry and its benefits provide for expansion of tradition silica chemistry.

Because the silica nanoparticles mentioned throughout this thesis have been suggested as potential NCT agents, their cytotoxic effects must be studied if they are to be used in biological applications. In addition to conducting cytotoxic studies, work needs to be done to determine the location of the particles with respect to the cells, to predict the effect of the irradiative damage. If the nanoparticles have little to no toxicity against normal cells, then ligands that targets tumor cells (gliomas have been the focus of BNCT agents) should be attached to the surface to determine if the nanoparticles meet the 3:1 tumor-to-normal cell requirement of BNCT. Lastly, the neutron capture of the particles should be studied to determine if these particles can undergo BNCT within the silica particle body, and to discover if they have significant cytotoxic effect when activated by the neutrons.[1]

Relaxivity measurements of the gadolinium-carrying nanoparticles should be performed to determine their suitability for use as MRI contrasting agents. It would also be beneficial to determine if the mesoporous nanoparticles carrying gadolinium have any

toxicity to the body, perhaps by gadolinium being released from the DTTA complexes. This is unlikely based on the evidence of other DTTA-Gd chelators,[2] but is still a potential issue that should be addressed with any newly developed particle carrying toxic metals. Another interesting study would be to determine through animal testing if the particles are excreted from the body.

Metal-chelating nanoparticles might also be beneficial as X-ray computed tomography (CT) agents.[3] This would involve chelating bismuth as the contrast agent. It is known that bismuth can be chelated by EDTA and EDTA analogs, so the difficulty would be in determining the particle dosage requirement that is needed for imaging. Additionally, bismuth-212 has potential in targeted alpha therapy (TAT) of cancer, [4] so once again the metal-chelating particle may have a theranostic application.

Since novel vinyl ORMOSIL nanoparticles have been developed, the next step is to synthesize additional mesoporous or surface-rough structures from different organosilanes. Additionally, if two organosilanes were co-condensed,[5] it would create a mesoporous or surface-rough structure with two organic functionalities without the need for postmodification. For example, it has been suggested that boron and gadolinium might work well together for NCT. This could be accomplished by co-condensation of VTMS with SiDTTA, since that would provide two organic functionalities, one (DTTA) that can chelate gadolinium and the other (vinyl) that can be hydroborated to incorporate boron atoms.

As was discussed briefly in Chapter 3, the rvSNPs have a potential in creating water-repelling glass. This is due to the large surface area and high vinyl density on the

surface. To further explore this application, water contact angle should be determined to see if the rvSNPs do in fact have a superhydrophobic surface.[6]

The development of these silica nanoparticles for medical usage is going to be a lengthy process. Even though potential applications of the particles have been discussed, they may be medically useless because of potential biological complications. Nonetheless, the synthetic strategies we developed will allow us to consider alternative applications for silica nanoparticles.

## 5.3 References

[1] Coderre, J.A.; Morris, G.M. *Radiat. Res.* **1999**, *151*, 1-18.

[2] Li, Z.; Zhang, Y.; Shuter, B.; Idris, N.M. *Langmuir* **2009**, *25*, 12015–12018.

[3] Rabin, O.; Perez, J.M.; Grimm, J.; Wojtkiewicz, G.; Weissleder, R. *Nature Materials* **2006**, *5*, 118-122.

[4] Montavon, G.; Le Du, A.; Champion, J.; Rabung, T.; Morgenstern, A. *Dalton Trans.* **2012**, *41*, 8615-8623.

[5] Ottenbrite, R.M.; Wall, J.S.; Siddiqui, J.A. *J. Am. Ceram. Soc.* **2000,** *83,* 3214-3215.

[6] Li, X.; He, J. *ACS Appl. Mater. Interfaces* **2012** dx.doi.org/10.1021/am3002082.